Numerical Cavity-Resonance Modelling of Impulse Excited Pi 2 Pulsations in the Magnetosphere

by

HERCULES PEKRIDES

Submitted in partial fulfilment of the
requirements for the degree of
Doctor of Philosophy,
at the
Space Physics Research Institute,
University of Natal, Durban.

Republic of South Africa
April 1993

To my Parents,
Christina
and
Panayiote.

Preface

The work described in this thesis was carried out at the Space Physics Research Institute (SPRI), Department of Physics, University of Natal, Durban, South Africa, from April 1989 to July 1992, under the supervision of Professor A. D. M. Walker of the SPRI, and co-supervision of Dr. P. R. Sutcliffe of the Hermanus Magnetic Observatory, Hermanus, South Africa.

The studies documented in this thesis represent original work by the author and have not been submitted in any form to another university. Where use was made of the work of others it has been duly acknowledged in the text.

Portions of chapters 4, 5 and 6 have been presented as a paper at the 1990 South African Institute of Physics Annual Conference, University of Port Elizabeth, South Africa, as a poster at the XXth General Assembly of the International Union of Geodesy and Geophysics (IUGG), Vienna, Austria, 11-24 August 1991, and as a paper at the Tenth National Congress of the Australian Institute of Physics, University of Melbourne, Victoria, Australia, 10-14 February 1992.

Acknowledgements

I gratefully acknowledge all persons who where of assistance during the course of this thesis. In particular, I would like to thank the following:

supervisor Professor A. D. M. Walker of the SPRI, for his keen interest, availability and helpful advice,

co-supervisor Dr. P. R. Sutcliffe of the Hermanus Magnetic Observatory, South Africa, for assisting with the clarification of Pi 2 observational aspects and for providing useful spectral analysis programs,

the personnel of the Hermanus Magnetic Observatory, for their kind assistance provided in the retrieval of Pi 2 archived data during April 1989,

Miss T. M. Holloway of the SPRI, for computer hardware and software assistance,

Dr. M. J. Alport, of the Plasma Physics Research Institute, University of Natal, Durban, for graphics software support,

Dr. J. P. S. Rash, Dr. E. Mravlag and Mrs. J. A. E. Stephenson for proof-reading this thesis,

my parents, for their moral and financial support, and

my God, He made it possible.

I would also like to thank the University of Natal for financial support through Graduate Scholarship Awards during 1989 and 1990, as well as travel funds granted by the University Research Grant Committee toward travel to the IUGG conference, Vienna, 1991. Finally, thanks to the Foundation for Research and Development for major financial assistance provided during 1989 and 1990.

Abstract

A magnetohydrodynamic (MHD) cavity-resonance model is developed to study the ultra low frequency (ULF) response in the magnetosphere to an external compressional impulse. It is assumed that the magnitude of the impulse is small enough such that non-linear terms remain negligible. The MHD differential equations are derived in a cold, non-uniform plasma imbedded in a cylindrical ambient field geometry and are solved using numerical finite difference integration methods. The crucial feature of the model is that it allows for the investigation of the response within the magnetospheric cavity to an impulse that has both temporal and spatial form.

There is strong observational evidence that low-latitude Pi 2 pulsations have, or are associated with, a global propagation mechanism. Evidence alluding to the global nature of low-latitude Pi 2 is the characteristically low azimuthal (or axial) wavenumbers, ($|m| \lesssim 1$). Further evidence of the global nature of Pi 2 is the lack of arrival time difference between globally separate events, as well as the similarity in the spectral content of globally separate events. As an application, the cavity-resonance model is applied to investigate the Pi 2 pulsation event. The cavity-resonance waves are excited by an impulsive perturbation at the magnetopause which is centred about the midnight meridian. The excitation signal is chosen representing the causal Pi 2 mechanism thought to be associated with the sudden, short circuiting of the cross-tail current to the auroral oval.

Various aspects of the cavity-resonance wave modes are investigated and the appropriateness of this type of modelling for the study of Pi 2 is evaluated. Numerical integration and well as Fourier and Laplace methods are used to investigate the transmission of the impulsive signal through the magnetosphere. Coupling between the isotropic (cavity) and the transverse Alfvén (resonance) mode is studied. The effect of the plasmapause is considered. Longitudinal variations of polarization as well as the latitudinal phase variations of the perturbed fields are computed. Computational results are compared with observational features of the Pi 2 event.

Contents

APPENDICES

List of Symbols

$\mathbf{b}$	perturbation magnetic field.
$\mathbf{B}$	background magnetic field.
$\mathbf{E}_0$,E	zero order and perturbation electric fields resp.
$\mathbf{J}_0$,$\mathbf{J}$	zero-order and perturbation current densities resp.
m	azimuthal wave number field quantities vary as $e^{-im\phi}$.
a, R_e	radius of the earth.
$\mathbf{V}$	plasma drift velocity.
$\mathbf{A}$	Alfvén speed, $B/\sqrt{\mu_0\rho}$.
$\rho_{0,i,eq}$	background, ionospheric and equatorial plasma densities
P, T	poloidal and toroidal electric field sobriquets
$\bar{P}$,$\bar{T}$	Laplace transformed poloidal and toroidal electric field components
$\bar{\mathcal{P}}$,$\bar{\mathcal{T}}$	Fourier and Laplace transformed P, T
κ	ionospheric damping decrement
n	field aligned standing wave harmonic

List of Acronyms

AFGL	Air Force Geophysics Laboratory
BGS	British Geological Survey
FAC	field aligned current
KHI	Kelvin-Helmholtz Instability
MHD	magnetohydrodynamic
MLT	magnetic local time
SABRE	Sweden and British Radar Auroral Experiment
SAMNET	U.K. Sub-Auroral Magnetometer Network
SCW	substorm current wedge
STARE	Scandinavian Twin Auroral Experiment
UCLA	University of California, Los Angeles
ULF	ultra low frequency
VLF	very low frequency

Chapter 1

Introduction

Within the earth's magnetosphere there are a multitude of ongoing geophysical processes. The energy source for all these processes lies ultimately in the solar radiation and solar wind's interaction with the magnetosphere. These interactions cover a broad spectral range, from cosmic and X-rays to VLF (very low frequency) and ULF (ultra low frequency) waves.

ULF waves form an important part of the dynamic processes occurring in the magnetosphere. The study of these waves is of significance because it helps to identify specific magneto-plasma processes occurring in the magnetosphere. Pi 2 are a class of ULF pulsations that are of particular importance because they are closely associated with a major geophysical event - the magnetospheric substorm. Specifically, Pi 2 are related to the sudden formation of the magnetosphere-ionosphere current system at substorm onset which is a major contributor to the transport of energy from the magnetotail to the ionosphere.

Pi 2 have been studied in some detail during recent years and much progress has been made toward the understanding of these events. However, there are aspects relating to the Pi 2 propagation mechanism that are not yet clearly understood. For instance, the event's high latitude characteristics conflicts with what is seen at mid and low latitudes. At auroral latitudes, Pi 2 pulsations are observed to be spatially confined in Local Time to within a few hours about midnight. Low-latitude Pi 2, on the other hand, are observed at all Local Times and have features which tend to suggest a global mode structure.

As a consequence of the contrasting nature between high-, mid- and low-latitude Pi 2, theoretical developments have been divided according to the latitudinal zones. These models are remarkably successful in explaining observed Pi 2 features in the latitudinal zones for which they were intended, but inaccurate when applied outside these zones.

In fact, none of these models is able to explain the relationship between the high- and low-latitude Pi 2 characteristics. For low latitudes, few models have been developed and none explain the global nature of low-latitude Pi 2. A further puzzle is the process responsible for producing the secondary amplitude maximum and phase reversal of Pi 2 observed at mid latitudes.

In this thesis, a Pi 2 propagation model is proposed and developed. The problem is approached in the following manner: first, observed characteristics of the event are reviewed (chapter 2). This is followed by a brief look at some recent model descriptions (chapter 3) for Pi 2. From these studies a scenario is proposed for the propagation of Pi 2 (section 3.2.4). This scenario is based on the premise that Pi 2 are MHD waves extending throughout the magnetospheric cavity. Consequently, developments in the field of cavity and global mode modelling are reviewed.

In ULF-global mode modelling, the entire magnetosphere or plasmasphere is most often chosen as the cavity within which the MHD waves are confined to propagate. The geometry of these cavities is generally assumed to be either a box (straight magnetic field lines) or a cylinder or a dipole. The more accurate geometrical descriptions give rise, (as usual), to more complicated wave equations. The usual assumption within the magnetosphere is applied i.e. that the magnetic field and plasma are frozen into each other. Suitable models for the plasma distribution within the cavities are chosen. These types of wave equations are known as cavity-resonance equations and are characterized by two Alfvén wave modes, the fast isotropic (cavity) and the transverse Alfvén (resonance) wave modes. In a non-uniform plasma distribution these modes are coupled, resulting in field line resonances and damped global modes.

Historically, the cavity-resonance equations were studied using analytical methods. However, this approach was made tractable by assuming extensive, (and consequently severely limiting), simplifications. For example, the equations are reduced one dimension if one assumes azimuthal symmetry of the wave fields. Essentially, this means that the problem is reduced to the description of the wave equations in a two-dimensional meridian plane. Choosing a simple geometry for the geomagnetic field is another way in which to keep the equations in an analytically tractable form. Naturally, curvature terms are neglected in this case. Choosing simple power-law relationships to describe the plasma distribution within the model cavity is another method of reducing complexity. Without any of these simplifying assumptions, the equations are mathematically intractable and require the application of numerical integration methods in order to solve. Even so, the number of computational iterations required to solve the full three-dimensional problem dramatically increases from the box model cavity to cylindrical or dipolar cavities. Only with the aid of the most powerful supercomputers are solutions to the equations derived in a dipolar geometry possible in a reasonable amount of time.

In this thesis a cavity-resonance model, based on the earlier work of *Allan et al.* [1985b], is adapted so that the spatio-temporal response of waves generated within the cavity, by an externally incident excitation pulse, may be investigated (chapter 4). The model of *Allan et al.* [1985b] is modified in two major ways. First, the equations are derived in full three-dimensional form, allowing for wave fields to be determined at any longitude within the cavity. Secondly, the excitation signal is no longer assumed to be purely time dependent and now includes a transverse spatial component (in this case axial). For the specific study of Pi 2 pulsations, the spatial part of the excitation signal is chosen to best describe the scale of the perturbation in the region thought to be associated with the causative mechanism of Pi 2 (chapter 5). The importance of the spatial structure of the excitation signal has been emphasized in the global mode modelling of *Southwood and Kivelson* [1990]. They found that the response within the cavity depended not only on the time scale of the change, but also, and importantly, on the spatial scale of the perpendicular pressure change (to the magnetic field) at the outer cavity boundary.

The spatio-temporal evolution of the modelled waves within the cavity, (with appropriate background plasma and magnetic parameters), is investigated (chapter 6). The study is commenced with an investigation of the nature of cavity modes and their coupling to the field line resonance mode. Features such as the amplitude, phase and polarization are computed and discussed. Computational results are compared with observations wherever appropriate.

The study is concluded with a summary of the important findings, and an assessment of the MHD cavity-resonance approach to the modelling of Pi 2 (chapter 7). The model's merits and short-comings are outlined, and recommendations are made for improvements to the model described in this thesis.

Chapter 2

Observational Features of the Pi 2 Pulsation Event

Pi 2 pulsations are well established amongst the family of geomagnetic ULF pulsations having been extensively studied by many authors. A complete and comprehensive review of these studies would be beyond the scope of this thesis. Rather, we briefly review major Pi 2 features, and in particular, those features which may be compared with the model descriptions in later chapters.

2.1 Definition

The Pi class of magnetic pulsations are defined as damped, quasi-sinusoidal oscillations with an irregular waveform (*Jacobs*, [1970]). This class is subdivided into two classes, Pi 1 and Pi 2, according to frequency (*Jacobs et al.*, [1964]). Pi 1 are classified as those pulsations with a period of $1 - 40$ seconds ($1000 - 25$ mHz), while Pi 2 are classed as those pulsations with a period of $40 - 150$ seconds ($25 - 6.67$ mHz).

2.2 Role

Pi 2 pulsations are thought to be transient signals related to the sudden formation of a magnetosphere-ionosphere current system at the onset of the geomagnetic substorm. The coupled magnetosphere-ionosphere system is formed when cross-tail currents in the magnetotail collapse and are diverted (or short-circuited) into the auroral oval in the local midnight sector as field aligned currents (FAC). The precise link between Pi 2

and FAC is unclear, but their close association underscores the importance of Pi 2 in the transport of energy from the magnetotail to the ionosphere. It has been suggested that FAC are associated with the transverse Alfvén wave mode since this is the only mode that will carry them (*Baumjohann and Glassmeier*, [1984]).

Pi 2 also serve as useful indicators for the exact onset time of the substorm expansive phase in polar regions (*Sakurai and Saito*, [1976]; *Saito et al.*, [1976b]; *Rostoker and Olson*, [1978]; *Saito* [1979]; *Rostoker and Samson*, [1981]; *Southwood and Stuart*, [1980]; *Sutcliffe*, [1980]). The reliability of Pi 2 as a substorm indicator, as opposed to the substorm bay, was apparent in early studies (*Holmberg*, [1953]; *Kato et al.*, [1953]) and may be attributed to unique Pi 2 characteristics. It is known that the amplitude of substorm bays decreases rapidly with decreasing latitude. The amplitude of Pi 2 signals, on the other hand, bears no relation to the magnitude of the associated bays (*Saito*, [1969]). Thus even at low-latitudes, where substorms are barely detectable by the AE index, Pi 2 are detected in a one-to-one correspondence with substorms (*Saito et al.*, [1976a]). Furthermore, during multiple-onset events, magnetic bay signatures are often indistinct because the interval between onsets may be less than the bay development time. Pi 2, however, develop and decay much faster than bays and therefore are clearly observable. Mid- to low-latitude Pi 2 events serve as particularly good substorm onset indicators because they are clearly observable, unlike their high-latitude (auroral zone) counterparts which are contaminated by background electrojet noise. Moreover, low-latitude Pi 2 can be detected at globally separate locations, further highlighting their use as substorm onset indicators.

2.3 Overview of Observations

The observational aspects of Pi 2 pulsations have been extensively researched and there are a number of works on this subject (see reviews of *McPherron*, [1980]; *Hughes*, [1983]; *Yumoto*, [1986]). The majority of Pi 2 investigative studies have been made using ground based magnetometer stations (*Pashin et al.*, [1982]; *Samson*, [1982]; *Lester et al.*, [1983,1984]). These studies have been complemented by satellite observations (*Singer et al.*, [1983]; *Sakurai and McPherron*, [1983]) and, most recently, by auroral radar (*Sutcliffe and Nielsen*, [1990,1992]; *Yeoman et al.*, [1991]).

The main morphological features such as amplitude, frequency and polarization were established in the 1960's and 1970's (*Saito*, [1969]; *Jacobs*, [1970]; *Orr*, [1973]; *Lanzerotti and Fukunishi*, [1974]; *Southwood and Stuart*, [1980]; *McPherron*, [1980]). Originally, it was thought that the events were confined to high latitudes in the night sector. Later observations revealed them to occur at lower latitudes. At low latitudes events were detected at Local Times extending to the day sector. Most recently, multi-station ground

and satellite observation studies have focused on the global aspects of Pi 2 (*Hughes*, [1983]; *Samson and Rostoker*, [1983]; *Sakurai and McPherron*, [1983]; *Baumjohann and Glassmeier*, [1984]; *Verő*, [1986]) which allude to a cavity mode nature (*Yeoman and Orr*, [1989]; *Sutcliffe and Nielsen*, [1990]; *Yeoman et al.*, [1990]; *Sutcliffe and Yumoto*, [1991]).

2.4 Pi 2 and Associated Events

At high latitudes, Pi 2 events are closely associated with polar magnetic substorms, the formation and brightening of the auroral arc, the enhancement of the auroral electrojet, the westward travelling surge, X-ray intensifications, riometer absorption events and energetic particle precipitation (*Stuart and Barsczus* [1980]; *Samson*, [1982,1985]). Within the auroral zone, there is also a close association between Pi 2 and the poleward border of the electrojet (*Olson and Rostoker*, [1977]). Poleward of the initial electrojet position, it has been found that there is little pulsation activity until the poleward border of the electrojet passes overhead, at which point a large amplitude Pi 2 is detected (*Olson and Rostoker*, [1977]).

The relationship between Pi 2 and the expansion phase of a substorm is illustrated in Fig. 2.1 using the Canadian magnetometer network (the location of each station of the network is shown in Fig. 2.2 and Table 2.1). The sudden negative bay identifying the onset of the expansive phase of a substorm was recorded first at Fort Chipewyan (FTCH), where Pi 2 activity was also initiated. Thereafter, Pi 2 spread northward with the poleward border of the electrojet. Pi 2 located equatorward of the electrojet were observed at the same time as substorm onset.

Peak Pi 2 intensities are observed in the region of brightest auroras associated with the westward travelling surge and the breakup region (*Pashin et al.*, [1982]). Almost all correlative studies have shown that the Pi 2 begin at or before the breakup phenomena which strongly suggests that Pi 2 are closely associated with the enhancement of the field aligned currents. In particular, the upward field aligned currents along the westward edge of the auroral system are thought to play an important role in Pi 2 generation (*Samson*, [1982]).

Pi pulsations sometimes appear to be associated with and/or trigger low-latitude daytime Pc 3 (*Stuart and Barsczus*, [1980]). Some of the longer period Pi 2 have similar period, diurnal variation of period, latitudinal amplitude variation, and K_p dependence of period as Pc 4. The major difference between the two types of pulsation events is their duration, a possible reflection of the different excitation mechanisms (*Fukunishi and Hirasawa*, [1970]). As far as the K_p index is concerned, Pi 2 periods in general

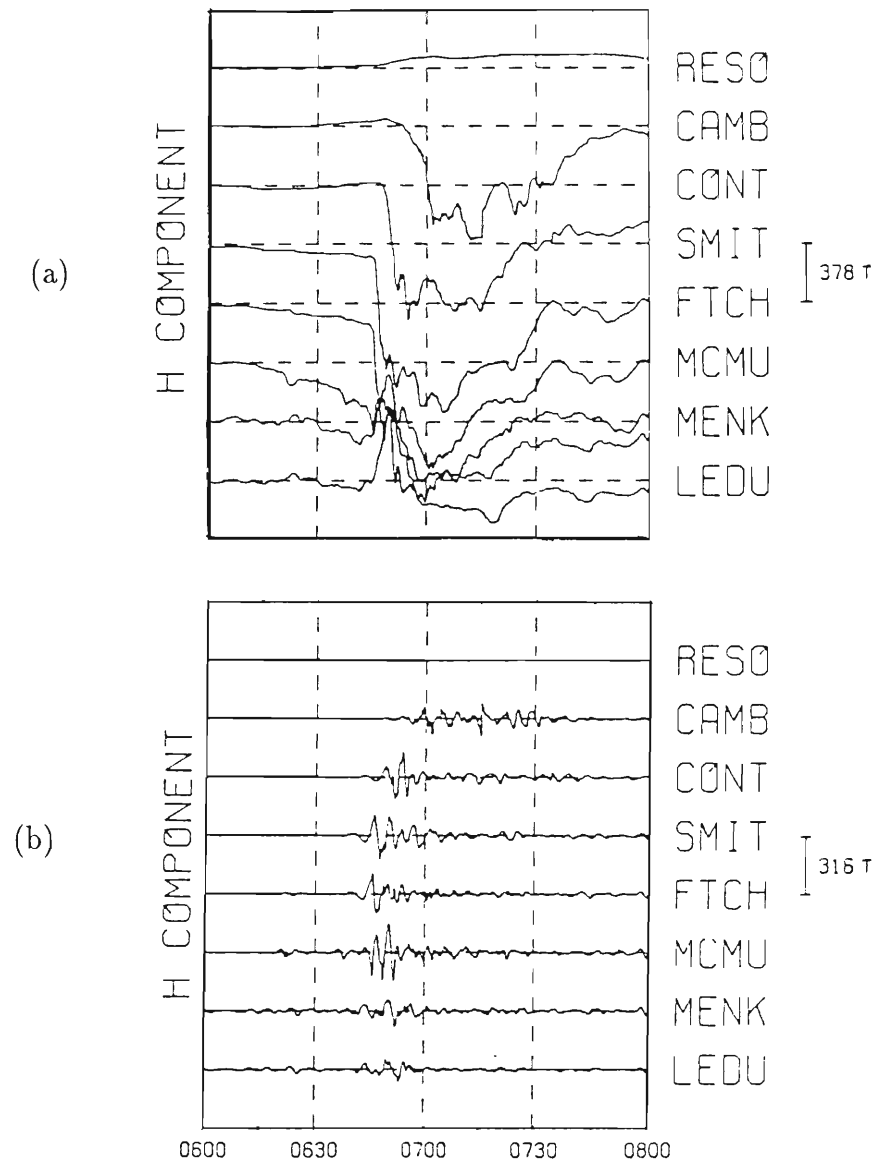

Figure 2.1: (a) Broad-band and (b) band pass filtered (filter corner frequencies are 1 and 20mHz) H-component magnetogram records during the substorm on 23 Nov 1970 from the Canadian network of observatories (after *Olson and Rostoker,* [1977]).

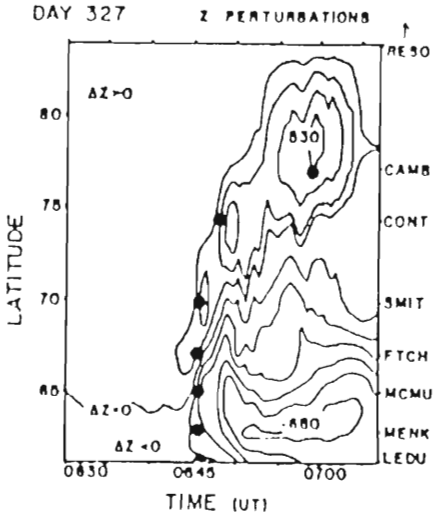

Figure 2.2: Geographical Location of Canadian Magnetometer Network.

Station	Mnemonic	Centred Dipole	L
		Lat. Long.	
Resolute Bay	RESO	83.0 289.4	71.4
Cambridge Bay	CAMB	76.8 296.6	19.5
Contwoyto Lake	CONT	72.6 295.8	11.3
Fort Smith	SMIT	67.3 300.0	6.8
Fort Chipewyan	FTCH	66.3 302.1	6.2
Fort McMurray	MCMU	64.2 303.5	5.4
Meanook	MENK	61.9 300.8	4.5
Leduc	LEDU	60.6 302.9	4.2

Table 2.1: Centred dipole coordinates of each station used in Fig 2.1.

shorten with higher K_p index (*Nishida*, [1978]).

2.5 The Global Nature of Pi 2

2.5.1 Spectra

During quiet magnetic conditions, the period of night-time Pi 2 is generally fairly constant over large latitudinal and Local Time ranges (*Stuart and Barsczus*, [1980]). For example, Pi 2 have been observed at mid and equatorial latitudes with no period differences (*Stuart and Hunter*, [1975]). *Yeoman and Orr* [1989] calculated the power spectra for a set of Pi 2 pulsations at three ground observatories separated longitudinally by $5\frac{1}{2}$ hours of MLT, and found their spectral peaks to coincide. Using the four stations of the BGS (British Geological Survey) latitudinal array, they also observed Pi 2 having dominant H and D frequencies with additional second harmonic components.

Sutcliffe and Yumoto [1991] pointed out that Pc 3 pulsations observed at three ground stations separated by 35^0 (in longitude) had different eigenfrequencies and found them to be dependent on the localized differences in plasma conditions as predicted by field line resonance theory. On the other hand, the frequencies of Pi 2 observed across this array were found to be almost identical. They concluded that local plasma differences did not affect the Pi 2 pulsations, and that this was evidence that Pi 2 are associated with a global, rather than a field line dependent pulsation mechanism. *Yumoto et al.* [1990] corroborate this finding. They found that for $L < 7$, events measured at widely separated stations had identical periods, but different to those measured by spacecraft in the outer magnetosphere for $L > 8$. From the ground data they suggested a global mode Pi 2, possibly bounded by the plasma sheet. Sometimes it seems as if there is some decoupling of the H- and D-components, each component having a different dominant spectral peak (*Lester et al.*, [1983]). This observation indicates that the two components possibly represent different wave modes.

At auroral latitudes, Pi 2 band spectra show a relative increase in energy and are found to be broad and chaotic, (because of background broad band electrojet noise), as opposed to low latitudes where Pi 2 band spectra are sharply peaked (*Stuart and Booth*, [1974]). However, the frequency of the Pi 2 spectral peaks remains unchanged with latitude. Synchronous satellite data usually display no discernable peaks at Pi 2 frequencies, and the spectra appear similar to those observed at auroral zone stations (*Gelpi et al.*, [1985a,1985b]; *Olson and Rostoker*, [1977]). *Sakurai and McPherron* [1983], using digital power spectra and coherency analysis techniques on data from the UCLA fluxgate magnetometer on board ATS 6, were able to divide Pi 2 events at

geosynchronous orbit into three categories: the superposition of an approximately 100 s Pi 2 oscillation with large amplitude, high frequency Pi 1 activity; an approximately 100 s Pi 2 wave with no Pi 1 activity; and a pure transverse Pi 2 wave. A similar finding had been made by *Kuwashima* [1978], which may be an indication of the nature of the Pi 2 source: in the auroral zone, Pi 2 consist of two parts; one a localized irregular burst seemingly dependent on locally related transient phenomena, and the other a more regular signal similar to the Pi 2 signal more widely observed at mid and low latitudes. *Samson,* [1982] pointed out that is important to distinguish between the two types of oscillations observed at high latitudes since they probably come from a different source.

As far as diurnal variations are concerned, the dominant spectral component of day-time Pi 2 is in general shorter than night-time Pi 2 as illustrated in Fig. 2.3. This is generally true for ULF pulsations and may be attributed to the relative compression of the dayside, compared to the nightside, magnetosphere (For the same latitudinal position on the surface of the earth, a relatively more compressed magnetosphere means that the corresponding magnetic fields line there are shorter and hence the characteristic frequency of the local Alfvénwave is higher).

2.5.2 Range of the Event

The detection of Pi 2 is found to be dependent on latitude and local time. Peak occurrences are in the 21:00-1:00 LT sector (e.g. *Smith,* [1973]; *Sakurai and McPherron,* [1983]) and at high latitudes ($L > 4$) ground based observations are localized in longitude to within 1-2 hours in LT (*Olson and Rostoker* [1977]; *Kuwashima,* [1978]). In the midnight sector, mid latitude ($2 < L < 4$) ground observations have in the past been made over at least 60^0 in longitude (e.g. *Singer et al.,* [1983]). *Sakurai and McPherron* [1983] were able to detect mid latitude ground station events (using the Air Force Geophysical Laboratory (AFGL) magnetometer network) concurrently with the ATS 6 satellite at geosynchronous orbit, provided the satellite was located in the 19:00-03:00 LT sector. *Gelpi et al.* [1985a] found that the region of magnetic disturbance in the near geosynchronous orbit was more azimuthally localized (i.e. in Local Time) than the mid-latitude Pi 2 signature. Further studies of GEOS 2 and GEOS 3 satellite data by *Singer et al.* [1983] indicated the event to be longitudinally localized to within 30^0 of the 23:00 LT meridian at geosynchronous orbit.

At low latitudes, the longitudinal extent over which Pi 2 are observed does not appear to be a function of substorm intensity (*Sutcliffe,* [1980]). They cover a much larger longitudinal extent than their higher latitude counterparts, often the whole night sector (*Saito et al.,* [1976b]) and most of the dayside magnetosphere (*Yumoto,* [1987]; *Sutcliffe*

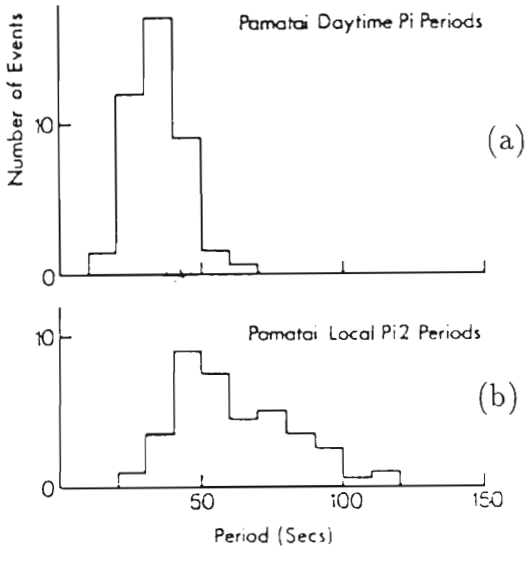

Figure 2.3: Occurrence histograms representing the periods of (a) daytime and (b) night-time Pi 2 events, recorded at Pamatai, Tahiti (Geographic coordinates $17^0 34'\mathrm{S}, 210^0 24'\mathrm{E}$; Geomagnetic coordinates $15.3^0, 282.7^0$) (after *Stuart and Barsczus,* [1980]).

and Yumoto, [1989]) with no apparent preference in Local Time. In the equatorial dip region, Pi 2 are usually detectable at any Local Time (*Yanagihara and Shimizu*, [1966]; *Stuart and Barsczus*, [1980]; *Yumoto*, [1986]). Detection of day-time Pi at mid latitudes is obscured because of regular day-time background Pc activity which tends to mask the Pi signal. *Stuart and Barsczus* [1980] studied dayside magnetometer data from a number of mid latitude stations ($2.3 < L < 5.3$) and found no evidence of Pi 2 activity.

Sutcliffe and Nielsen [1990] made first-time observations of Pi 2 with the STARE radar system. This followed earlier work by *Sutcliffe and Yumoto* [1989] who developed a data adaptive filtering technique to identify dayside Pi 2 pulsations at mid to low latitudes which normally are concealed by commonly occurring Pc 3 activity. Using this method, they showed that low-latitude Pi 2 are a common dayside phenomenon, and, more significantly, they sometimes detected mid-latitude events. Prior to these findings it was generally accepted that mid-latitude Pi 2 were confined to a 60^0 longitudinal zone in the midnight sector.

2.5.3 Simultaneous Observations

One of the earliest identifications of day-time (near equator) Pi 2 occurring in association with night-time (mid latitude) events was made by *Yanigihara and Shimizu* [1966]. Further studies revealed that low-latitude and equatorial Pi 2 occur simultaneously in the day and night sectors within a time accuracy of ± 1 minute (e.g. *Orr and Barsczus,* [1969]; *Saito et al.*, [1976b]; *Sastry et al.*, [1983]; *Yumoto*, [1987]). *Stuart and Barsczus* [1980] found that the majority of day-time Pi 2 events occurred simultaneously with night-time counterparts within a time accuracy of ± 30 s.

More recently, *Sutcliffe and Yumoto* [1989] supported the observation that dayside, low latitude Pi 2 occur simultaneously with night-time events. *Sutcliffe and Yumoto* [1991] not only presented further evidence that low- to mid-latitude Pi 2 occur simultaneously in both the day and nightside hemispheres, but also showed that the spectra are similar (see section 2.5.1). This finding is illustrated in Fig. 2.4 which shows H-component spectra of an event observed at Hermanus, where it was close to local midnight, and at Onagawa, where it was a few hours after dawn. From the figure it can be seen that the dominant peaks are coincident at about 25 mHz ($T \approx 40$ s).

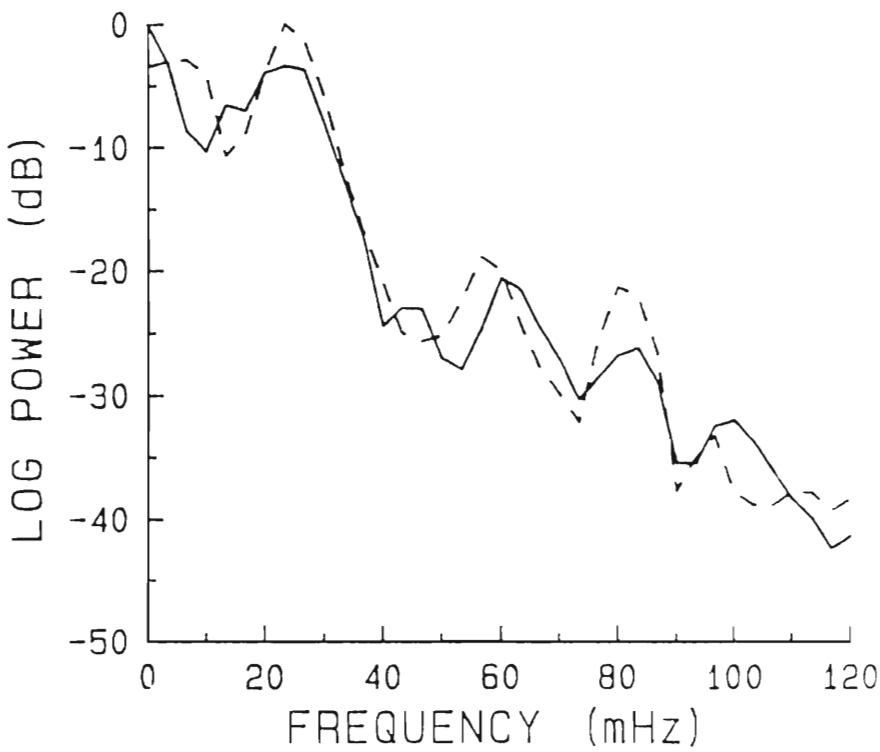

Figure 2.4: H-component log power spectra at Hermanus (solid line) and Onagawa (dashed line) during the 10 minute interval 22:34-22:44 UT on day 236, 1986 (*Sutcliffe and Yumoto,* [1991]).

2.5.4 Dipolarization

Dipolarization may be understood as the result of the sudden disappearance of the cross-tail current sheet from the near Earth portion of the tail (with accompanying more dipole-like reconfiguration of the geomagnetic field). Magnetic field dipolarizations detected by satellite (e.g. AMPTE CCE, see *Yumoto et al.*, [1989]) are noted to have corresponding ground Pi 2 pulsations. Using Pi 1-2 data obtained on the ground at low latitude conjugate stations (L=$1.2-2.1$) and in the near Earth magnetotail by the AMPTE CCE spacecraft, *Yumoto et al.*, [1989] found that the onset of the substorm tends to be detected by ground observations of Pi 2 earlier than at $\sim 8R_E$ in the near earth tail. The time lag is a minimum at midnight and increases as the satellite position shifts east or west from midnight. This result is consistent with that of *Nagai*, [1982], whose data also suggested that the time lag increases as the satellite moves earthward, which was interpreted as an earthward movement of the region of dipolarization. Pi 2 were also observed that had no corresponding dipolarization at CCE, consistent with previous observations in that Pi 2 are a global indicator of the expansion phase onset of a substorm (whereas dipolarization occurs over a limited region of the near earth magnetotail).

2.5.5 Azimuthal Phase and Wavenumber

Initial phase velocity observations were often conflicting. Pi 2 were generally observed to have westward phase velocity, with the occasional detection of an event with eastward phase. Observed azimuthal wavenumbers (m) were also highly conflicting, with reports of values ranging from as high as $10-20$ to less than 1. However, these conflicts were resolved when a latitudinal-Local Time ordering was established.

Phase

At auroral latitudes a predominantly westward Pi 2 phase motion is observed (*Gelpi et al.*, [1985a,1985b]). Besides a predominantly westward phase velocity, there is also a component of the H oscillation which propagates poleward, in step with the poleward movement of the poleward border of the auroral electrojet (*Yumoto et al.*, [1989]). At high latitudes, *Samson and Harrold* [1985] reported phase velocities of Pi 2 to be eastward to the east of the FAC region and westward to the west of this region. At mid latitudes, *Lester et al.* [1984] observed westward propagating events dominating to the west of the substorm current wedge (see section 3.2.2 for description of the substorm current wedge (SCW) model) and eastward propagating phase events dominating to the east of the SCW. (The east/west boundaries of the SCW may be said to be roughly

coincident with the east/west boundaries of the FAC).

There are few low-latitude Pi 2 phase studies, but indications are that the phase is westward during the pre-midnight sector and eastward during post-midnight (*Yumoto*, [1987]).

AFGL array studies by *Gelpi et al.* [1985b] have shown that the apparent longitudinal phase propagations of the magnetic H- and D-components behave differently. On the other hand, *Yumoto et al.* [1990] studied four Pi 2 events detected during small substorms in the midnight sector and found the H and D components to be nearly in-phase between night and dayside stations at low latitudes. Furthermore, they found that the components of H and D oscillate nearly anti-phase and in-phase between high and low latitude stations respectively. This means that there is a 180^0 phase shift between high and low latitude events. *Yeoman and Orr* [1989] located this 180^0 phase shift of the H-component along the British Geological Survey (BGS) latitudinal chain and speculated that is was associated with the plasmapause. Earlier, *Lester and Orr* [1983] used satellite plasma density measurements to locate the plasmapause in conjunction with Pi 2 observations from two meridian magnetometer chains and concluded that there is a variation of the H-component phase across the plasmapause which is not seen in the D-component. Early ground based studies showing a 180^0 phase reversal of B_H at L= $3-4$ were presented by *Bjőrnsson et al.* [1971] and *Fukunishi* [1975]. A recent study by *Takahashi et al.* [1992] of AMPTE CCE satellite observations has indicated the field aligned and transverse (radial) magnetic components to be in phase when the satellite is at L<3 and 180^0 out of phase when L>3.

Symmetry along field lines

Conjugate studies (e.g. *Kuwashima and Saito,* [1981]), indicate the H-component (D-component) to be in phase (out of phase) in the northern and southern hemispheres. This phase symmetry can be explained by assuming an odd mode oscillation along the field lines. This result was also inferred from the conjugate studies of *Fukunishi* [1975]. Most recently, *Takahashi et al.* [1992] have studied Pi 2 events detected by AMPTE CCE and on the ground at Kakioka and found the compressional magnetic components to be symmetric, with anti-symmetric transverse components.

Azimuthal Wavenumber (m)

The azimuthal wave number is found to depend on latitude. At high latitudes $|m| \sim 3-20$ (*Lester et al.*, [1985]; *Samson and Harrold*, [1985]; *Yumoto et al.*, [1988b]), $|m| \sim 2-4$ at mid latitudes (*Green and Stuart*, [1979]; *Mier-Jedrzejowicz and Southwood*,

[1979]; *Lester et al.*, [1983,1984]; *Yumoto et al.*, [1988b]), $|m| < 2$ at low latitudes (*Yumoto* [1986]), and $|m| \ll 1$ at very low to equatorial latitudes (*Kitamura et al.*, [1988]). From these studies, it is clear that the longitudinal phase velocity

$$v_\phi = \frac{\omega}{k_\phi} = \frac{2\pi f a L}{m}$$

(where f is the wave frequency, a is the earth radius and m is the azimuthal wavenumber) of Pi 2 is latitude dependent, slower at higher latitudes where m is larger, and faster at lower latitude where m is smaller.

2.6 Amplitude Variations

The largest amplitude Pi 2 pulsations are observed in the region of the brightest auroras associated with the westward travelling surge and the breakup region (*Pashin et al.*, [1982]). (This suggests the generation mechanism to be located in the outer magnetosphere where the field lines are connected to the auroral region (*Kitamura et al.*, [1988])). In the local midnight sector, Pi 2 amplitudes decrease from high to low latitudes (*Saito*, [1969]). The amplitude also decreases with Local Time moving away from the midnight region, decreasing rapidly at high latitudes and slightly at low latitudes (see also section 2.5.2). It is notable that the quality of the day-time response does not seem to relate to the quality or amplitude of the night-time event (*Stuart and Barsczus*, [1980]).

At mid latitudes there appears to be a secondary amplitude maximum (e.g. *Bjőrnsson et al.*, [1971]; *Raspopov et al.*, [1972]; *Lester and Orr*, [1981]; *Kuwashima and Saito*, [1981] and *Yeoman and Orr*, [1989]). This Pi 2 secondary amplitude maximum was first observed at about 50^0 geomagnetic latitude by *Jacobs and Sinno* [1960] on an array covering North America and the Pacific. *Yeoman and Orr* [1989] have pointed out that the secondary maximum appears to be located near the plasmapause, although *Lester and Orr*, [1981] observed the secondary maximum well earthward of their projected position of the equatorial plasmapause. The relationship between the plasmapause and this secondary amplitude maximum remains to be explained.

2.7 Equatorial Signal Enhancements

Most reports of day-time Pi 2 reports have placed them in the equatorial ($L < 1.1$) region. One of the earliest observations was that of *Yanagihara and Shimizu* [1966] who were able to correlate the event with a night-time, mid latitude event. They found the amplitude of the day-time event at the dip equator to be enhanced relative to the night-time counterpart (see also *Stuart and Barsczus*, [1980]). Furthermore, they reported the amplitude of day-time Pi 2 observed at a station near the dip equator to be enhanced by a factor of 2 to 5 relative to an observation made at 26^0 N. *Sastry et al.* [1983] also observed events with enhanced amplitudes at the dip equator during the day-time. They used H_x component data from two stations, one at the dip equator (Etaiyapuram - ET, geomagnetic $-0^0.6, 147^0.5E$), and the other in the equatorial belt but away from the dip equator (Choutuppal - CH, geomagnetic $7^0.5, 149^0.3E$), and computed the ratio $R_x = \frac{H_{x,E.T.}}{H_{x,C.H.}}$. They were able to show (see Fig. 2.5) that during the day, there was a definite enhancement in the amplitude of the events at the dip equator over those at the station further away from the dip, with a maximum enhancement occurring during $11 - 12$ LT.

2.8 Ground Based Polarization Patterns

The sense of the horizontal polarization ellipse is determined by the ground based H and D magnetic field components. It has been established that the polarization sense is dependent on latitude and Local Time as we shall see in the next two sections.

2.8.1 Polarization Azimuth

At very low latitudes Pi 2 polarization patterns are, in general, linearly polarized approximately along the magnetic meridian (i.e. the magnetic D-component is small compared to the H-component). This is illustrated in Fig. 2.6 where it is clear that D-component perturbations are smaller than the H-component perturbations at the lower latitude stations. A further illustration is given by Fig. 2.7 where it can be seen that the H- and D-components are of comparable amplitude at mid latitudes (SANAE, $L = 4.1$), while at low latitudes (Hermanus, $L = 1.7$) the D-component is far smaller than the H-component. This trend extends over the dayside (*Yumoto,* [1987]) except at the dawn and dusk hours when the D-component is enhanced by an inhomogeneity in the ionospheric conductivity (see *Saka et al.*, [1988]). From these examples, it is clear that at higher latitudes the relatively larger amplitude of the D-component results in a more elliptical polarization.

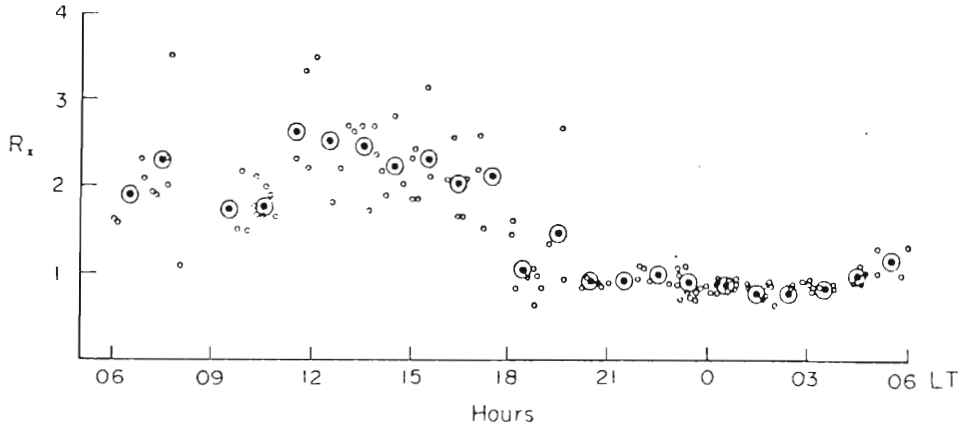

Figure 2.5: Local time variation of the ratio $R_x = \frac{H_{x,E.T.}}{H_{x,C.H.}}$ for Pi occurring simultaneously at CH and ET (*Sastry et al.,* [1983]).

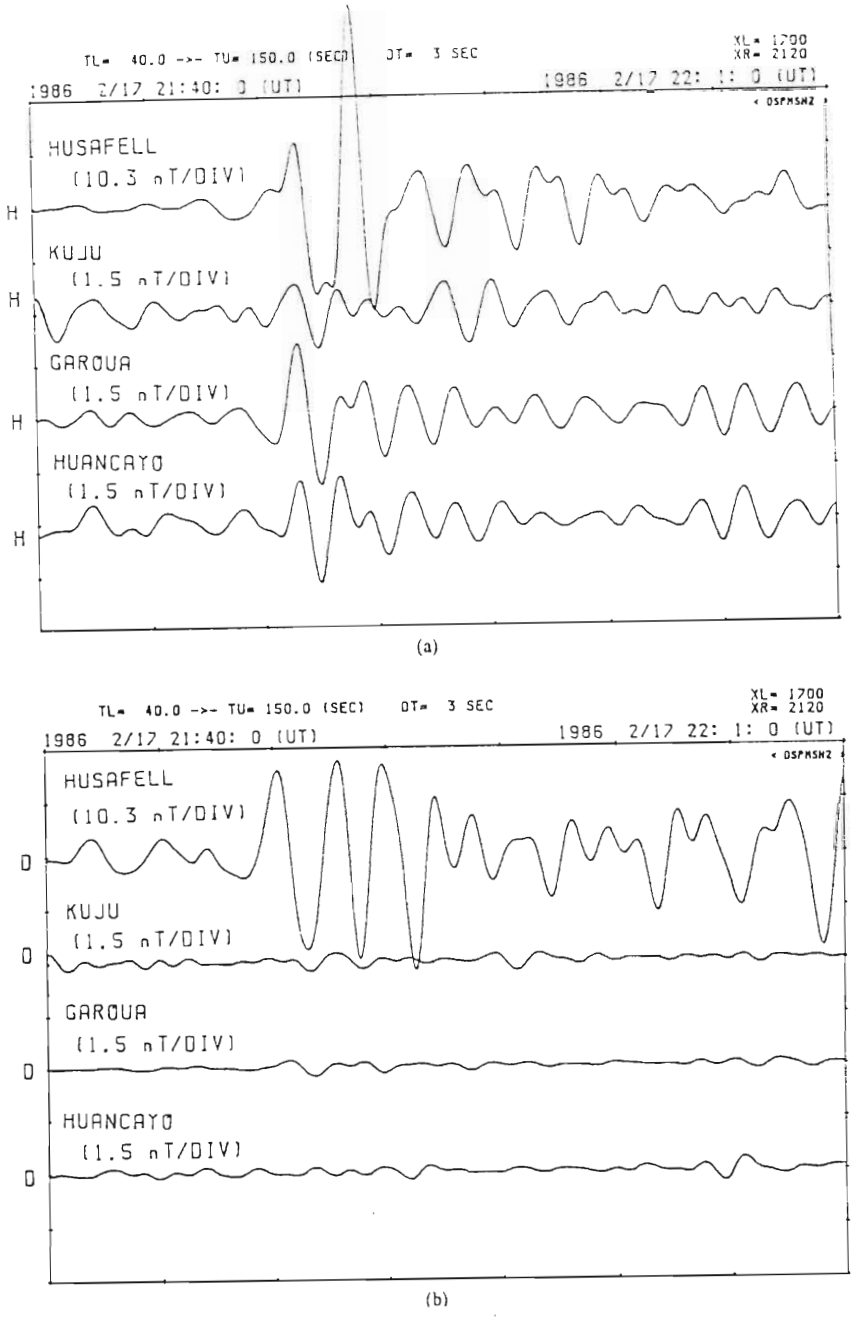

Figure 2.6: H- and D-component magnetograms of a Pi 2 event on 17/2/1986, 21:40-22:01 UT. The coordinates of the stations are : Husafell 64.7, 339.0 Geographic, 70.0, 73.9 Geomagnetic; Kuju 33.2, 130.0 Geographic, 27.5, 201.1 Geomagnetic; Garoua 9.3, 13.4 Geographic, −2.1, 83.9 Geomagnetic; Huancayo, −12.1, 284.7 Geographic, 0.8, 355.6 Geomagnetic (*Kitamura et al.*, [1988]).

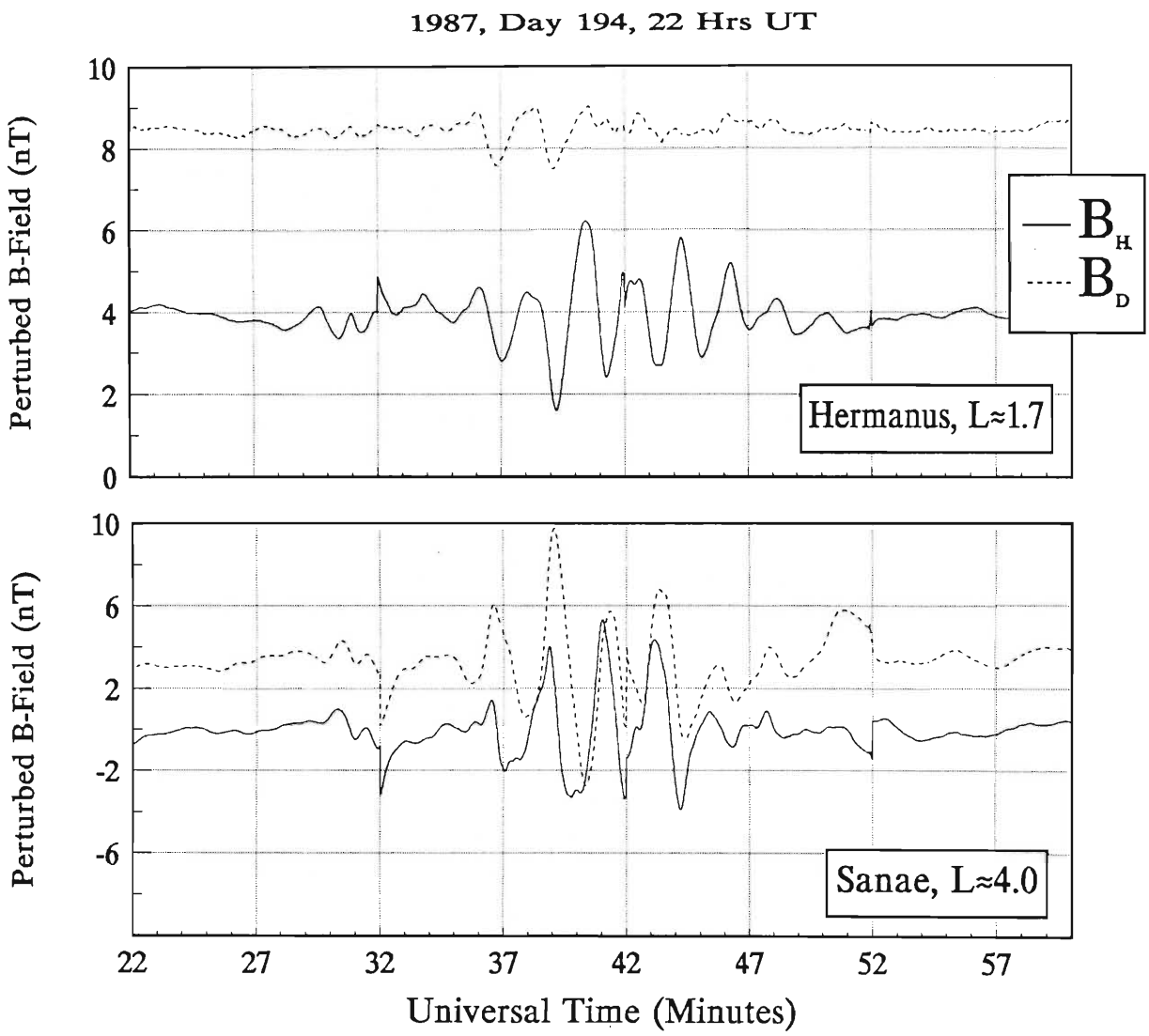

Figure 2.7: H- and D-components magnetograms at Hermanus and Sanae on day 194, 1987, 22:22-23:00 UT.

The major axis of the Pi 2 horizontal polarization ellipse follows a pattern with Local Time similar to that predicted by the bay variations of the substorm current wedge model (*Rostoker*, [1967]; *Bjőrnsson et al.*, [1971]; *Lester et al.*, [1983,1984,1989]). (For a description of the substorm current wedge, in particular polarization predictions of this model, see section 3.2.2). In Fig. 2.8 *Lester et al.*, [1984] summarize the horizontal polarization pattern for a set of mid-latitude Pi 2 observations in terms of a substorm current wedge coordinate system. West of the wedge centre, azimuths are predominantly in the north-east quadrant, while east of the centre, they are in the north-west quadrant. This means that the major axis of the polarization ellipse rotates in a right-handed[1] sense as one proceeds westward at constant geomagnetic latitude. The centre of the pattern is defined as the longitude where the major axis lies along the H axis. *Lanzerotti and Medford* [1984] using data from three magnetometers spaced in latitude near $L \sim 1.9$, found that the ellipse orientation in the horizontal plane generally changes from a northeast/southwest direction for pre-midnight events to northwest/southeast for post-midnight events. *Yeoman et al.,* [1990], using Pi 2 data from the SAMNET (U.K. Sub-Auroral Magnetometer Network) array, have also found the polarization azimuth pattern as a function of longitude to agree with that of the SCW model. That is to say, if one assumes that the centre of the SCW is in the near midnight meridian then these results are in agreement with the findings of *Lester et al.* [1984].

In a further polarization study carried out by *Lester et al.* [1989] at low latitudes, it was determined that inside the SCW the polarization pattern is similar to that for mid latitude stations (see Fig. 2.9). Events having azimuths between 0^0 and 90^0 dominate to the west of the central meridian, and events with azimuths between 90^0 and 180^0 dominate to the east of the central meridian. The difference at low latitudes arises for events to the west of the wedge which show azimuths of between 0^0 and 90^0, the same as those for events inside the wedge and west of the central meridian (wedge centre). Similarly east of the wedge the azimuths are predominantly in the northwest quadrant (azimuths between 90^0 and 180^0), opposite to that found at mid latitudes. This does not agree with mid latitude results (*Lester et al.*, [1983,1984]) which showed that the events tended to change azimuth quadrants at the edges of the wedge (the longitude at which $\Delta H = 0$). *Lester et al.* [1989] postulated that the differences between the mid and low latitude wave azimuths could be explained in terms of a Local Time increase in the wedge width with decreasing latitude.

[1] A right handed sense of rotation is defined as clockwise (CW), and a left-handed sense as anti-clockwise (ACW), when looking down the ambient field lines in the northern hemisphere.

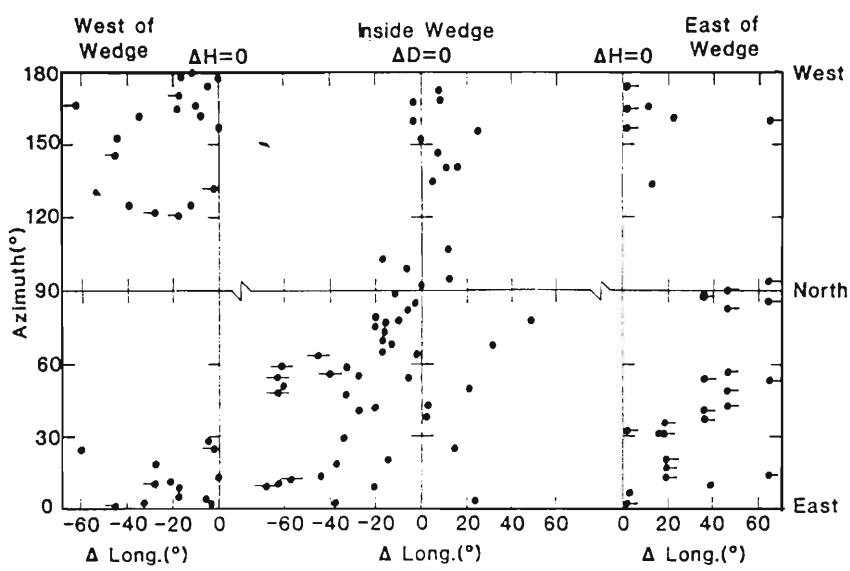

Figure 2.8: Major axis azimuth of the horizontal polarization ellipse vs longitude for a set of mid-latitude Pi 2 events (detected at the AFGL East-West network). Azimuth is measured counterclockwise from 0^0 east. Left, central and right panels correspond to points west, inside and east of the wedge respectively. ΔH and ΔD represent the H- and D-component bay signatures respectively. The centre and edges of the wedge are defined where $\Delta D = 0$ and $\Delta H = 0$ respectively (after *Lester et al.,* [1984]).

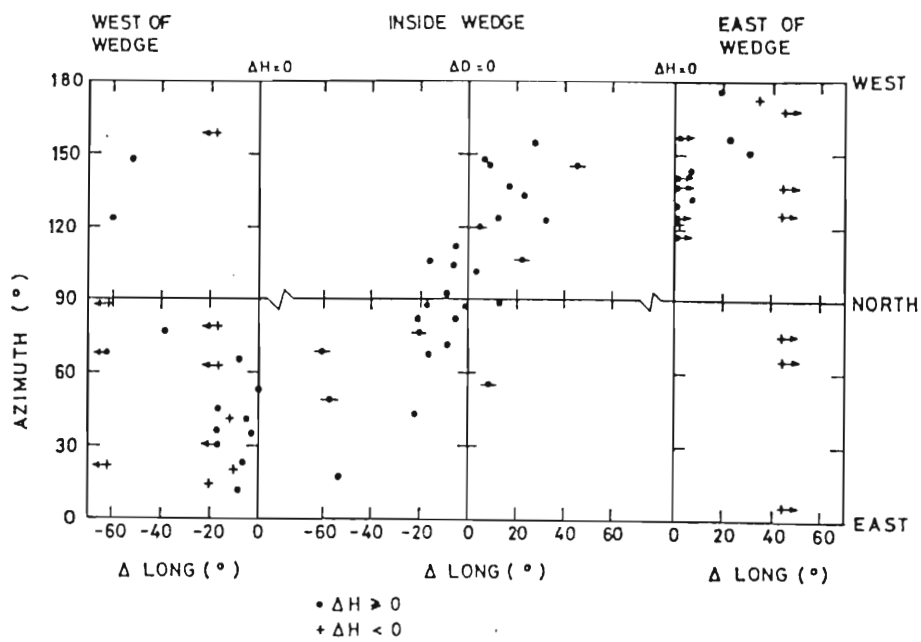

Figure 2.9: Low-latitude Pi 2 horizontal polarization azimuth plotted in current wedge coordinates (*Lester et al.*, [1989]), as for Fig. 2.8.

2.8.2 Polarization Ellipticity Sense

At high (auroral) latitudes[2], the Pi 2 polarization sense is occasionally found to be left-handed (ACW) (e.g. *Gelpi et al.*, [1985b]). Most are, however, right-handed (CW) reversing to a left-handed (ACW) sense at lower latitudes. The position of the polarization reversal (from high to low latitudes) is often close to the plasmapause position (*Fukunishi,* [1975]; *Lester and Orr,* [1981,1983]). *Yeoman et al.* [1990] recorded events, using the U.K. Sub-Auroral Magnetometer Network (SAMNET), that had a right-handed (CW) polarization poleward of a predicted plasmapause position (i.e. in the auroral region) and left-handed (ACW) equatorward of this position (mid latitudes). *Stuart and Baransky* [1982], using United Kingdom and Scandinavian meridian profiles, were able to infer that the sense of polarization and the spectral structure of Pi 2 changed at the plasmapause, and that a minimum in the H-component amplitude occurred there.

Numerous mid-latitude Pi 2 observations by *Lester et al.* [1983,1984] indicate a predominantly left-handed (ACW) ellipticity. This trend agrees with other mid latitude results (e.g. *Fukunishi*, [1975]; *Mier-Jedrzejowicz and Southwood*, [1979]; *Lester and Orr*, [1981]).

Low latitude ($< 40^0$) work by *Lester* [1989] established that to the east and inside the substorm current wedge the sense of polarization is predominantly left-handed (ACW), as observed at mid latitudes. West of the wedge, the sense of polarization is observed to be largely right-handed (CW), suggesting that there was a polarization reversal west of the wedge between the stations at mid ($\sim 55^0$) and low ($\sim 40^0$) latitudes. This low-latitude Pi 2 polarization behaviour corroborates early work of *Saito* [1969], *Sutcliffe* [1981] and *Yumoto et al.* [1988] who found that before local midnight, the polarization was predominantly right-handed (CW), and after midnight predominantly left-handed (ACW). *Lanzerotti and Medford* [1984] do not observe this pattern, finding instead a left-handed (ACW) ellipticity at magnetometer stations near $L \sim 1.9$.

At geosynchronous orbit, ATS 6 investigations by *Sakurai and McPherron* [1983] indicated a polarization reversal around midnight, with left-handed polarization pre-midnight and right-handed post-midnight, similar to that observed by ground based stations equatorward of the auroral electrojet.

The post-1980 polarization observations described above are depicted pictorially in Fig. 2.10. For each latitudinal category, there are two panels, the upper panel showing the polarization pattern ordered according to the SCW model, and the lower panel those patterns which have been ordered according to Local Time. We point out that

[2]Unless otherwise specified, the results mentioned here apply to the northern hemisphere because the majority of observational studies are carried out there.

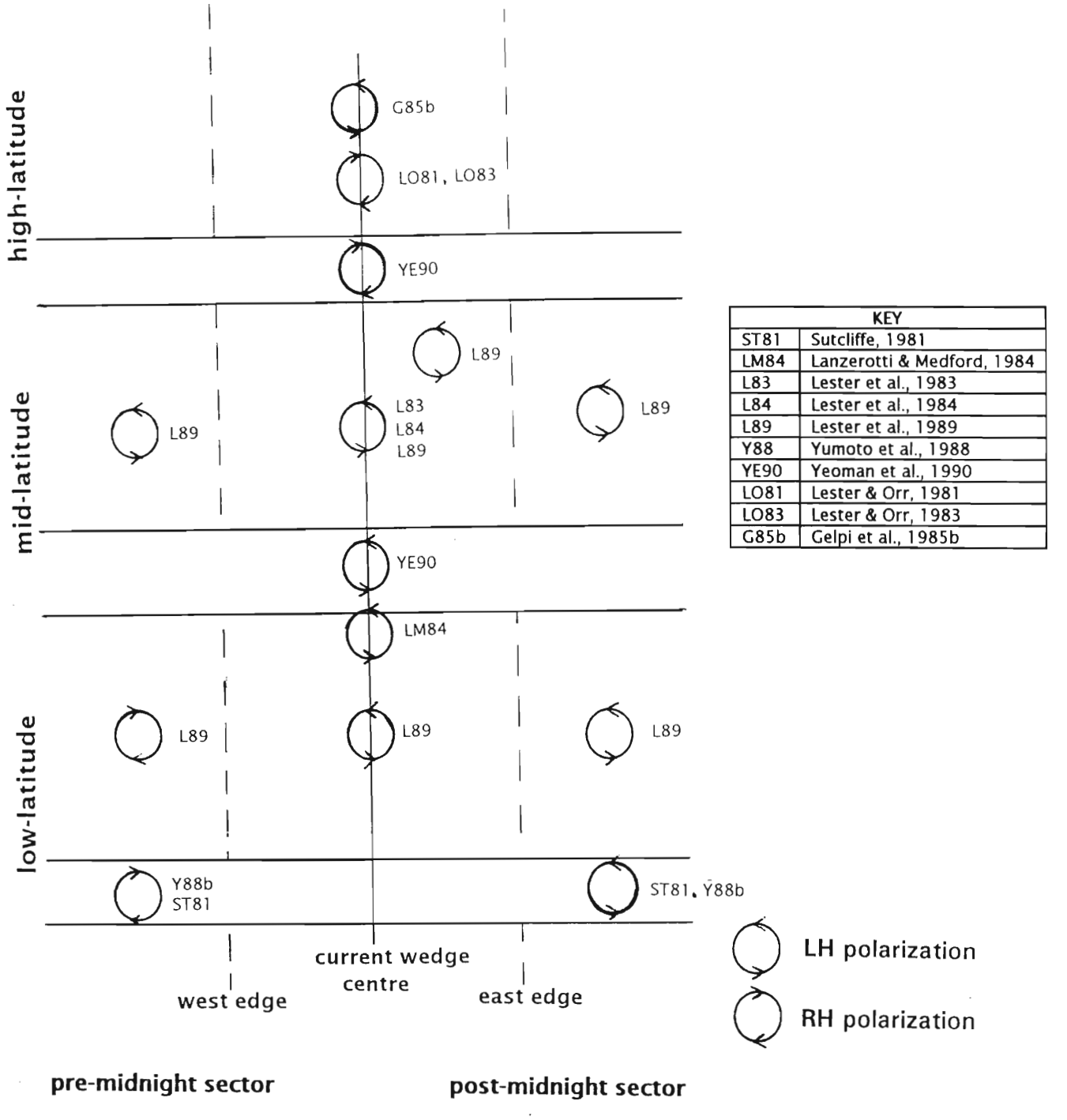

Figure 2.10: Latitudinal-Local Time dependence of the horizontal polarization sense in the northern hemisphere. Events located with respect to a SCW system are placed in panels indicating the wedge limits (dashed lines).

although Local Midnight does not necessarily coincide with the centre of the SCW coordinate system, the difference between the two is small. The pattern of Fig. 2.10 compares favourably with the pre-1980 polarization pattern compiled by *Sutcliffe* [1979] in Fig. 2.11.

2.9 Bay Signatures

Yumoto [1987] showed that at mid and low latitudes, Pi 2, as well as bay variations, appear almost simultaneously within ± 1 minute. An equatorial enhancement of the day-time bay variations was also noted. H-component bays observed between 09:00 and 19:30 LT were enhanced and positive at mid and low latitude stations, as shown in Fig. 2.12a, indicating the possible existence of a dayside storm-associated field aligned current. The D-component bay variations changed from positive to negative (from west to east) across the array of stations. This characteristic of bay variation indicates the possibility that a day-time substorm associated current wedge, similar to the nightside wedge, is set up during the substorm onset and contributes to magnetic variations at mid and low latitudes in the day-time sector. Along the central meridian at low latitude, the magnitudes of the H-component bays tend to decrease with decreasing magnetic latitude (see Fig. 2.12b), with a notable equatorial enhancement. This suggests that the day-time bay enhancements near the equator are predominantly due to an equatorial ionospheric current induced by a substorm-associated electric field transmitted almost instantaneously from high latitudes in the wave-guide bounded by the ionosphere and the earth's surface. (The geographic and geomagnetic coordinates used in the above study are listed in Table 2.2.)

Investigations by *Lester et al.* [1983,1984,1989] have shown that the mid-latitude Pi 2 polarization azimuth as a function of longitude (Local Time) has a pattern similar to, and often coincides with, the location of the substorm current wedge (see section 3.2.2). Fig. 2.13 shows the H- and D-component bay signatures of the current wedge, as well as the predicted mid latitude polarization pattern for Pi 2. The predicted polarization pattern compares well with observation (see section 2.8.1). Also in the figure, the longitudes at which $\Delta H = 0$, and ΔD are extrema, coincide with the location of the FAC. Note that they refer to the region inside the wedge as the region in which $\Delta H > 0$. This positioning is not strictly correct, as *Gelphi et al.* [1987] point out, because the head of the westward travelling surge occurs east of the longitude where $\Delta H = 0$.

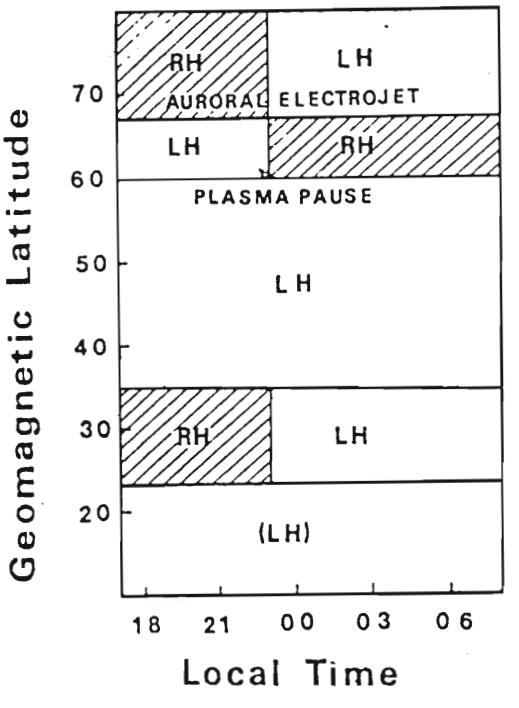

Figure 2.11: Latitudinal-Local Time dependence of Pi 2 polarization sense (northern hemisphere) (*Sutcliffe* [1979]).

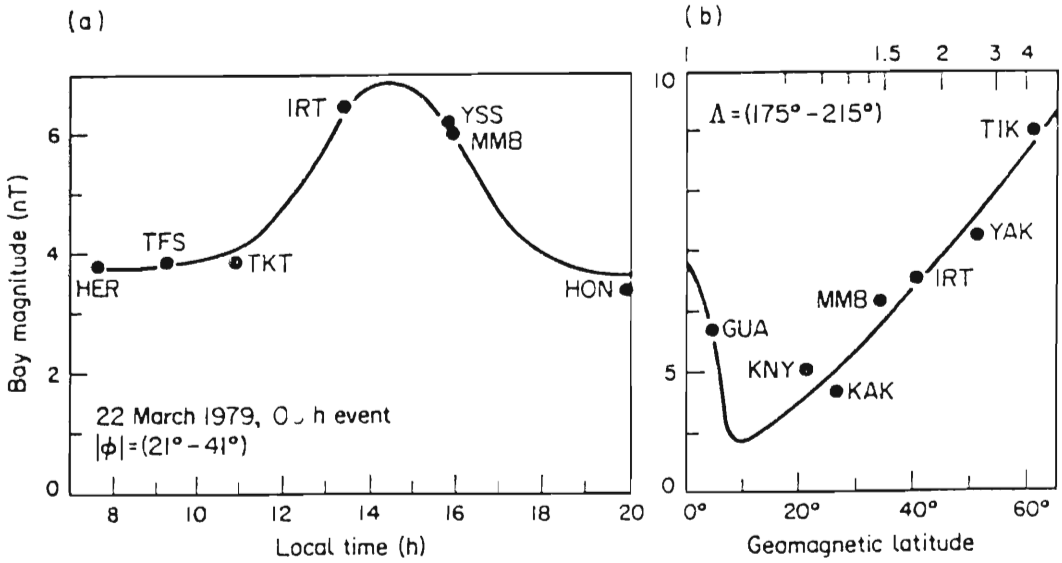

Figure 2.12: H-component bay magnitudes as functions of (a) Local time and (b) latitude (in the data period 14:00-16:00 LT and between magnetic latitudes $21^0 - 41^0$)(*Yumoto et al.*, [1987]).

Station		Geographic		Geogmagnetic		*DL*
		Lat.	Long.	Lat.	Long.	
Hermanus	HER	-34.42	19.23	-33.57	82.44	1.44
Tbilisi	TFS	42.08	44.70	36.55	123.47	1.55
Tashkent	TKT	41.33	69.62	32.38	145.45	1.40
Irkutsk	IRT	52.17	104.45	41.00	176.10	1.76
Tixie Bay	TIK	71.58	129.00	60.80	192.65	4.20
Yakutsk	YAK	62.02	129.72	51.35	195.23	2.56
Kanoya	KNY	31.42	130.88	20.94	199.69	1.15
Kakioka	KAK	36.23	140.18	26.45	207.59	1.25
Onagawa	ONW	38.43	141.47	28.75	208.45	1.30
Memambetsu	MMB	43.90	144.20	34.44	210.04	1.47
Yuzhno Sakhalinsk	YSS	46.95	142.72	37.32	208.26	1.58
Guam	GUA	13.58	144.87	4.41	214.60	1.01
Cape Wellem	CWE	66.17	190.17	62.25	238.95	4.61
Honolulu	HON	21.32	202.00	21.43	268.36	1.15

Table 2.2: Names and Coordinates of the Magnetometer Stations Shown in Fig 2.12.

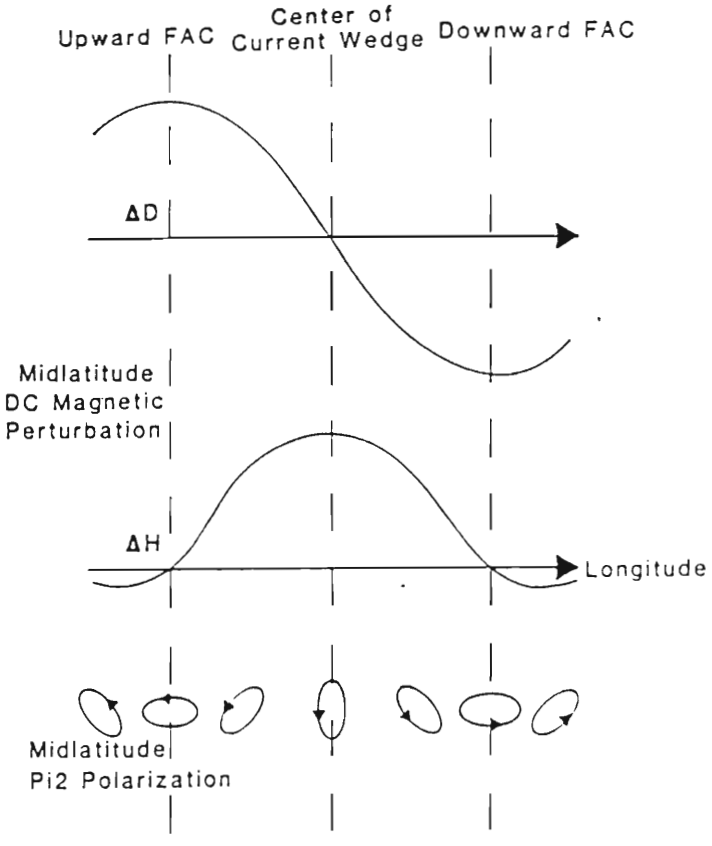

Figure 2.13: A schematic representation of the longitudinal H- and D-magnetic bay components, resulting from the substorm current wedge. The bottom panel shows the predicted Pi 2 azimuth pattern associated with the current wedge model (*Lester et al.*, [1984]).

Chapter 3

Contemporary Pi 2 Modelling

This chapter comprises two principal sections. In the first part, proposals for the excitation and propagation of Pi 2 are considered. Particular attention is given to impulsive type source mechanisms. This is followed by a Pi 2 propagation scenario in terms of a MHD cavity wave mechanism, which will form the basis of the modelling strategy adopted later in this thesis. In the second part of the chapter, selected contemporary global-cavity mode pulsation models are briefly reviewed.

3.1 Introduction

Considerable attention has been given to the interpretation and modelling of Pi 2 observations. Most of these studies have focused on the explanation of high-latitude (e.g. *Samson*, [1982]; *Kan et al.*, [1982]; *Lester et al.*, [1983]; *Baumjohann and Glassmeier*, [1984]; *Rothwell et al.*, [1986,1988]) and mid-latitude (e.g. *Lester et al.*, [1984]; *Samson et al.*, [1985]; *Southwood and Hughes*, [1985]) polarization features. Some of this modelling has been highly successful. The modelling of *Samson* [1982], for example, is able to predict the high latitude Pi 2 polarization pattern. The problem with high- and mid-latitude models is that their results do not extend to lower latitudes. This is largely because the nature of high- and mid-latitude Pi 2 is distinctly different to their low-latitude counterparts. A major difficulty in modelling has been the explanation of the observed latitudinal variation of the Pi 2 azimuthal wavenumber (see section 2.5.3). Another has been the 180^0 phase change which occurs between mid- and low-latitudes (see section 2.5.5). How Pi 2 waves propagate from the high latitude midnight sector to low latitudes remains unclear (*Yumoto*, 1986]; *Verö*, [1986]; *Kitamura et al.* [1988]). To add to this, there is mounting observational evidence that low-latitude Pi 2 exhibit a global propagation nature. A model is therefore required which would ideally satisfy

both high and low-latitude morphology (*Stuart and Barsczus*, [1980]).

3.2 Proposed Pi 2 Propagation Mechanisms

3.2.1 Source Mechanisms

The Pi 2 driving mechanism is very much an open question (*Yumoto*, [1988]). Proposed Pi 2 mechanisms may be categorized in two principal groups according to the different approaches used for the interpretation of data. One approach is to consider Pi 2 as transient ULF wave-resonances, where the ionosphere is essentially treated as an inactive reflecting boundary. In this approach it is assumed that the damped oscillations are the result of a sudden change (dipolarization) in the physical state of the magnetotail-ionosphere system (*Nishida*, [1978]; *Sato*, [1982]; *Lysak an Dum*, [1983]; *Kan and Sun*, [1985]; *Rothwell et al.*, [1986]). These sudden changes may be represented as a step function in the current and voltage sources launched at, and reflected by, the ionospheres (*Hopcraft and Smith*, [1986]; *Southwood and Hughes*, [1985]; *Yumoto et al.*, [1989]). The other approach is to consider Pi 2 in terms of current fluctuations where the ionosphere is treated as an active part of the ionosphere-magnetosphere coupling system (e.g. *Tamao and Miura*, [1982]) via, say, the Sato feedback instability (*Sato*, [1982]). Pi 2 have also been interpreted as the oscillating components of the localized field-aligned currents in the substorm current wedge (*Pashin et al.*, [1982]; *Samson and Rostoker*, [1983]; *Sakurai and McPherron*, [1983]; *Glassmeier et al.*, [1988]). Whatever the approach, it appears that the rapid change in the magnetospheric convection and change associated with the substorm onset, as a result of short-circuiting of the cross tail current to the auroral oval via field aligned currents, plays an integral role in the excitation and propagation of Pi 2.

Early research indicated the midnight sector as the probable of origin of Pi 2 (e.g. *Raspopov*, [1968]; *Stuart*, [1972]; *Olson and Rostoker*, [1977]; *Kuwashima*, [1978]). The general consensus is that primary Pi 2 are generated on the last closed field line of the night-time magnetosphere (*Stuart and Barsczus*, [1980]), supporting the idea that the generating mechanism is related to an instability associated with field lines and plasma in the magnetotail region.

3.2.2 Magnetosphere-Ionosphere Current Coupling Models

During substorm onset, magnetic energy stored in the magnetotail is suddenly released by the short circuiting of the cross-tail current (see reviews by *Akasofu*, [1977]; *Nishida*,

[1978]; *Atkinson*, [1979]; *McPherron*, [1979]) and diversion along magnetic field lines (as FAC) to the auroral ionospheres. The fact that Pi 2 occur in association with the brightening of the auroral arc during the substorm expansive phase suggests that the morphology of high- and mid-latitude Pi 2 magnetic fields may be largely influenced by FAC and the ionospheric currents near arc brightening. *Samson* [1985], for example, used Pi 2 intensity and polarization studies to deduce that a significant portion of the Pi 2 magnetic field comes from field-aligned and ionospheric currents.

Substorm Current Wedge

The relationship between Pi 2 polarization and the current system causing the substorm magnetometer bays was first investigated by *Rostoker* [1967]. Studies of high-latitude Pi 2 pulsation equivalent currents in the ionosphere have shown them to have a vortex structure coincident with the ionospheric intersection of the substorm current wedge field aligned currents (*Pashin et al.*, [1982]; *Lester et al.*, [1985]). For this reason many authors conveniently position Pi 2 features in terms of the substorm current wedge model. For example, the mid-latitude Pi 2 longitudinal polarization ellipse behaviour has been ordered in terms of the substorm current wedge model (e.g. *Lester et al.*, [1983,1984]; *Gelpi et al.*, [1985b]). The position of the substorm current wedge is determined from the magnetic substorm bays (*Lester et al.*, [1983,1984]; *Samson and Harrold*, [1983]; *Singer et al.*, [1984]; *Samson et al.*, [1985]; *Gelpi et al.*, [1985b,1987]).

The substorm current wedge system described by *McPherron et al.* [1973] and developed further by *Clauer and McPherron* [1974] is illustrated by Fig 3.1. With the collapse of the tail fields, cross-tail current is diverted along the field lines (FAC) into the auroral zone (upper panel). In the ionosphere this current flows as the westward electrojet, returning to the tail region via upward FAC. In the tail, the perturbation may be represented as an equivalent eastward current (consider lower panel, right). The magnetic FAC footprints and equivalent current flow with field variations in the ionosphere is illustrated in Fig 3.2. Also in this figure are the predicted Pi 2 azimuth if Pi 2 were assumed to be the result of the oscillation of the current system.

Lester et al. [1983] used the AFGL mid latitude chain of magnetometers to investigate the relationship between Pi 2 and the substorm current wedge. For 65% of the events studied, the centre of the Pi 2 and substorm current systems were were found to be collocated (in meridian), suggesting that the two systems are not necessarily connected. These results are illustrated in Fig 3.3 where the horizontal polarization azimuth variations, as a function of longitude, are plotted in terms of the SCW coordinate system. The dashed line represents Pi 2 polarization azimuths for the case when the substorm current wedge system and the Pi 2 system were collocated. In general there is good correlation (events denoted by dots) between the SCW and the Pi 2 systems. How-

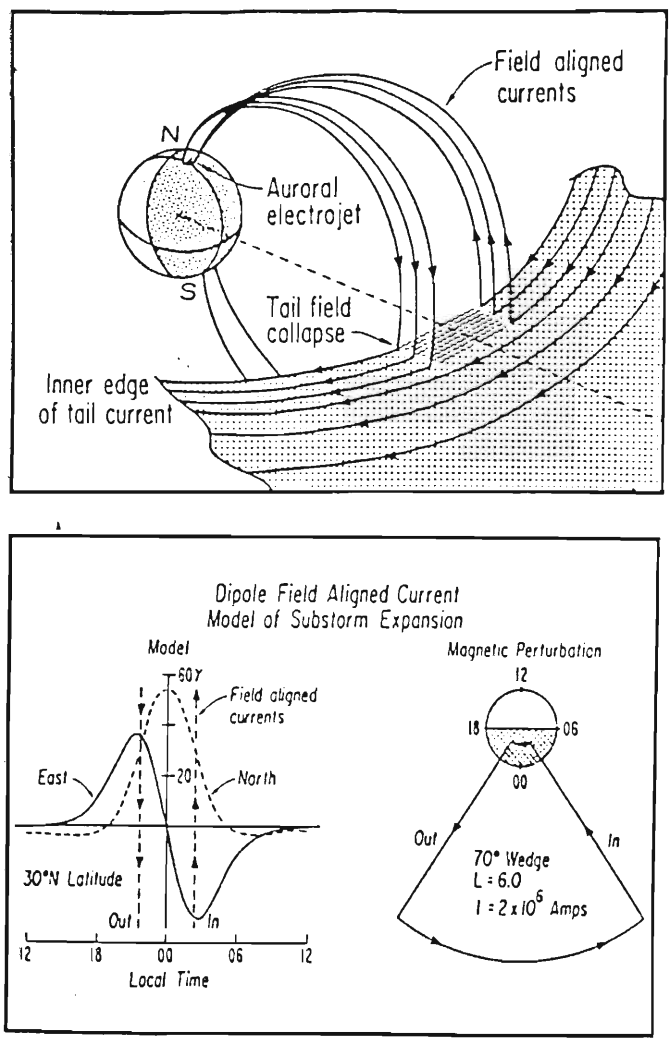

Figure 3.1: Schematic model of the substorm current wedge (upper panel), with the equivalent current system and model parameters (lower panel) as determined by *Clauer and McPherron* [1974]. The bottom panel (left) summarizes the calculated sense and magnitude of the mid-latitude magnetic bay expected after substorm onset. The solid and broken curves represent the East-West and North-South magnetic fields respectively as a result of the FAC.

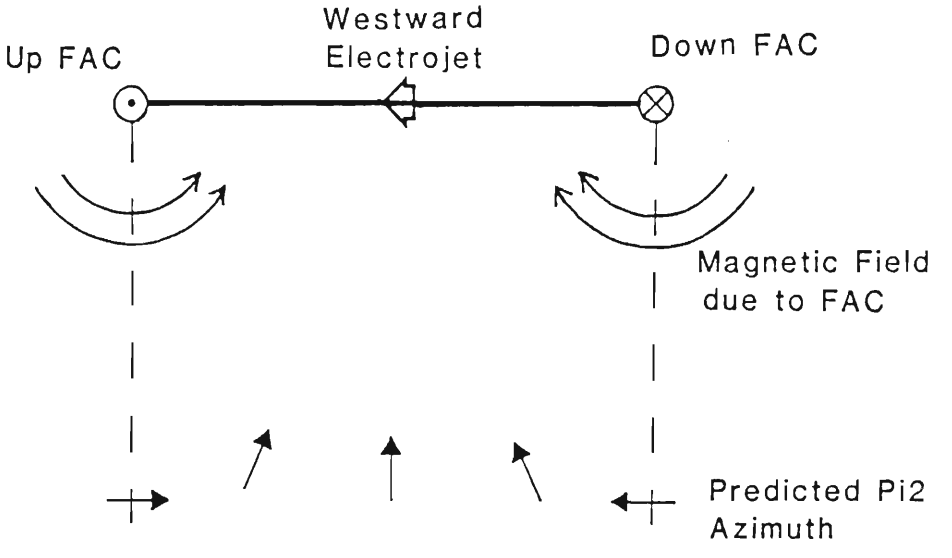

Figure 3.2: Schematic view of the field aligned current footprints in the ionosphere, with the predicted mid-latitude Pi 2 polarization azimuths (*Lester et al.,* [1983]).

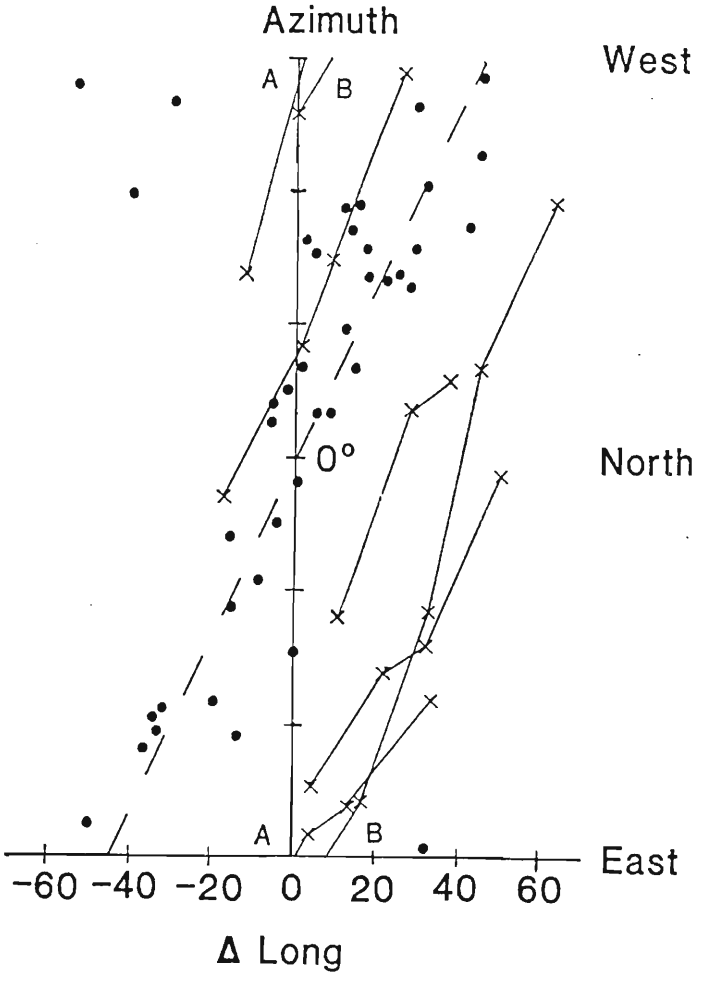

Figure 3.3: Azimuth versus longitude (ΔLong) for Pi 2 events as studied by *Lester et al.* [1983]. ΔLong= 0 corresponds to the centre of the SCW. Tick marks on the azimuth axis are every 30^0 ($0^0 \equiv$ north-south azimuth). Dots represent events where the two methods for locating the center of the current system agree and crosses where they disagree.

ever, there are a number of events which are displaced from the current wedge centre (events denoted by crosses) indicating a relative Local Time displacement of the centre of the Pi 2 system, either to the east or west of the substorm current wedge. *Lester et al.* [1983;1984] explain that the relative displacement of the Pi 2 and SCW systems is caused by the background ionospheric current. For instances when there is no background current, the two systems coincide.

3.2.3 Hydromagnetic Transient-Response Wave Models

High latitude, night-time Pi 2 have been interpreted as transient hydromagnetic waves occurring in association with the sudden change in the physical state of the magnetosphere (dipolarization) at substorm expansion onset (*Baumjohann and Glassmeier*, [1984]; *Southwood and Hughes*, [1985]; *Yumoto,* [1988]). *Baumjohann and Glassmeier* [1984] explain that dipolarization may be linked to the substorm current wedge system. This idea is illustrated in Fig 3.4 where it can be seen that upward and downward FAC cause respective eastward and westward deflections of the magnetic field in the equatorial plane (upper panel). A compressional or field aligned magnetic component is also generated by an equivalent dusk to dawn (eastward) current as a result of the sudden disappearance of part of the dawn to dusk directed cross-tail current. These signatures are observed as dipolarization (lower panel).

The global nature of Pi 2 at low latitudes has prompted the idea that Pi 2 are forced field line oscillations on a global scale coupled with resonance waves in the inner magnetosphere (*Yumoto et al.*, [1990]). *Saito and Matsushita* [1968] were first to suggest that the substorm activity in the magnetotail could result in a compression of the closed field lines of the inner magnetosphere causing them to ring as compressional mode cavity resonances and hence producing the mid- to low-latitude Pi 2 signatures.

The Transverse Alfvén Resonance Waves

High latitude nightside Pi 2 have been interpreted by some authors as transient standing field line resonances (*Maltsev et al.*, [1974]; *Olson and Rostoker*, [1977]; *Kuwashima*, [1978]; *Stuart et al.,* [1979]), with the inner edge of the plasmasheet suggested as the possible site for Alfvén resonant oscillations (*Fukunishi et al.,* [1975]; *Saito et al.*, [1976a]). Predictions of the frequencies of low-latitude Alfvén resonances do not however match those of Pi 2 observations. The frequency of field line resonance waves is latitude dependent while that of Pi 2 is independent of latitude (see section 2.5.1). *Sutcliffe and Yumoto* [1991] made comparative studies of the frequency spectra of low-latitude Pc 3 and Pi 2 and found that Pc 3 frequencies were higher by a factor of 2

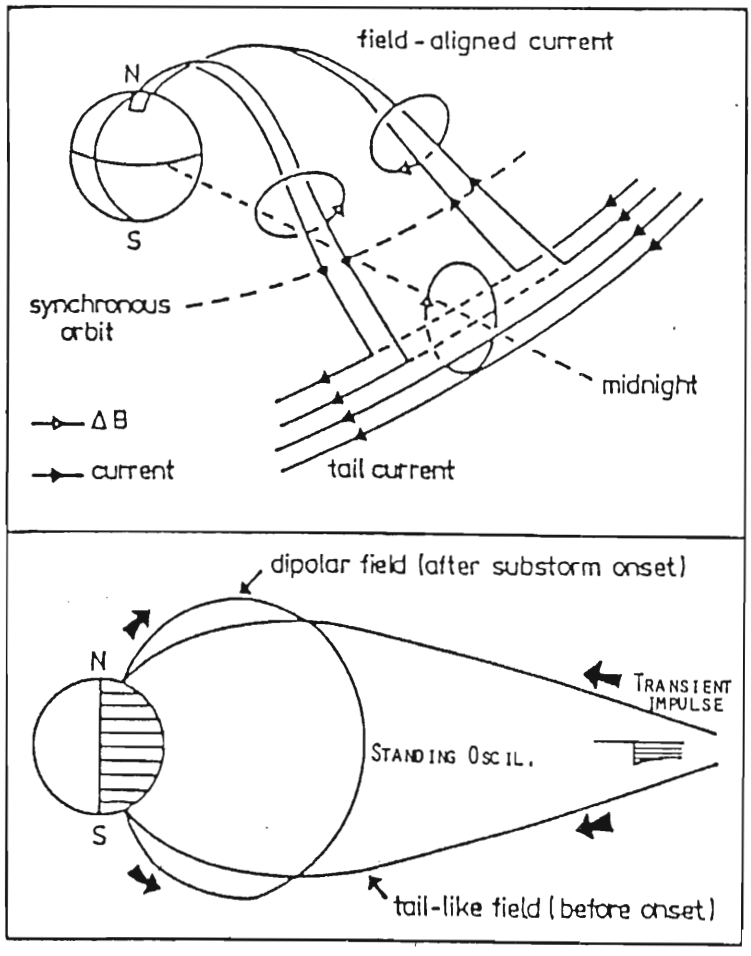

Figure 3.4: Transient change in the current convection caused by the formation of a substorm current wedge (top panel) with equivalent magnetic dipolarization (bottom panel) (after *Baumjohann and Glassmeier*, [1984]).

to 3 times. They pointed out that since Pc 3 are believed to be fundamental field line resonances, Pi 2 having lower frequency, cannot be a field line resonance oscillation. Polarization predictions of the field line resonance theory also conflict with that observed for low-latitude Pi 2 (*Lanzerotti and Medford,* [1984]).

Surface and Plasmapause Waves

There have been suggestions that mid- and low-latitude Pi 2 are field line oscillations originating at the plasmapause (e.g. *Fukunishi and Hirasawa*, [1970]; *Lanzerotti and Fukunishi*, [1974]; *Stuart*, [1974]; *Orr*, [1975]; *Saito et al.*, [1976a]). The idea is that hydromagnetic signals are transmitted through the magnetosphere from high latitudes to the plasmapause where field line coupling would occur as a result of the sharp radial gradient of the plasma generating a surface wave. The nature of the waves at low latitudes would largely be attributed to the surface wave excited at the plasmapause.

The surface wave mechanism has merit in that it predicts the subauroral Pi 2 secondary amplitude peak (*Baumjohann and Glassmeier*, [1984], see also section 2.6 regarding the Pi 2 secondary amplitude maximum). Furthermore, a surface wave mechanism would give rise to a transient wave with frequency which is independent of latitude and longitude. Although Pi 2 spectral peaks observed at longitudinally separated stations coincide (section 2.5.1), changes in the relative amplitude of the spectral peaks conflicts with that expected from a plasmapause surface wave (*Yeoman and Orr*, [1989]).

Superposition of Waves

Southwood and Hughes [1985] have shown that the mid-latitude Pi 2 polarization pattern can be reproduced by superposing two oscillating field aligned current systems associated with shear Alfvén waves, one propagating westward and another, relatively smaller, propagating eastward. Fig 3.5 illustrates this idea. The figure sketches hodograms for waves as would be seen at seven observatories along an east-west line. The top row of hodograms illustrate a westward travelling anti-clockwise rotating polarized wave and the second row an eastward travelling clockwise polarized wave with amplitude half that of the westward travelling wave. The bottom row is the superposition of the waves in the top two rows. The result is an anti-clockwise, elliptically polarized wave with a net westward motion. The resultant ellipse pattern is similar to Pi 2 polarization patterns observed at mid latitudes (see Fig 2.13).

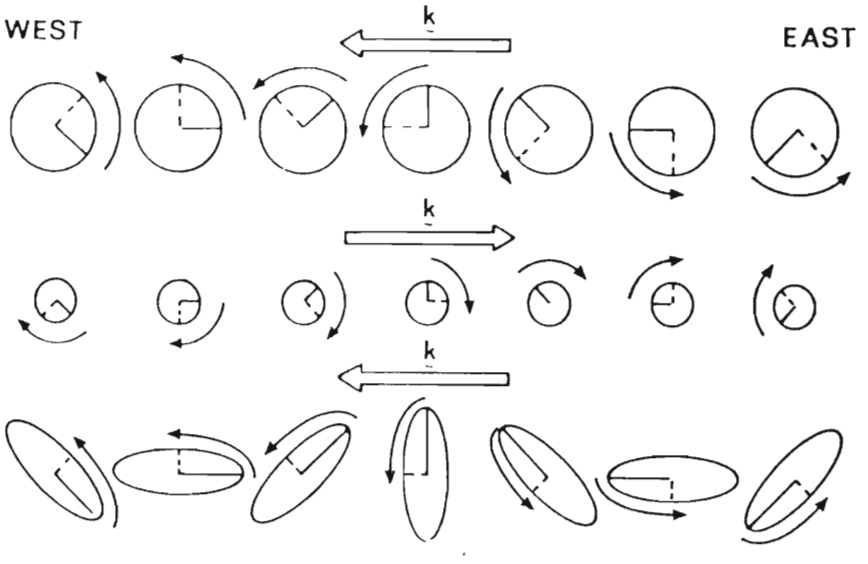

Figure 3.5: Hodograms illustrating how two waves may be superposed to reproduce the Pi 2 polarization pattern (after *Southwood and Hughes*, [1985]).

The Ionospheric Wave-Guide

A contemporary problem regarding the propagation of Pi 2 is that of finding a suitable explanation for the small arrival time differences between signals observed at high and low latitudes (see section 2.5.3). The problem with a MHD mechanism is that it would take a high latitude night-time wave $\approx$ 100 s to travel through the magnetosphere to the day sector (*Stuart and Barsczus,* [1980]). One of the earliest proposals for Pi 2 propagation mechanism was that waves generated in the night sector could propagate from auroral zones to mid-latitudes via the ionosphere (*Rostoker,* [1965]; *Jamet et al.,* [1969]). Such a wave travelling at the top of the ionosphere at a speed of say 3000 kms^{-1} would take $10 - 30$ s to travel from the night to the dayside (*Stuart and Barsczus,* [1980]).

Pi 2 Global or Cavity Mode Waves

In recent years, much evidence has emerged suggesting that low-latitude Pi 2 are in some way associated with a global or cavity mechanism (*Kitamura et al.*, [1988]; *Sutcliffe and Yumoto*, [1989]; *Yeoman and Orr*, [1989]; *Yumoto et al.*, [1989]; *Takahashi et al.,* [1992], see also section 2.5). The idea that a low-latitude Pi 2 is the signature of a magnetospheric cavity mode is not a new one (e.g. *Saito and Matsushita*, [1968]; *Mainstone*, [1970]; *Doobov and Mainstone*, [1973]; *Stuart*, [1974]; *Lester and Orr*, [1981]). *Sutcliffe and Yumoto* [1991] presented compelling evidence that besides low-latitude Pi 2, mid-latitude Pi 2 are also a common dayside phenomenon and are related to a cavity or global type mechanism. They suggested an impulsive MHD signal to originate at high latitudes, (in the midnight sector), spreading in Local Time at lower latitudes to set up global cavity resonance oscillations (see also *Kivelson and Southwood*, [1985]) confined to the plasmasphere (as modelled by *Allan et al.,* [1986a,1986b]).

Yumoto et al. [1989] were able to link cavity-resonance modelling (*Allan et al.*, [1986a,-1986b]) to some of their observations. Their interpretation was that an impulsively stimulated plasmasphere cavity wave would drive local field line resonance at the L-shell where the frequency of two modes match. The magnetic D-component of the Pi 2 pulsation would be largely due to the localized toroidal mode oscillation excited by a second harmonic cavity mode (similar to that predicted by *Allan et al.* [1986b]). *Kitamura et al.* [1988] also postulate that a compressional type wave propagating from the outer magnetosphere would couple to a local transverse Alfvén resonance wave. The compressional wave would be attenuated in the process, the degree of which would depend on the axial wavenumber, m. It turns out that the coupling efficiency between the two wave modes is greater for larger m (i.e the greater the inhomogeneity, the better the coupling). In the case of perfect axial symmetry i.e. $m = 0$, the two

modes are decoupled. At low latitudes the wavenumber spectrum of an arbitrary Pi 2 disturbance is expected to have a peak at a finite m, denoted by m_L say on curve (a) in Fig 3.6. Pi 2 observed at relatively higher latitudes would be localized to a greater degree and hence would be associated with larger m, for example, curve labelled (b) in Fig 3.6. The spectrum of the disturbance would include an $m = 0$ component, this component being greater when the source region is larger in spatial scale (longitude). Fig 3.6 illustrates that coupling between the wave modes is more efficient at higher latitudes because the wavenumbers are larger there.

Even at relatively high latitudes, Pi 2 often appear as compressional fast mode hydromagnetic waves (*Lin and Cahill*, [1975]). *Yeoman et al.* [1991] combined data from the SABRE ionospheric radar (Sweden and Britain Radar auroral Experiment) and the SAMNET magnetometer network to enable them to determine the MHD wave mode for observed Pi 2 pulsations. Their results showed that Pi 2 are largely transverse Alfvén in nature at auroral latitudes and largely compressional mode at lower latitudes. The sub-auroral region was found to be a transition region between the two wave types.

It has been argued that the absence of large systematic delays in the arrival time differences of low-latitude Pi 2 and bay variations at globally separated observatories does not favour the hydromagnetic propagation mechanism. This argument relies on the assumption that the excitation mechanism is localized in the near midnight sector. However, it is possible for a transient change to occur simultaneously through-out the magnetosphere. The instantaneous formation of a dayside current wedge during the substorm onset (*Yumoto*, [1987]) could, for example, be associated with such a large scale change.

3.2.4 The Cavity Mode Pi 2 Scenario

Although there have been a number of model plasmaspheric and cavity-resonance investigations (e.g. *Kivelson et al.*, [1984]; *Allan et al.*, [1986a,1986b]; *Krauss-Varban and Patel*, [1988]), none has been specifically applied to the study of Pi 2. In this thesis a propagation scenario similar to that outlined above by *Kitamura et al.* [1988] and *Yumoto et al.* [1989] is proposed. It is assumed that the Pi 2 causative mechanism is associated with the collapse of the tail fields in the near-earth plasma sheet during substorm expansion onset. The precise mechanism of the excitation is not important in our modelling. It is assumed, however, that some mechanism is responsible for launching broad-band hydromagnetic signals which excite the cavity modes. The resulting disturbances in the cavity are assumed to comprise a fast isotropic (or compressional) mode and a transverse Alfvén mode. The fast mode compressional waves propagate

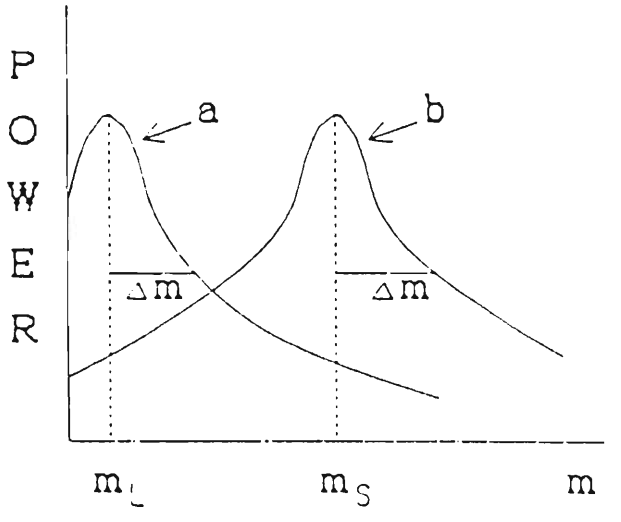

Figure 3.6: Expected power spectra of disturbances at the generation region of Pi 2 in the magnetosphere. Spectrum labelled (a) represents that due to a large scale disturbance having a peak at m_L with a considerable $m = 0$ component. Spectrum (b) is that of a smaller scale disturbance having a peak at $m_S (> m_L)$ with a smaller $m = 0$ power component (*Kitamura et al.*, [1988]).

from the outer magnetosphere across the ambient magnetic fields to the ionosphere (where they are reflected) setting up standing waves which span the magnetosphere cavity (cavity or global modes). The cavity waves couple to the transverse Alfvén mode resulting in resonances at latitudes where the frequencies of the two modes match.

3.3 Global Mode Modelling

Sudden sharp increases in the solar wind dynamic pressure have been known to initiate resonant field oscillations in the outer magnetosphere (e.g., *Baumjohann et al.,* [1984]; *Sibeck et al.*, [1989]) as well as transient high latitude pulsations (e.g. *Friis-Christensen et al.*, [1988] and *Potemra et al.*, [1989]). Recent observations suggest that the magnetosphere has a distinct set of responses to applied solar wind and magnetotail related pressure fluctuations (e.g. *Samson et al.*, [1991]). In particular, there is strong evidence that low-latitude Pi 2 are associated with a global or cavity mode oscillation mechanism (see chapter 2). Hence this chapter is concluded with a brief review of ULF global or cavity mode modelling. Until now, global or cavity mode modelling has yet to be applied specifically for the investigation of Pi 2, this being the subject of the thesis.

3.3.1 Origin of Global Modes

Global or cavity mode waves may be understood in terms of ULF standing waves set up across a cavity in the magnetosphere. The MHD approach has been successful in describing a number of ULF type pulsations. In general, a single plasma species is assumed. The resulting MHD equations are characterized by two magneto-plasma wave modes. If one assumes a model magnetosphere to have a non-isotropic plasma distribution with curved geomagnetic geometries and asymmetric wave disturbances then the two modes couple. *Dungey* [1968] (using a dipole field geometry) pointed out that if one assumed axis-symmetric disturbances, i.e. axial wavenumber $m = 0$, then the two wave modes were separable, one called a toroidal mode and the other a poloidal mode. The toroidal oscillations are characterized by electric field perturbations which are radial with magnetic field and velocity component perturbations being azimuthal. In the idealized case, the magnetic L-shells decouple and oscillate azimuthally independent of each other with frequency L-dependent. The axisymmetric poloidal mode has an azimuthal electric field perturbation with radial motions of the plasma and magnetic field components. In this case, the entire magnetosphere undergoes a radial expansion and compression with frequency that is L-independent.

Toroidal oscillations are important in describing transverse ULF pulsations propagating along the field lines. The poloidal modes are strongly related to the compressional waves since the field lines oscillate in the radial directions and hence the magnetic shells can directly interact with each other (*Dungey*, [1968]). In practice, the two modes are coupled and no pure mode exists.

Analytic investigations of the theory described above has proved to be difficult because of the mathematical complexity characterizing the MHD wave equations, particularly when a dipole magnetic field geometry is chosen. Under certain simplifying assumptions, such as azimuthal symmetry, an analytic treatment is possible (see early work of *Dungey*, [1954]).

Often, a simple geometry is chosen to represent the magnetospheric cavity. The simplest geometry is the 'box' model or straight field line model. Once the appropriateness of the modelling has been established, a more realistic field model may be chosen which, for example, would include the effect of field curvature. Even for relatively simple geometries, the complexity of the governing MHD equations necessitates the use of numerical methods in order to obtain solutions. Advances in the numerical throughput of computers (e.g. *Krauss-Varban and Patel* [1988] used a Cray X-MP), as well as improvements in numerical algorithms, make it possible for this problem to be solved in reasonable time (minutes and hours rather than weeks and months). The finite differences and finite element numerical integration methods have been popularly used for the integration of the MHD waves in model magnetospheric cavities (e.g. *Allan et al.*, [1985b]; *Krauss-Varban and Patel*, [1988]; *Lee and Lysak*, [1989]).

In the simplest approach to the modelling of cavity-resonance waves in the magnetosphere, all field nonuniformity is ignored (box model field geometry). The ionosphere is treated as a perfectly conducting boundary and the magnetosphere as a bounded plasma permeated by straight magnetic field lines. The boundaries of the system are the equatorial ionosphere, magnetopause and the north and south auroral ionospheres. Despite these simplifications, *Southwood and Kivelson* [1990] have shown that the characteristic responses to an external pressure perturbation are present. Furthermore, using the box model approach they were able to qualitatively deduce how a more complex system would behave. *Krauss-Varban and Patel* [1988] also carried out similar numerical investigations of the coupled hydromagnetic wave equations using a box magnetosphere model geometry. Despite the limitations of the straight field line geometry, they were able to make some useful deductions. For example, they found that in the uncoupled case the toroidal equations give rise to singular solutions and a continuous spectrum, while the poloidal component possesses regular solutions with a discrete spectrum. Coupling of the two modes can lead to discrete solutions containing a singularity where the poloidal mode frequency matches that of the standing field line resonance.

Boundaries of the System

The magnetopause is often assumed to be a quasi free boundary subjected to externally imposed pressure perturbations. Adjacent to the outer magnetopause boundary exists a compressible plasma that can sustain waves and thus the boundary does not necessarily act as a total reflector. The ionosphere, plasmapause and magnetopause are the usual boundary choices on the grounds that the plasma density gradient is relatively steep there (*Southwood and Kivelson*, [1990]). Most workers assume a perfectly conducting ionosphere. On the other hand, finite ionospheric conductivity may cause significant dissipation of the waves (*Newton et al.*, [1978]; *Glassmeier et al.*, [1984]) or even an ionospheric coupling effect via the Hall conductance (e.g. *Allan and Knox*, [1979]). Within the magnetosphere itself, there are many different regions which may be considered as cavities (see *Doobov*, [1973]). *Krauss-Varban and Patel* [1988], for example, consider the plasmapause as a boundary and consider the cavity therein. They assume reflection from the ionosphere and plasmapause boundaries, and imposed a periodic boundary condition in the azimuthal direction. Recently, *Walker and Samson* [1992] demonstrated the existence of cavity boundaries defined by the partial reflection of earthward travelling fast Alfvén waves.

3.3.2 Nature of Excitation

Steady state (e.g. Kelvin-Helmholtz (K-H) instability, see *Chen and Hasegawa*, [1974]; *Southwood*, [1974]), and impulsive type perturbations have been considered as external ULF excitation mechanisms. The nature of the response triggered within the magnetosphere is expected to depend on the excitation signal. Impulsive sources are likely to excite a broad band of field line resonances with frequencies which are latitude dependent (*Poulter and Nielsen*, [1982]; *Hasegawa et al.*, [1983]; *Allan et al.*, [1985a]). A continuous, narrow band signal source is unlikely to excite global modes since it does not have the necessary bandwidth. For the investigation of cavity or global modes, a compressional excitation pulse is assumed. These boundary perturbations generate compressional waves which propagate across the ambient field lines causing the whole magnetosphere to ring as a global compressional response (*Kivelson and Southwood*, [1985,1986]; *Sibeck et al.*, [1989]; *Southwood and Kivelson*, [1990]). The development of global modes by an impulsive stimulus at the boundary has been illustrated by numerical cavity-resonance investigations using box, cylindrical and dipolar cavity models (*Allan et al.*, [1985b,1986a,1986b]; *Inhester*, [1987]; *Krauss-Varban and Patel*, [1988]; *Lee and Lysak*, [1989, 1990]).

The nature of the temporal and spatial part of the pressure change at the boundary is an important consideration. The time scale of change in pressure must be shorter

than the time taken for an MHD wave to travel through the magnetosphere($\sim$ 10min) in order for a compressional wave to propagate through the system (*Southwood and Kivelson*, [1990]). The spatial scale length of the pulse perpendicular to the magnetic field is also of significance in determining the type of response within the modelled cavity (*Southwood and Kivelson* [1990]).

The study of global modes has resulted in some important findings. *Southwood and Kivelson* [1990] showed that time dependent pressure perturbations at the magnetospheric boundary can excite internal fast and transverse mode eigen-oscillations with temporal response reflecting the temporal nature of the source. They also found that the response of the system at a given point within the cavity depended critically on whether the local Alfvén resonance frequency was near the central frequency of the source perturbation. In a nonuniform plasma, a broad band source time signal would potentially lead to the excitation of globally damped quasi-eigen-oscillations which would preferentially feed energy into a discrete set of localized field aligned resonance regions in the long time limit. After a few reflections, phase differences between modes ensure that the individual normal modes in the response become more apparent. It was noted that the transverse Alfvén waves had a character similar to a surface wave, i.e. amplitude decaying from the boundary. Energy was found to be transferred irreversibly from the fast mode to the transverse Alfvén mode. Hence, the fast mode was damped even if there was no dissipative mechanism. They concluded that the fast modes were not true eigen-oscillations but damped oscillatory transients appearing as a consequence of a damped impulse on the system.

Krauss-Varban and Patel [1988] studied global modes that had periods of oscillation within the Pc 3 range. They found that the discrete modes situated inside the Alfvén continuum are the best candidates for explaining observed hydromagnetic resonances.

In the numerical global mode modelling carried out by *Lee and Lysak* [1989], global modes corresponding to eigenperiods of $T \sim 37, 27, 17$ and 11s were found. They observed that a transient impulse leads to a quasi-stationary state after about 3-4 min. The energy transfer between the compressional mode and the toroidal mode was only active during the transient interval.

3.3.3 Conclusion

In chapter 2 it was noted that some mid- and low-latitude Pi 2 features allude to a global or cavity mode propagation mechanism. Even high-latitude Pi 2 appear to have a dual nature with part of the signal having qualities of the compressional Alfvén wave mode. In this chapter, the modelling of global or cavity type MHD waves in the earth's magnetosphere was considered. A possible scenario for the propagation of

Pi 2 in terms of cavity oscillations was presented. In the following chapters, a cavity-resonance model is adapted for the investigation of Pi 2. The appropriateness of the model will be established by comparing the computed results with Pi 2 observational features.

Chapter 4

The Cavity-Resonance Model

In this chapter, a magnetohydrodynamic cavity-resonance model is developed to study the response triggered in a magnetospheric-like cavity by an externally imposed perturbation. The formalism is based on the original work of *Radoski* [1974], and later developments of *Allan et al.* [1985b,1986a,1986b]. The cavity-resonance modelling developed by *Allan et al.*, [1985b] is extended so that the temporal and spatial response, to an impulse that has arbitrary temporal and spatial form, can be investigated.

4.1 MHD Theory Development

4.1.1 The Magnetohydrodynamic Wave Equation

In this section, the wave equation is derived from a set of fundamental hydromagnetic equations in a collisionless, perfectly conducting cold magnetized plasma of a single species. Let the magnetic, electric, current density and velocity fields be represented by $\mathbf{B} = \mathbf{B}_0 + \mathbf{b}$, $\mathbf{E} = \mathbf{E}_0 + \mathbf{E}$, $\mathbf{J} = \mathbf{J}_0 + \mathbf{J}$ and $\mathbf{V} = \mathbf{V}_0 + \mathbf{V}$, where each quantity is the sum of a zero order plus a first order perturbed component. It is assumed that there are no field aligned currents and that the background unperturbed plasma is at rest. Thus zero order terms involving the field aligned current $\mathbf{J}_0$, the background electric field $\mathbf{E}_0$, and the plasma drift velocity $\mathbf{V}_0$, are zero. Substituting the above field parameters into the low frequency form of Maxwell's equations and linearising, leads to the first order equations

$$\nabla \times \mathbf{b} = \mu_o \mathbf{J} \tag{4.1}$$

$$\nabla \times \mathbf{E} = -\frac{\partial \mathbf{b}}{\partial t} \tag{4.2}$$

supplemented by the frozen-in field line condition

$$\mathbf{E} = -\mathbf{V} \times \mathbf{B}_0 \tag{4.3}$$

and the force equation

$$\rho_0 \frac{\partial \mathbf{V}}{\partial t} = \mathbf{J} \times \mathbf{B}_0 \tag{4.4}$$

The electric field form of the wave equations is derived. Consider the curl of Faraday's Law 4.2,

$$\nabla \times (\nabla \times \mathbf{E}) = -\frac{\partial}{\partial t}(\nabla \times \mathbf{b}) = -\mu_o \frac{\partial \mathbf{J}}{\partial t}$$

The current density, $\mathbf{J}$, may be substituted by

$$\mathbf{J} = -\frac{1}{B_0^2}[(\mathbf{J} \times \mathbf{B}_0) \times \mathbf{B}_0] = -\frac{\rho_0}{B_0^2}(\frac{\partial \mathbf{V}}{\partial t} \times \mathbf{B}_0) = \frac{\rho_0}{B_0^2}\frac{\partial \mathbf{E}}{\partial t}$$

Since there is no field aligned electric field component, the resulting vector wave equation is given by

$$\begin{aligned} [\nabla \times (\nabla \times \mathbf{E})]_\perp &= -\frac{1}{A^2}\frac{\partial^2}{\partial t^2}\mathrm{E}_\perp \\ \mathrm{E}_\parallel &= 0 \end{aligned} \tag{4.5}$$

where $A = \frac{B_0}{\sqrt{\mu_0 \rho_0}}$ is the Alfvén velocity.

4.1.2 Geomagnetic Field Model

There are three idealized magnetospheric geometries that are popularly used to model the geomagnetic field in MHD studies. They are the dipole, cylindrical and box (or straight) field line geometries.

The box model is the simplest and is often used for preliminary investigations of new theoretical approaches (e.g. *Zhu and Kivelson*, [1988,1989]; *Southwood and Kivelson*, [1990]). The derived equations in a straight field line geometry are often uncomplicated, lending themselves to analytical solutions. The major disadvantage of the straight field line geometry, as opposed to the curved field line geometry, is that curvature effects are neglected (terms arising from the cylindrical form of the Laplacian).

The dipole geometry is a good first approximation to the near-Earth geomagnetic field. The problem with the dipole field model is that the derived MHD equations are analytically intractable and numerical methods have to be used to obtain solutions. This complexity can be reduced by making certain assumptions, for example, about the azimuthal symmetry. In the two-fluid MHD modelling of Pc 5 compressional pulsations with large azimuthal wavenumber by *Walker* [1987], *Taylor and Walker* [1987] and *Pekrides* [1988] the complexity of the equations was greatly reduced by applying the

condition $m \rightarrow \infty$. Without any prior simplifying assumptions, the problem remains essentially a three dimensional one. The magnitude of iterations required in order to obtain a solution to this problem, in reasonable time, means that powerful computers have to be used (*Lee and Lysak*, [1989] used a CRAY X-MP).

The cylindrical field line geometry given below represents a compromise; the wave equations are less complex than in the dipole case making computations feasible on mini-computer systems (e.g. VAX 3100, HP9000-350 series), while at the same time a limited form of the curvature effect is included.

4.1.3 Cylindrical Coordinates

The magnetosphere is approximated by a half cylinder of finite axial length with the magnetic field lines represented by semi-circles centered at the equator as shown in Fig. 4.1. This model is based on that used by *Radoski* [1974] and later by *Allan et al.* [1985]; the important difference being that in their case, they assumed axial symmetry which implied a magnetospheric model of infinite axial length.

The cylindrical coordinate system is defined by coordinates (r, θ, s) (see Fig. 4.1), where $\hat{\theta}$ is directed along the field lines, $\hat{r}$ points radially outward in the meridian plane and is perpendicular to $\hat{\theta}$, and $\hat{s} = \hat{r} \times \hat{\theta}$ is azimuthally westward, completing the triad. The Earth's ionosphere is represented by a flat plane with the southern and northern ionospheres located at $\theta = 0$ and π respectively with the equator at $\theta = \pi/2$. The magnetic field lines are chosen to be centered at $r = 0$, coinciding with the values $r = constant$, and thus have an r^{-1} dependence. The last r shell ($r = r_0$) defines the magnetopause. In the equatorial plane, the quantity $1 + r/a$ (a is the radius of the earth) may be identified with the McIlwain parameter L of a dipole field. The axial coordinate s, may be identified with longitude, with $s = 0$ chosen to define the midnight meridian plane. Note that the axial coordinate s, is cyclic because there must be continuity of the fields after a displacement s_0, say equivalent to the length of the model magnetospheric cavity. Therefore, along the axial coordinate there is a periodic condition $s_k = ks_0$, where k is an integer.

4.1.4 Development of Wave Equation

We define the first order, perturbed electric field amplitude components as

$$E_r(r, \theta, s, t) = T(r, s, t) f(\theta) \tag{4.6}$$

$$E_s(r, \theta, s, t) = iP(r, s, t) f(\theta) \tag{4.7}$$

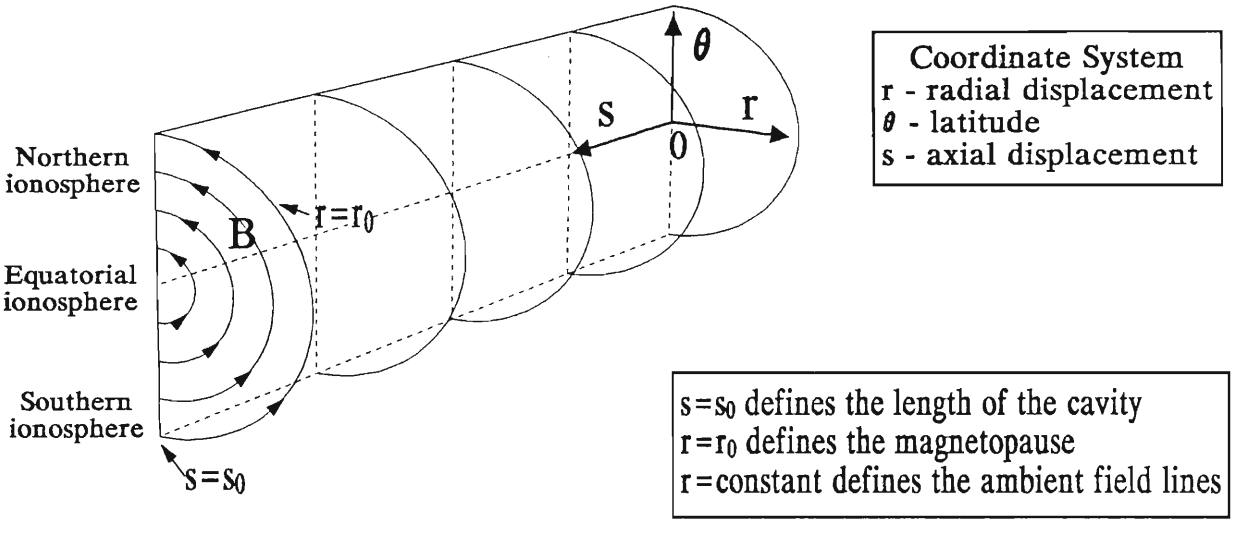

Figure 4.1: The magnetospheric cavity model using a cylindrical coordinate system (r, θ, s).

Amplitudes $T(r,s,t)$ and $P(r,s,t)$ derive their labelling historically because they are associated with motion of the magnetic components in the axial and radial directions respectively. As will be seen later, toroidal motions are represent the transverse or guided Alfvén wave modes while poloidal motion represent the isotropic wave modes.

At this point, the equations are transformed to a normalized coordinate system, conveniently suited to numerical integration. First, we define the scaled Alfvén speed at the magnetopause as $A(r = r_0) = A_0$, and scaled time $t_0 = r_0/A_0$. Next, we define the normalizing transformations

$$x = r/r_o,\ z = s/r_o,\ \tau = t/t_o \tag{4.8}$$

In the axial direction, a displacement equivalent to the length of the cavity is now defined by $z_0 = s_0/r_0$ and by $z_k = s_k/r_0 = ks_0/r_0 = kz_0$ thereafter. The domain of interest is thus $0 \leq x \leq 1$, $0 \leq \theta \leq \pi$ and $\tau > 0$. In normalized coordinates the electric field components are represented by

$$E_r \ \Rightarrow E_x = \ T(x,z,\tau)f(\theta) \tag{4.9}$$

$$E_s \ \Rightarrow E_z = iP(x,z,\tau)f(\theta) \tag{4.10}$$

and therefore wave equation 4.5 may be written as

$$\left[\frac{1}{A_N^2}\frac{\partial^2}{\partial\tau^2} - \frac{1}{x^2}\frac{1}{f(\theta)}\frac{\partial^2}{\partial\theta^2}f(\theta) - \frac{\partial^2}{\partial z^2}\right]T(x,z,\tau) \ = \ -i\frac{\partial}{\partial z}\left[\frac{\partial}{\partial x}P(x,z,\tau)\right] \tag{4.11}$$

$$\left[\frac{1}{A_N^2}\frac{\partial^2}{\partial\tau^2} - \frac{1}{x^2}\frac{1}{f(\theta)}\frac{\partial^2}{\partial\theta^2}f(\theta) - \frac{1}{x}\frac{\partial}{\partial x}(x\frac{\partial}{\partial x})\right]iP(x,z,\tau) \ = \ -\frac{\partial}{\partial z}\left[\frac{1}{x}\frac{\partial}{\partial x}(xT(x,z,\tau))\right] \tag{4.12}$$

where $A_N(x) = A(x)/A_o$ is the normalized Alfvén speed (see Appendix A for detailed derivation). Equations 4.11 and 4.12 are the generalized form of the cavity-resonance wave equations. If a pre-determined function for $f(\theta)$ is chosen, the problem is essentially a three dimensional one (in x, z, and τ). If it is further assumed that the field perturbations in the axial direction go as $\sim e^{imz}$ (e.g. *Allan et al.*, [1985b,1986a,1986b]) then the partial derivatives with respect to z are replaced by factors of im, and the system of equations 4.11 and 4.12 is reduced to a two dimensional problem in x and τ (see section 3.2.3). However, we would like to study the spatial evolution of the waves, in the cavity, triggered by a realistic axial pulse form being a synthesis of wavenumbers, m. The study of the cavity-resonance response to a pulse with axial spatial form represents new work in this field and is the subject of this thesis.

Along the field line, a quasi standing-wave structure is assumed, as adopted by *Allan et al.*, [1985b], of the form

$$f_n(\theta) = \cosh\kappa(\frac{\pi}{2} - \theta)\sin(n\theta) - i\sinh\kappa(\frac{\pi}{2} - \theta)\cos(n\theta) \tag{4.13}$$

where κ is a damping decrement (which accounts for ionospheric Joule heating) and n is an integer representing the harmonic order number. The form of $f_n(\theta)$ is shown in Fig. 4.2 for $n = 1, 2$ and selected values of κ. Substituting equation 4.13 for $f(\theta)$ into equations 4.11 and 4.12 gives

$$\left[\frac{1}{A_N^2}\frac{\partial^2}{\partial\tau^2} + \frac{(n+i\kappa)^2}{x^2} - \frac{\partial^2}{\partial z^2}\right] T(x,z,\tau) = -i\frac{\partial}{\partial z}\left[\frac{\partial}{\partial x}P(x,z,\tau)\right] \quad (4.14)$$

$$\left[\frac{1}{A_N^2}\frac{\partial^2}{\partial\tau^2} + \frac{(n+i\kappa)^2}{x^2} - \frac{1}{x}\frac{\partial}{\partial x}(x\frac{\partial}{\partial x})\right] P(x,z,\tau) = i\frac{\partial}{\partial z}\left[\frac{1}{x}\frac{\partial}{\partial x}(xT(x,z,\tau))\right] \quad (4.15)$$

The above equations describe coupled isotropic and Alfvénic motion. The frequency of the Alfvén mode depends on the ambient magnetic field strength, ($\mathbf{B}_0$), the length of the field line and the plasma density, (ρ_0). In a realistic magnetosphere, $\mathbf{B}_0$ and ρ_0 are functions of the radial distance from the Earth and hence the Alfvén mode is characterized by a continuum of frequencies. The isotropic mode propagates across the field lines, and is reflected by the ionosphere to set up standing waves across the cavity (cavity modes). These cavity eigenmodes couple to the Alfvén waves at the L-shell where the frequency of the cavity mode matches that of the Alfvén mode.

4.1.5 Boundary Conditions

Along the axial coordinate the fields must be continuous after a length $z = z_0$ (equivalent to the longitudinal length of the magnetosphere) i.e. periodic and therefore

$$P(x, z_k, \tau) = P(x, kz_0, \tau) \quad (4.16)$$

$$T(x, z_k, \tau) = T(x, kz_0, \tau) \quad (4.17)$$

where $z_0 = 2\pi$ and k is an integer. The northern and southern ionospheric boundary values are fixed by equation 4.13. At the equatorial ionosphere,

$$P(x = 0, z, \tau) = -i\frac{E_\theta}{f(\theta)} = I(z)G_1(\tau) \quad (4.18)$$

$$T(x = 0, z, \tau) = \frac{E_z}{f(\theta)} = I(z)G_2(\tau) \quad (4.19)$$

where $G_i(\tau)$ is a response function to the impulse applied at the magnetopause boundary. The function $I(z)$ is determined by the ionospheric conductivity along the equator.

At the magnetopause, the imposed signal will be made up of a temporal and axial part,

$$T(x = 1, z, \tau) = H(\tau)M_1(z) \quad (4.20)$$

$$P(x = 1, z, \tau) = H(\tau)M_2(z) \quad (4.21)$$

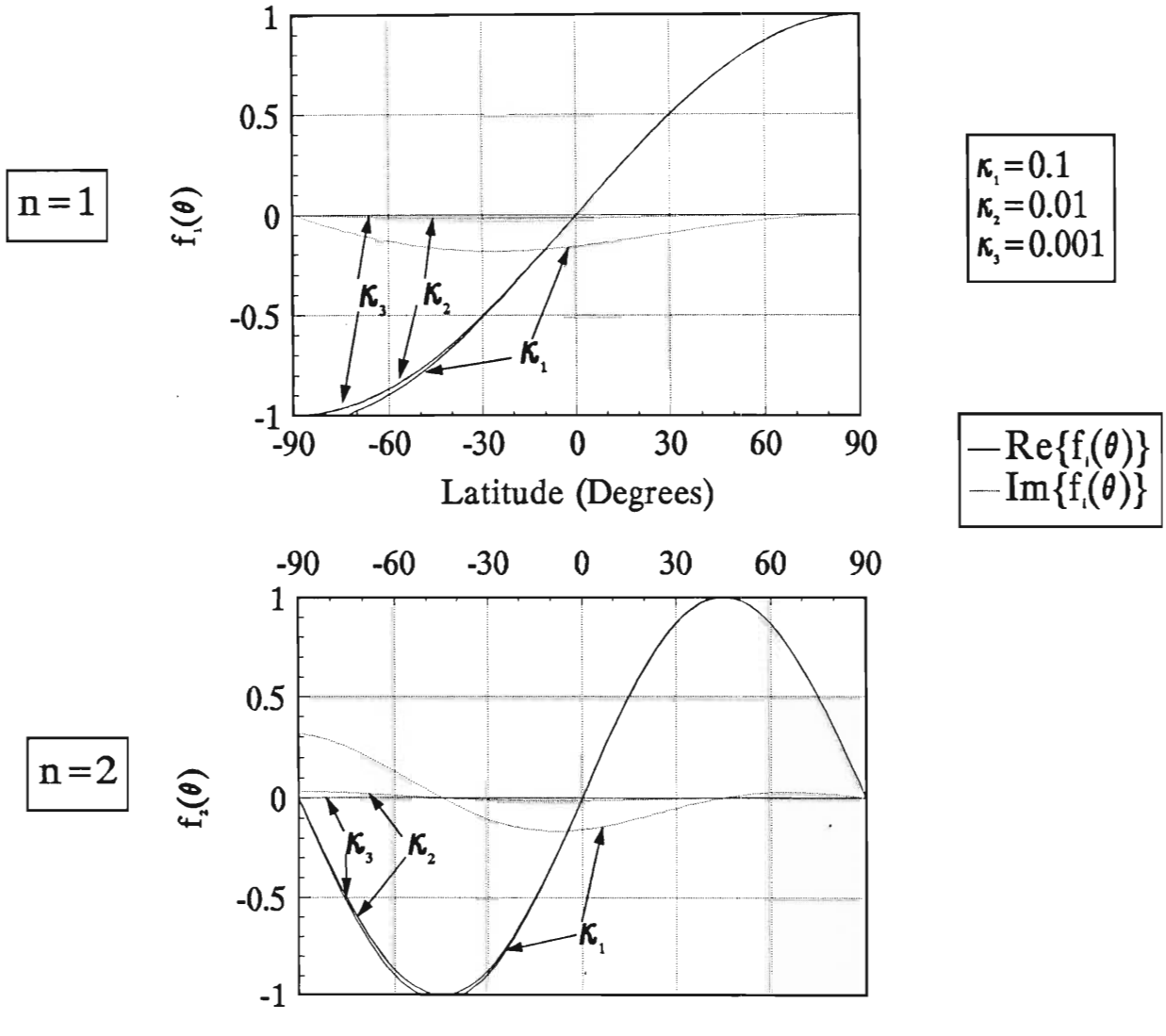

Figure 4.2: Field aligned wave structures of $f_1(\theta)$ (fundamental, odd harmonic) and $f_2(\theta)$ (second, even harmonic) for selected values of damping decrements (κ).

where $H(\tau)$ is the incident signal such that $H(\tau \leq 0) = 0$. In the case of a purely compressional signal, $M_1(z) = 0 = T$. The function $M_2(z) = M(z)$ describes the axial structure of the compressional components of the incident pulse. The periodicity condition defined by equation 4.16 means that $M(z)$ may be written as a Fourier synthesis of the spatial components in m, i.e.

$$M(z) = \sum_{j}^{N} c_j e^{-im_j z} \tag{4.22}$$

The choice of $H(\tau)$ and $M(z)$ must characterize the causative pulse. As an application of this cavity-resonance model we will consider impulse functions as first approximation descriptions of the excitation signal that initiates the Pi 2 pulsation event in the following chapter.

4.2 Method of Solution

The system 4.14 and 4.15 is solved as follows. First, a Laplace transform is applied with respect to time, τ. This is followed by a Fourier transform with respect to the z coordinate. This leaves two one-dimensional differential equations with respect to x. This system is reduced to a single, second order differential equation in x by substitution. The resulting equation is integrated numerically along x using finite difference methods. The final solution is obtained by applying numerical inverse Fourier and inverse Laplace transforms.

4.2.1 Defining the Fourier and Laplace Transforms

Given that $E(z)$ is continuous and z real, we define the Fourier transform pair as

$$\mathcal{E}(m) = \mathcal{F}\{E(z)\} = \int_{-\infty}^{\infty} E(z) e^{-imz} dz \tag{4.23}$$

$$E(z) = \mathcal{F}^{-1}\{\mathcal{E}(s)\} = \frac{1}{2\pi} \int_{-\infty}^{\infty} \mathcal{E}(m) e^{imz} dm \tag{4.24}$$

with the properties

$$\frac{\partial \mathcal{E}(m)}{\partial z} = im\mathcal{E}(m)$$

$$\frac{\partial^2 \mathcal{E}(m)}{\partial z^2} = -m^2 \mathcal{E}(m)$$

Let τ be real and p complex, then the Laplace transform is defined as the integral

$$\bar{E}(p) = \mathcal{L}\{E(\tau)\} = \int_0^\infty E(\tau)e^{-p\tau}d\tau \tag{4.25}$$

with the properties

$$\begin{aligned}\frac{\partial}{\partial\tau}\bar{E}(p) &= -p\bar{E}(p)\\ \frac{\partial^2}{\partial\tau^2}\bar{E}(p) &= p^2\bar{E}(p)\end{aligned}$$

4.2.2 Application of Fourier and Laplace Transform

Applying the Laplace transform to equations 4.14 and 4.15 with respect to the time coordinate τ, gives

$$\left[\frac{p^2}{A_N^2} + \frac{(n+i\kappa)^2}{x^2} - \frac{\partial^2}{\partial z^2}\right]\bar{T}(x,z,p) = -i\frac{\partial}{\partial z}\left[\frac{\partial}{\partial x}\bar{P}(x,z,p)\right] \tag{4.26}$$

$$\left[\frac{p^2}{A_N^2} + \frac{(n+i\kappa)^2}{x^2} - \frac{1}{x}\frac{\partial}{\partial x}(x\frac{\partial}{\partial x})\right]\bar{P}(x,z,p) = \frac{i}{x}\frac{\partial}{\partial z}\left[\frac{\partial}{\partial x}x\bar{T}(x,z,p)\right] \tag{4.27}$$

and the Fourier transform of the above system, with respect to z, is

$$\left[\frac{p^2}{A_N^2} + \frac{(n+i\kappa)^2}{x^2} + m^2\right]\bar{\mathcal{T}}(x,m,p) = m\left[\frac{\partial}{\partial x}\bar{\mathcal{P}}(x,m,p)\right] \tag{4.28}$$

$$\left[\frac{p^2}{A_N^2} + \frac{(n+i\kappa)^2}{x^2} - \frac{1}{x}\frac{\partial}{\partial x}(x\frac{\partial}{\partial x})\right]\bar{\mathcal{P}}(x,m,p) = -\frac{m}{x}\left[\frac{\partial}{\partial x}x\bar{\mathcal{T}}(x,m,p)\right] \tag{4.29}$$

Notice that the equations are coupled by gradient terms whose strength is proportional to m; m essentially being a measure of longitudinal asymmetry. When $m = 0$, then the above system is decoupled, equation 4.28 describing pure Alfvén guided oscillations (toroidal mode) in $T(x,z,\tau)$ and equation 4.29 describing the isotropic mode (poloidal mode) oscillations in $P(x,z,\tau)$.

4.2.3 Numerical Integration Procedure

Equations 4.28 and 4.29 may be put into a single, second order differential form in terms of $\bar{\mathcal{P}}(x,m,p)$ by substituting for $\bar{\mathcal{T}}(x,m,p)$, i.e.

$$\left(\frac{m^2}{\alpha} - 1\right)\frac{\partial^2}{\partial x^2}\bar{\mathcal{P}} + \left(\frac{m^2}{x}\left(\frac{\partial}{\partial x}\frac{x}{\alpha}\right) - \frac{1}{x}\right)\frac{\partial}{\partial x}\bar{\mathcal{P}} + \beta\bar{\mathcal{P}} = 0 \tag{4.30}$$

where

$$\alpha = \frac{p^2}{A_N^2} + \frac{(n+i\kappa)^2}{x^2} + m^2$$

$$\beta = \alpha - m^2$$

Equation 4.30 is in the ideal form for the application of a finite difference integration algorithm (this method is outlined in Appendix B). Essentially, the spatial and temporal domains are divided into integration grids. In this work, the radial and azimuthal spatial domains are divided into 128 and 256 grids respectively. The temporal/frequency domain comprises 256 grid points. First, the equations are integrated step by step along x. This is followed by numerical inverse Laplace and Fourier transforms along the frequency (p) and azimuthal wavenumber (m) ordinates respectively to obtain the final solution in $P(x,z,\tau)$. The numerical inverse Laplace transform method used in this work is based on that described by *Piessens and Branders*, [1971]. It is the same method as used by *Allan et al.*, [1985b, 1986a, 1986b, 1987]. It must be noted that this method gives unreliable results for $m > 10$. Thus, care is taken in this thesis when choosing azimuthal forms for the initiating pulse. The requirement is that the significant spectral components lie within the $m < 10$ range (i.e. components for $m > 10$ have negligible amplitude).

Finally $T(x,z,\tau)$ is determined by substituting the solution in x of $\bar{\mathcal{P}}$ into equation 4.29 and then solving in a similar way to that described above. The electric fields are determined from $T(x,z,\tau)$ and $P(x,z,\tau)$ using equations 4.9 and 4.10.

4.2.4 Magnetic Components

The components of magnetic perturbation follow directly from Faraday's Law 4.2. Referring to Fig. 4.1 and remembering that $E_\theta = 0$, the magnetic components are given by

$$\frac{\partial b_x}{\partial \tau} = -\frac{1}{x}\frac{\partial E_z}{\partial \theta} = -\frac{iP}{x}\frac{\partial f(\theta)}{\partial \theta} \tag{4.31}$$

$$\frac{\partial b_z}{\partial \tau} = \frac{1}{x}\frac{\partial E_x}{\partial \theta} = \frac{T}{x}\frac{\partial f(\theta)}{\partial \theta} \tag{4.32}$$

$$\frac{\partial b_\theta}{\partial \tau} = \frac{\partial E_z}{\partial x} - \frac{\partial E_x}{\partial z} = i\left(\frac{\partial P}{\partial x} - \frac{\partial T}{\partial z}\right) f(\theta) \tag{4.33}$$

Notice that b_θ represents the magnetic component parallel to the magnetic field lines and is therefore incident approximately normal to the ionosphere. In the case of a totally reflecting ionosphere, one expects this component to vanish there. If there is

partial damping, this component is expected to be finite but small at the ionosphere. Appendix C shows how the integral form of the magnetic components are used with a Laplace identity to obtain solutions for b_x, b_θ and b_z during the integration process .

4.2.5 The Poynting Vector

The Poynting vector is defined as

$$\mathbf{S} = \mu_0^{-1}\mathbf{E} \times \mathbf{b}^*$$

where the asterisk denotes the complex conjugate. Since the instantaneous Poynting vector is oscillatory, it would be more appropriate to determine the cumulative energy flow. The time-integrated Poynting vector is defined as (see *Allan et al.*, [1987])

$$\mathbf{F}(\tau) = \int_0^\tau \Re(\mathbf{E}) \times \Re(A_0\mathbf{b})d\tau \tag{4.34}$$

where $\mathbf{F}(\tau)$ is in units of electric field squared. Multiplying the integral by a factor $1/(\mu_o A_0^2)$ gives $\mathbf{F}(\tau)$ in energy flux units through a unit area up to a time τ (*Allan*, [1982]).

Chapter 5

Pi 2 Cavity-Resonance Modelling

5.1 Introduction

The cavity-resonance equations developed in the previous chapter are applied to the study of Pi 2 events. An impulse signal with temporal and spatial form describing the approximate causative signal is modelled. A realistic plasma distribution model, that includes the ionospheric and plasmapause features, is developed for the cavity.

5.2 Model of an Impulse at the Magnetopause

The temporal nature of the cavity-resonance waves with specific azimuthal wavenumber has been extensively investigated (see *Allan et al.,* [1985b,1986a,1986b,1987]). In this thesis we consider the response of the system to a series of azimuth spectra derived from a an impulse with spatial form. This enables the study cavity-resonance waves generated by a realistic pulse that has longitudinal form. Emphasis is therefore placed on the spatial, rather than the temporal, nature of the cavity response. Naturally, the temporal and spatial form of the impulse signal depends on its phenomenological origin. In order to investigate the cavity response due to a particular geophysical mechanism, an appropriate pulse signal must be modelled. For the earth's magnetosphere, there are a number of instability mechanisms which could cause pressure fluctuations at the magnetopause. For example, the nature of the cavity-resonances induced by sudden impulses (SI's are sudden increases in the solar wind velocity incident at the magnetopause over a broad front), can be studied by choosing an impulse signal that is likely to extend over most of the dayside hemisphere, having a maximum at midday and tapering toward the dawn and dusk terminators. Pc activity due to the Kelvin-Helmholtz

Instability (KHI) may be studied by choosing an incident signal characterized by a continuous monochromatic component with a spatial form that accounts for the observed noon-meridian phase change.

For the Pi 2 pulsation event, the impulse is chosen which, to a first approximation, resembles the sudden relaxation of the magnetospheric cavity during the substorm onset.

5.2.1 The Temporal Structure of Impulse

The precise form of the causative signal is unknown. We assume that the impulse signal is related to the collapse of the near-Earth tail field. The causal mechanism seems to be located at high latitudes, where observed Pi 2 band spectra are noisy and contain many spectral components (see section 2.5.1). These features are accounted for by ensuring a broadband signal with oscillating components. The modelled temporal part of the signal displays an initial steep amplitude ramp followed by less rapid decay. The general temporal form of the impulse is given by

$$H(\tau) = \alpha \tau e^{\beta \tau} \tag{5.1}$$

where $\alpha = \alpha_r + i\alpha_i$ and $\beta = \beta_r + i\beta_i$ with $\beta_r < 0$ to ensure signal decay. Note that τ is a normalized time i.e. $\tau = t/t_0$ where $t_0 \approx 100$ s (see section 4.1.4, equation 4.8). The oscillation nature and duration of the pulse depends on β. For small $|\beta_r|$ the signal will have sinusoidal behaviour lasting for a relatively large number of cycles. The period of these cycles is determined by β_i. Lastly α determines the steepness of the initial signal ramp.

In the analysis carried out in this thesis, a similar temporal pulse form to that used by *Allan et al.* [1985b] is modelled which allows for comparison of results where possible. Putting $\alpha = -13.8571i$ and $\beta = i - 5$, this give a signal of the form

$$H(\tau) = -13.8571 i \tau e^{-5\tau} e^{i\tau} \tag{5.2}$$

The form of this signal is shown as $H_1(\tau)$ in Fig. 5.1.

An important characteristic of any signal is its bandwidth. A signal that rises and decays relatively quickly is termed 'broad band'. This is because a Fourier synthesis of such a signal reveals that it is composed of a relatively larger range of frequency components than say a 'narrow band' signal. The delta function is the limiting case of a broad band signal, since it is the superposition of all possible frequency components, each equally weighted. A broad band impulse signal therefore serves as a useful diagnostic in studying the response of a system. Choosing the impulse to be of the correct

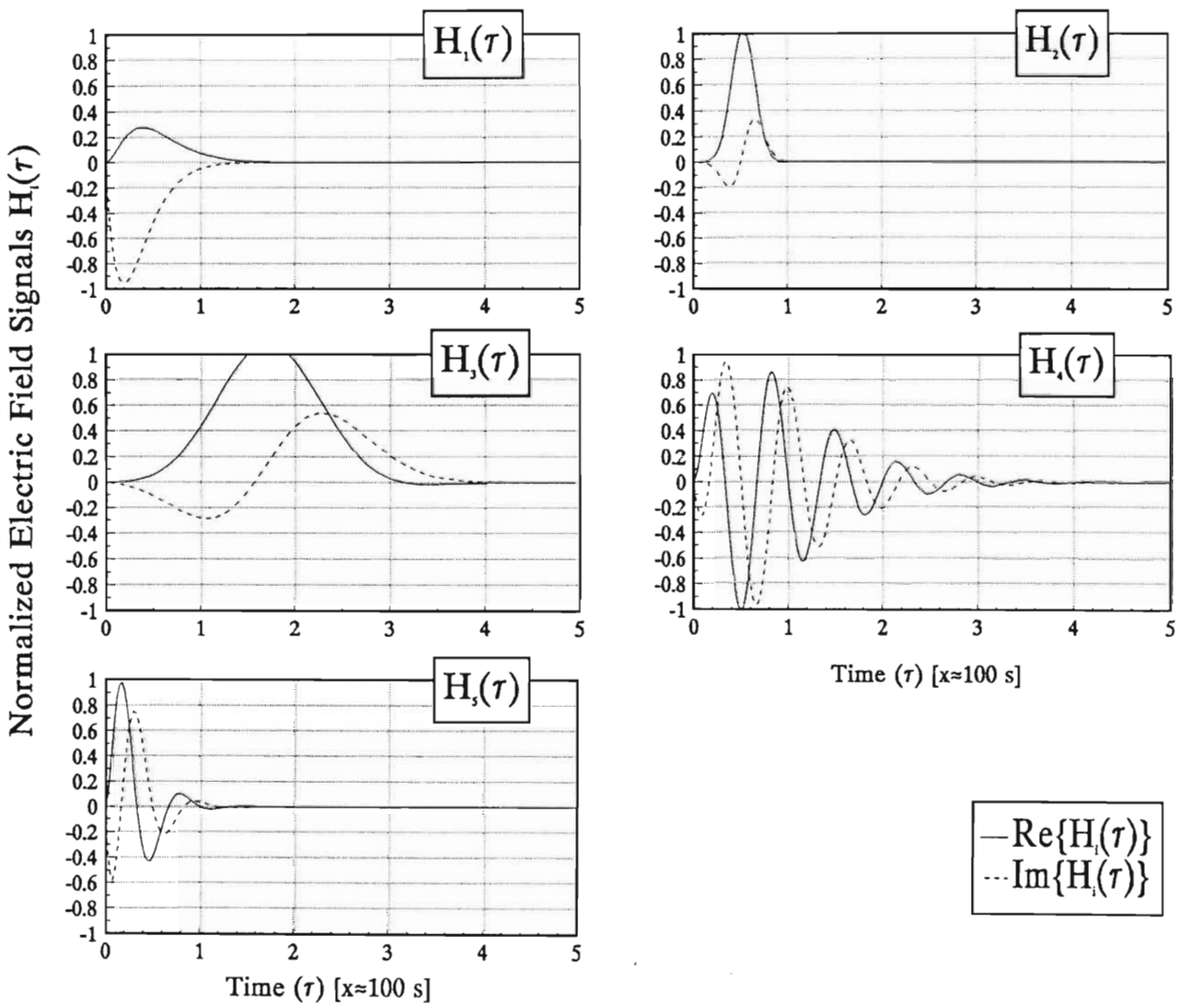

Figure 5.1: Temporal Forms of Model Compressive Impulses.

$H_i(\tau)$	Signal Form
$H_2(\tau)$	$-2\tau i e^{-\frac{(\tau-\frac{1}{2})^2}{(\frac{1}{5})^2}} e^{i\pi\tau}$
$H_3(\tau)$	$-\frac{2}{3}i\tau e^{-(\tau-\frac{3}{2})^2} e^{i\tau}$
$H_4(\tau)$	$-5.5\tau i e^{-2\tau} e^{3\pi i\tau}$
$H_5(\tau)$	$-16\tau i e^{-6\tau} e^{3\pi i\tau}$

Table 5.1: Some Examples of the Temporal Forms of Pulse Signals

band width is of critical importance in the study of cavity mode excitations (see e.g. *Lee and Lysak*, [1989] and *Southwood and Kivelson*, [1990]). Some examples of impulse signals are shown in Table 5.1 and displayed in Fig. 5.1.

Signal $H_2(\tau)$ is an example of a broad band signal. (We use the terms broad and narrow band in terms of the characteristic cavity time t_0, where $\tau = t/t_0$). This signal would be useful because it would excite many of the higher frequency cavity eigenmodes. Pulse $H_3(\tau)$ is an example of a narrow band signal. Pulse $H_4(\tau)$ may be used to investigate cavity-resonance waves generated by a transient oscillatory instability or generating mechanism in the magnetotail (see *Moortgat et al.*, [1990]).

Kitamura et al., [1988] postulated that the Pi 2 signal generating mechanism is located in the outer magnetosphere where the field lines are connected to the auroral region. Recent observations by the SAMNET array (*Yeoman et al.*, [1990]) indirectly suggest the sub-auroral region as a transitional region where there is a change in the nature of the Pi 2 signal from one dominated by the auroral zone wave to one dominated by the mid to low latitude wave. The high latitude signal is characteristically noisy and is thought to be related to the generating mechanism (see section 2.5.1). This noisy signal could then trigger the cavity mode which characterizes the lower latitude event. Signal $H_4(\tau)$ resembles a typical Pi 2 signal and is a first approximation to the noisy signal at high latitudes (see also section 2.5.1). Signal $H_5(\tau)$ is similar to $H_4(\tau)$, except that this signal decays much faster. In practice however, we found the temporal pulse given by $H_1(\tau)$ to be adequate in exciting the fundamental and second harmonic cavity modes which (as we will see in the next chapter) have frequencies falling within the Pi 2 range. The higher cavity modes oscillate at higher frequencies, suitable for producing waves in the Pi 1 domain. Using the excitation pulse $H_1(\tau)$ has the added advantage of being able to make comparison between the work carried out in this thesis and that of *Allan et al.* [1985b,1986a,1986b,1987].

5.2.2 The Spatial Form of Impulse

At high (auroral) latitudes Pi 2 events are fairly well spatially confined in Local Time to within about $1-2$ hours in Local Time near the midnight meridian (see section 2.5.2), indicating a causal mechanism that is localized in longitude ($\approx 15^0-30^0$). The simplest, most rudimentary representation of this feature is the square, or top hat, pulse signal centred about the midnight meridian. A better approximation is the Gaussian pulse. The general axial form is given by

$$M(z) = A[e^{-\frac{z^2}{w^2}} + e^{-\frac{(z_0-z)^2}{w^2}}] + C \tag{5.3}$$

where w is the signal width (in radians) at $1/e$ of its maximum amplitude and C is the dc off-set. The dc off-set is necessary because *Sakurai and McPherron* [1983] (using ATS 6 magnetometer Pi 2 events observed at geosynchronous orbit) estimated that Pi 2 bursts were superimposed on a dc shift in the azimuthal direction caused by field-aligned currents above the satellite. They also found that the initial Pi 2 perturbation is in the same sense as the dc shift caused by the field-aligned currents. Similarly, away from the FAC, the ring current also experiences a surge causing an initial increase in the H-component magnetic field at points outside of the ring current (and a corresponding initial decrease in the H-component earthward of the ring current). Fig. 5.2a is a plot of the function $M(z)$ for $w = 15^0(\times\frac{\pi}{180^0})$ and $C = -0.05$ and Fig. 5.2b for $w = 30^0(\times\frac{\pi}{180^0})$.

In this thesis, we wish to study the evolution of the system due to a purely compressional pulse form. It is worth pointing out that although the outer boundary of the model cavity coincides with the magnetopause on the dayside sector, this is not necessarily the case for the night sector. At the outer cavity boundary,

$$\begin{aligned} T(x=1,z,\tau) &= H(\tau)M(z) = 0, \text{and} \\ P(x=1,z,\tau) &= H(\tau)M(z) \end{aligned}$$

The fourier and Laplace equivalents are

$$\begin{aligned} \bar{T}(x=1,m,p) &= 0 \\ \bar{P}(x=1,m,p) &= \bar{H}(p)\mathcal{M}(m) \end{aligned}$$

where we have used the transforms defined in section 4.2.1.

Fig. 5.3 is a perspective view showing the spatial pulse incident on the modelled magnetospheric cavity.

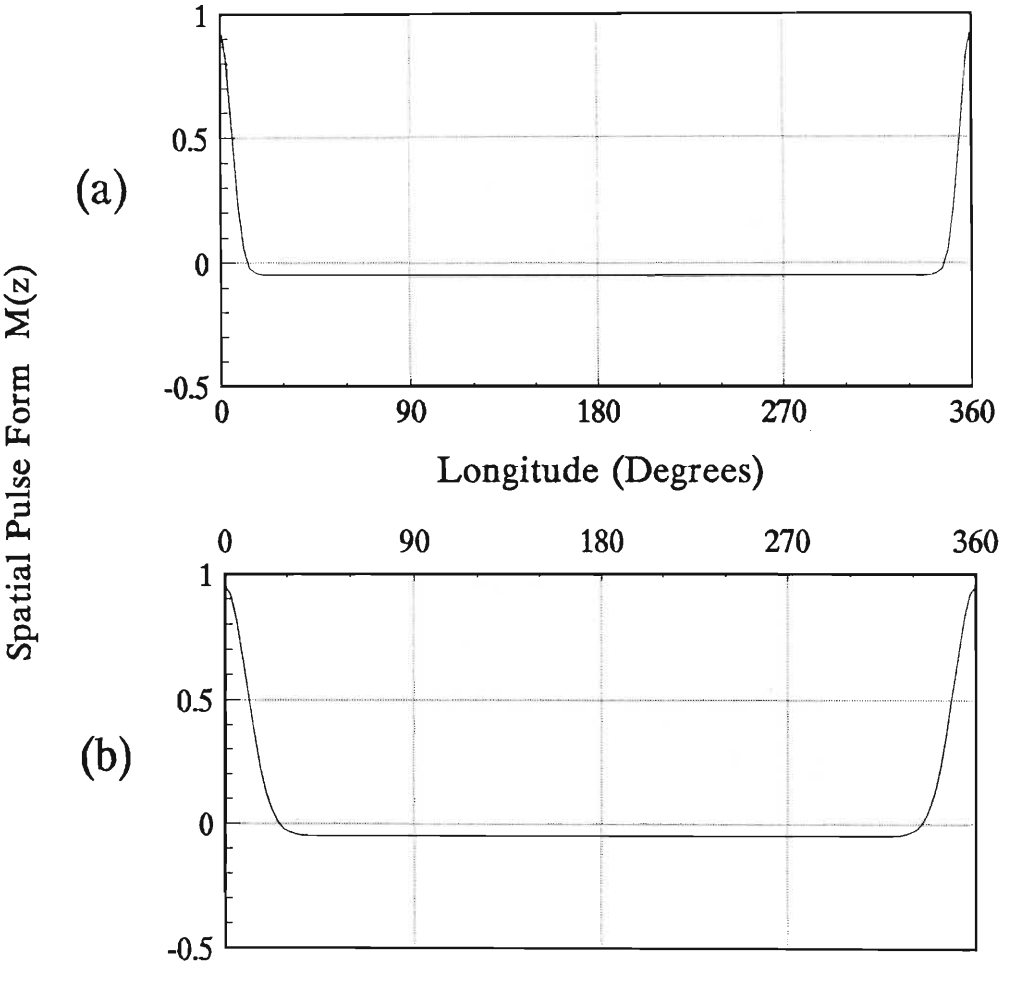

Figure 5.2: Modelled Spatial Pulse Form $M(z)$ incident at the magnetopause, with (a) $w = 15^0(\times\frac{\pi}{180^0})$ and $C = -0.05$ and (b) $w = 30^0(\times\frac{\pi}{180^0})$.

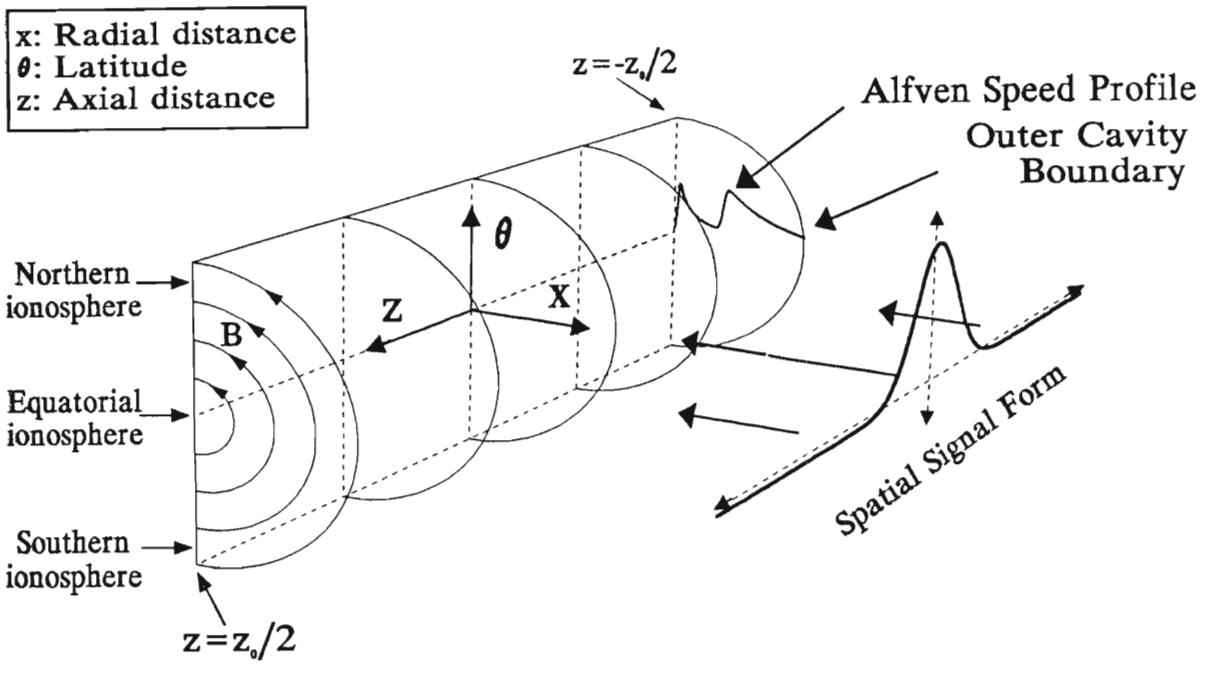

Figure 5.3: Model magnetospheric cavity (with normalized coordinates (x, θ, z)) showing the incidence of the spatial part of the impulse.

5.3 Ionospheric Conditions

For the preliminary investigations presented in this thesis, the ionosphere is assumed to be a perfect conductor. This means that the at the field amplitudes must be zero in the equatorial ionosphere. This is equivalent to putting $I(z) = 0$ (in equations 4.18 and 4.19) and hence

$$\begin{aligned} T(x = 0, z, \tau) &= 0 \\ P(x = 0, z, \tau) &= 0 \end{aligned}$$

with Fourier and Laplace transforms

$$\begin{aligned} \bar{T}(x = 0, m, p) &= 0 \\ \bar{P}(x = 0, m, p) &= 0. \end{aligned}$$

5.4 The Alfvén Speed Distribution Model

The plasma distribution in the magnetosphere is of particular importance. The inclusion of the plasmasphere in such a model would mean that many interesting questions can be addressed. Will the nature of the waves depend on the location of the plasmapause? How does the steepness of the plasmapause affect the waves? Will the incident waves be reflected at the plasmapause? Is there evidence of a surface wave at the plasmapause? These are some of the central questions pertinent to the understanding of low-latitude Pi 2.

In the following, an original plasma distribution model is developed (giving similar plasma distribution profiles to that of *Allan et al.,* [1986a,1986b]). This is a single species cold plasma theory and therefore it is the cold plasma distribution that is of interest. We point out that the preliminary investigative nature, and the simplistic approach of our modelling, does not justify sophisticated plasma distribution models that for example would include diurnal dependencies. The model must however be able to account for ionospheric ion increases, plasmapause ion decreases and include latitudinal movement of the plasmapause.

5.4.1 The Alfvén Speed

The Alfvén velocity depends on the magnetic field and plasma density. Once the Alfvén velocity has been determined, standard resonance theory is used to calculate the natural Alfvén wave period at a particular L-shell (see section 5.5).

The mass density, in the equatorial plane, is defined as

$$\rho_{eq} = \rho_i f(R) \tag{5.4}$$

where ρ_{eq} and ρ_i are the equatorial and plasma densities respectively. A suitable $f(R)$ is required that will characterize the plasma density variations with radial distance R in the magnetosphere. The dipolar magnetic field is given by

$$B = \frac{a^3 B_0}{r^3}(4 - 3\cos^2\theta) \tag{5.5}$$

where $r = aL\cos^2\theta$, θ is latitude, r is distance from the center to a point on the field, L is the McIlwain parameter and a is the radius of the earth. In the equatorial plane, let $r(\theta = 0) = aR$. In the equatorial plane the radial variation of the magnetic field is then

$$B_{eq} = \frac{B_i}{R^3} = B_i R^{-3} \tag{5.6}$$

where B_i is the magnetic field strength at the equatorial ionosphere. The Alfvén velocity in the equatorial plane is

$$A_{eq}(R) = \frac{B_{eq}}{\sqrt{\mu_0 \rho_{eq}}} \tag{5.7}$$

$$= \frac{B_i R^{-3}}{\sqrt{\mu_o \rho_i f(R)}} = A_i R^{-3} f^{-\frac{1}{2}}(R) \tag{5.8}$$

where $A_i = \frac{B_i}{\sqrt{\mu_0 \rho_i}}$ is the Alfvén velocity in the upper ionosphere. Normalizing at the magnetopause, one gets that

$$A_N(R) = \frac{A_i}{A_0} R^{-3} f^{-\frac{1}{2}}(R) \tag{5.9}$$

where $A(R = R_0) = A_0 = A_i R_0^{-3} f^{-\frac{1}{2}}(R_0)$ is the Alfvén velocity at the magnetopause. A suitable model function $f(R)$ will be determined in the next few sections.

5.4.2 Plasma Distribution Model

In the modelling carried out in this thesis, the cold plasma density distribution is characterized by four domains. Remember that this modelling applies to the semi-cylindrical magnetosphere defined earlier (section 4.1.2). The first domain (ionosphere)

is from the lower to upper F-region ionosphere, where the plasma density variations are dominated by heavy ion concentrations that have an approximate exponential decrease with height. The second domain (plasmasphere) begins at the upper ionosphere at a height of about $\approx 1.7 \times 10^3$ km, where the H^+ ions start to dominate, and ends at the plasmapause. In this domain, the ion fall-off is assumed to be $\propto R^{-N_1}$. The third domain (plasmapause) begins at the earthward boundary of the plasmapause, where an exponential drop off in the ion concentration is assumed until the outer plasmapause boundary is reached. Finally, between the outer edge of the plasmapause and the magnetopause is the plasmatrough where the plasma distribution fall-off is $\propto R^{-N_2}$.

The Ionosphere Region

Extensive observations of plasma distributions through out the ionosphere have been made by satellites and low orbiting rockets carrying particle detectors. A single, representative model is however not possible because of diurnal, seasonal, latitudinal variations and other factors which influence the ion concentrations. Since the depth of the ionosphere is a small fraction of the size of the magnetosphere, a precise ionospheric distribution in not critical in our study and we neglect the unnecessary complications of sophisticated models. Our modelling is based on a density profile determined by a superposition of low latitude ion distributions obtained from various workers by *Hattingh* [1987] in his study on the effects of the ionosphere on low latitude ULF pulsations. Fig. 5.4 is a diagram showing average concentrations of O^+ and H^+ and their altitude fall-off rates through the ionosphere.

The height at which maximum ion concentration occurs is chosen as the inner boundary of the magnetospheric cavity. This corresponds to the lower F region at a height of 300 km. The O^+ concentration there is $\approx 8 \times 10^{11}$ amu m^{-3}, (an effective mass density of $\approx 1.3 \times 10^{13}$ amu m^{-3}). An exponential fall-off rate is assumed up to the upper boundary of the region at a height of about 1700 km, (upper F region), where the heavier oxygen ion concentrations have decreased to the extent that the total mass density concentrations begin to be dominated by the H^+ ions. The total ion mass concentration at this height is $\approx 4 \times 10^{10}$ amu m^{-3}.

The plasma mass density in the F region is assumed to vary as

$$n(R) = \alpha e^{\beta R} \tag{5.10}$$

where α and β are determined as follows:

$$\ln[n(R)] = \beta R + \ln \alpha, \text{ and hence} \tag{5.11}$$

$$\beta = \frac{\ln[n(R_2)] - \ln[n(R_1)]}{R_2 - R_1}[O^+\text{ions}]$$

$$\alpha = \exp[\ln n[(R_1)] - \beta R_1][H^+\text{ions}] \tag{5.12}$$

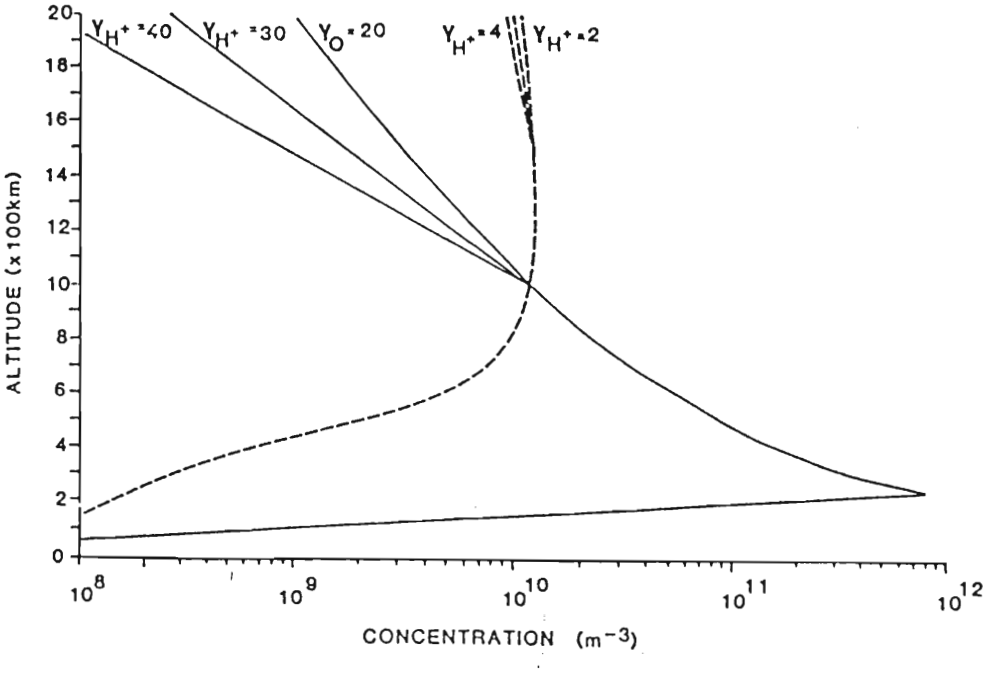

Figure 5.4: Average concentrations of O^+ (solid line) and H^+ (dashed line) as functions of altitude. The values 40, 30, 20 and 4, 2 refer to density fall off rates for oxygen and hydrogen assuming inverse power models. (*Hattingh*, [1987]).

and where $n(R_1)$ and $n(R_2)$ are given by:

$$\begin{aligned} n(R_1) &= n(300 \text{ km}) \approx 16 \times 8 \times 10^{11} \text{amu m}^{-3} \\ n(R_2) &= n(1700 \text{ km}) \approx 4 \times 10^{10} \text{amu m}^{-3} \end{aligned}$$

The Plasmasphere and the Plasmatrough

In the case where there is no plasmapause, the plasma density variation is assumed to be of the form (see *Cummings et al.*, [1969]),

$$\rho_{eq}(R) = \frac{\rho_i}{R^N} = \rho_i R^{-N} \tag{5.13}$$

In this case, the Alfvén velocity in equatorial plane is simply

$$A_{eq}(R) = \frac{B_{eq}(R)}{\sqrt{\mu_0 \rho_{eq}(R)}} = A_i R^{\frac{1}{2}(N-6)} \tag{5.14}$$

If the mass density variation is chosen to be $\propto R^{-3}$, (in keeping with *Allan et al.*, [1985b]), a simple speed variation is established,

$$A_{eq}(R) = A_i R^{-\frac{3}{2}} \tag{5.15}$$

Fig. 5.5 shows the normalized Alfvén speed and resonance frequency with radial distance (resonance frequency has been determined through classical resonance theory - see section 5.5 and Appendix F).

The plasmapause is accounted for by the following ion density model:

$$\begin{aligned} n_{H^+} &= \frac{n_i}{2}\left[\frac{1-\exp^{\frac{R-R_{pa}}{\Delta R}}}{1+\exp^{\frac{R-R_{pa}}{\Delta R}}}+1\right]\left(\frac{1}{R}\right)^{N_1} \\ &+ \frac{n_p}{2}\left[\frac{1-\exp^{\frac{R_{pb}-R}{\Delta R}}}{1+\exp^{\frac{R_{pb}-R}{\Delta R}}}+1\right]\left(\frac{R_{pb}}{R}\right)^{N_2} \end{aligned}$$

where

R_{pa} is the radial distance from the centre of the Earth to the inner plasmapause,
R_{pb} is the radial distance from the centre of the Earth to the outer plasmapause,
$\Delta R = R_{pb} - R_{pa}$ is the width of the plasmapause,
n_i is the plasma density at the upper ionosphere,
$n_p = \frac{n_i}{R_{pb}^{N_1}} \times \frac{1}{\Delta n_{pp}}$ is the plasma density on the outer edge of the plasmapause with $\Delta n_{pp} (\approx 100)$, being the relative plasma (density decrease) across the plasmapause.

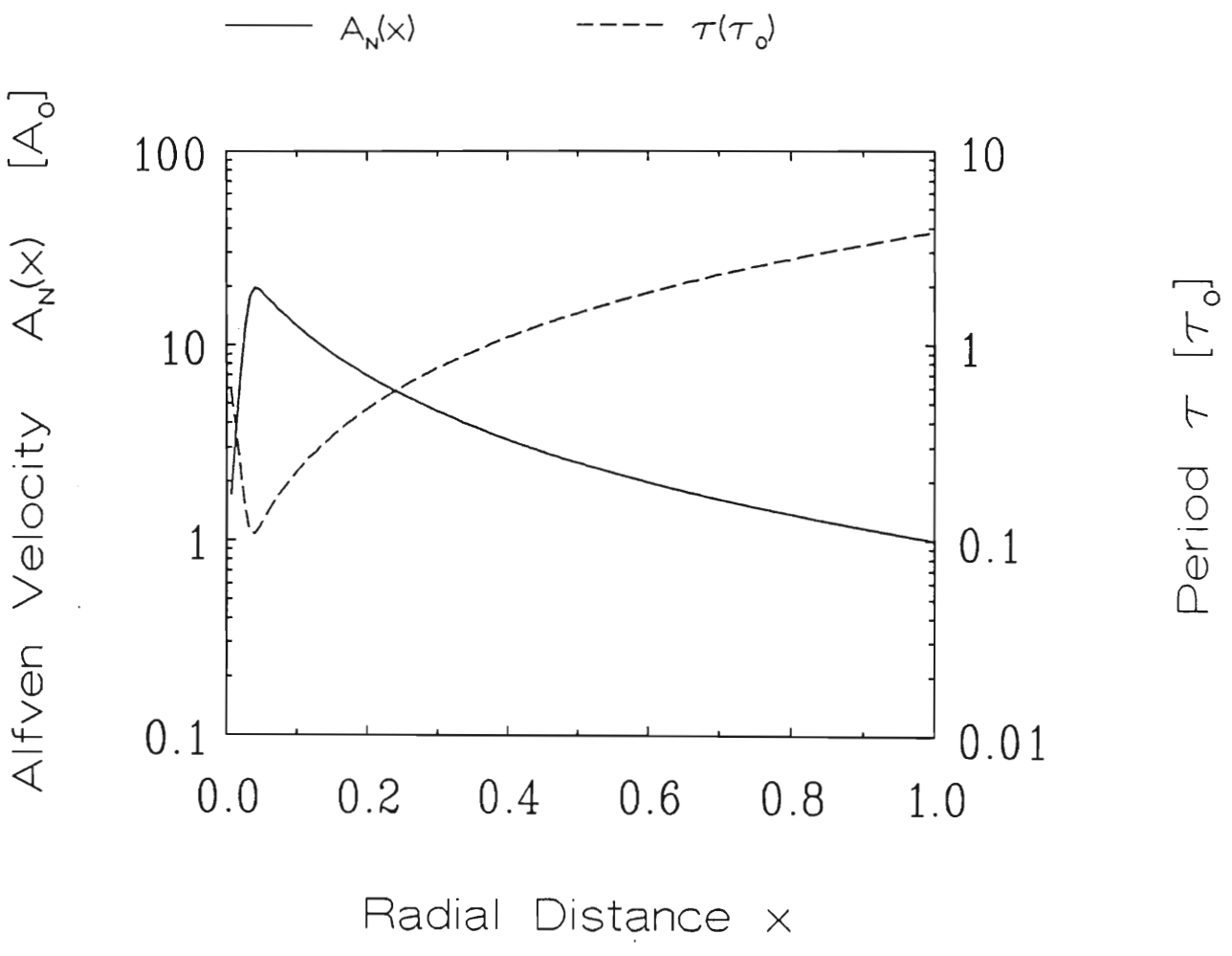

Figure 5.5: Equatorial Alfvén velocity distribution with corresponding characteristic resonance period.

Total Plasma Density Distribution

Putting all these terms together, the total plasma density distribution through the cavity is given by

$$\begin{aligned} n = \rho_{eq} = \rho_i f(R) \;=\; & \alpha e^{\beta R} \\ & + \frac{n_i}{2}\left[\frac{1-\exp^{\frac{R-R_{pa}}{\Delta R}}}{1+\exp^{\frac{R-R_{pa}}{\Delta R}}}+1\right]\left(\frac{1}{R}\right)^{N_1} \\ & + \frac{n_p}{2}\left[\frac{1-\exp^{\frac{R_{pb}-R}{\Delta R}}}{1+\exp^{\frac{R_{pb}-R}{\Delta R}}}+1\right]\left(\frac{R_{pb}}{R}\right)^{N_2} \\ & + n_{IMF} \end{aligned} \tag{5.16}$$

where n_{IMF} is the particle density at the magnetopause boundary.

In Fig. 5.6, the plasma mass density variation with radial displacement in the equatorial plane is shown for three magnetospheric conditions.

5.5 Resonance Eigenperiods

The characteristic period of oscillation of the guided Alfvén wave for each L-shell is determined by Alfvén toroidal-resonance theory. We make use of an empirical formula developed by *Taylor and Walker* [1984] from which a set of eigen-wavenumber values for k may be calculated (see Appendix F). The jth eigenperiod is given by

$$\begin{aligned} T_j(s) = \frac{1}{f_j} \;&=\; \frac{2\pi}{Ak_j} \\ \text{and hence } T_j(\tau_0) \;&=\; \frac{2\pi}{A_N(x)k_j(x)} \end{aligned} \tag{5.17}$$

Fig. 5.7, is a plot of the normalized Alfvén velocity and corresponding resonance eigenfrequency for the case when $L_{pp} = 4.5$. Fig. 5.8 shows the Alfvén speed in ms^{-1} for the same conditions.

In the following chapter, the transmission of this signal through the magnetosphere is studied and the results are compared with contemporary observations and models.

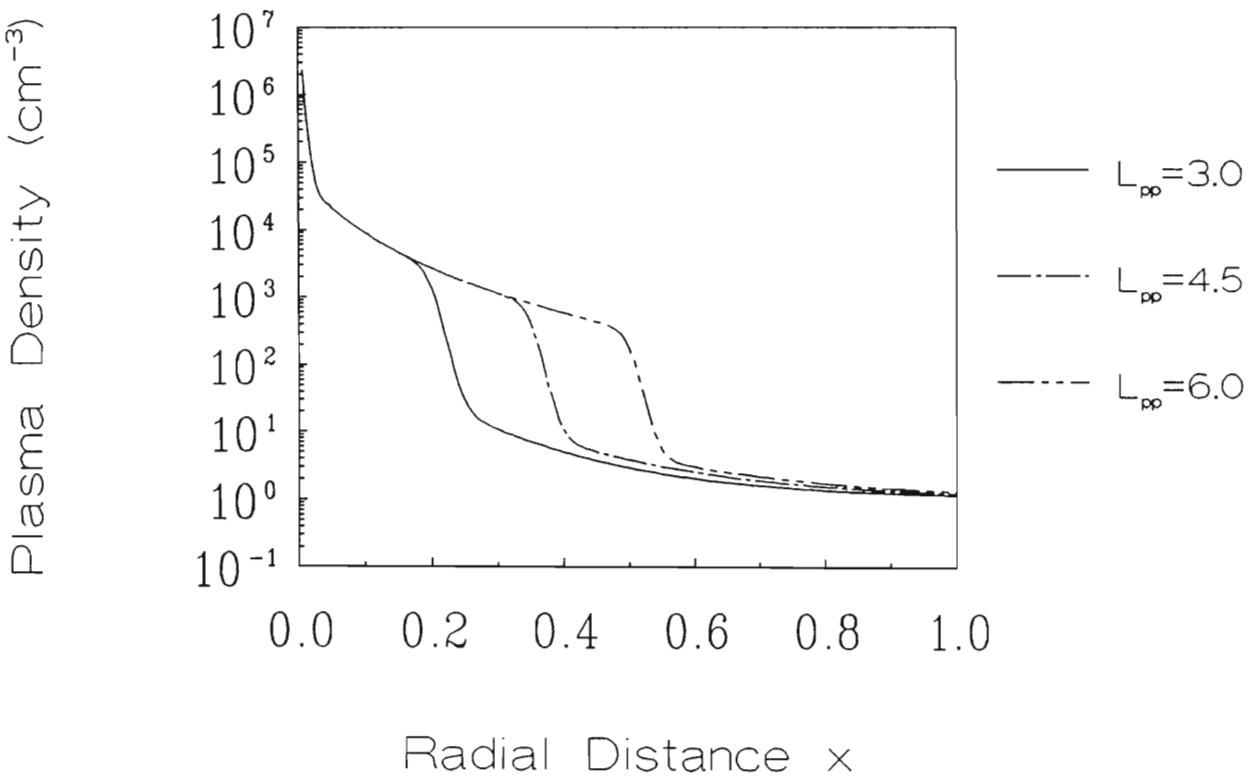

Figure 5.6: Plasma mass density profiles as a function of radial distance. The profiles are those where the plasmapause is located at $L_{pp} = 3.0, 4.5$ and 6.0. (The magnetopause is at L=11.)

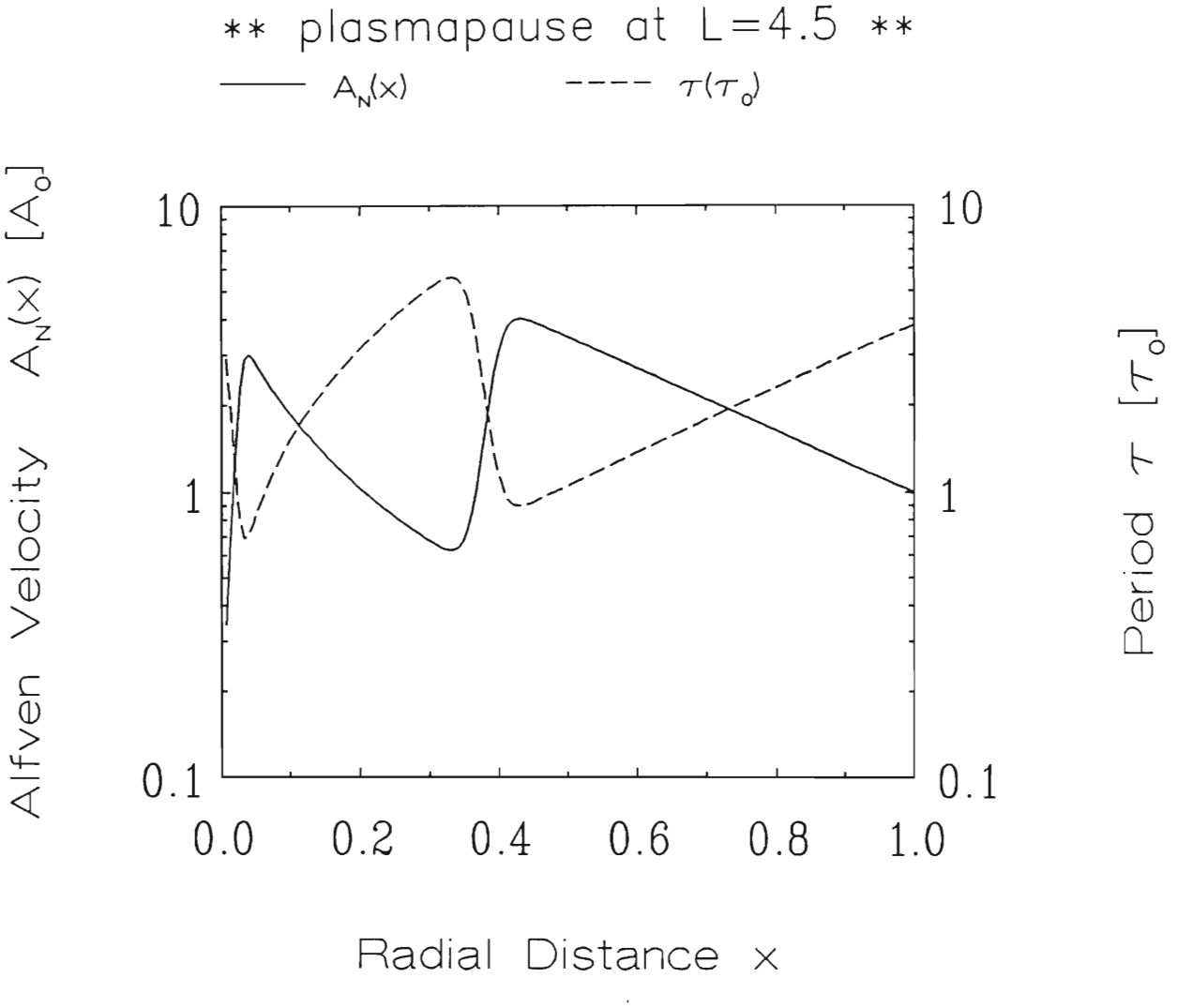

Figure 5.7: Normalized Alfvén velocity and characteristic Alfvén resonance period as a function of radial distance. $L_{pp} = 4.5$.

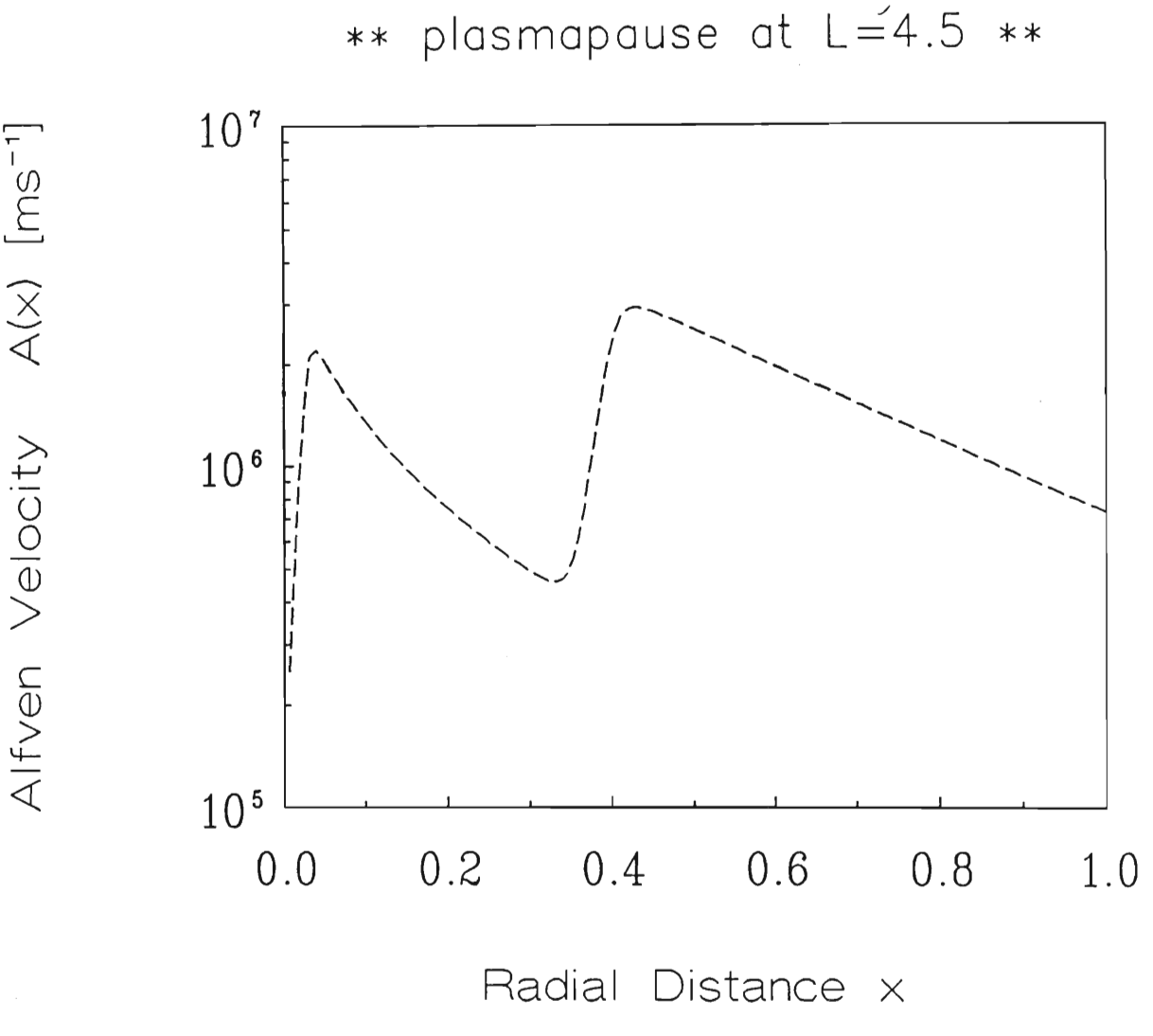

Figure 5.8: The Alfvén speed distribution in ms^{-1}.

Chapter 6

Computational Results

In this chapter, computational results of the cavity-resonance model developed in the previous chapters are presented and discussed. Due to the volume of calculations involved in this kind of three-dimensional modelling, computations require in the order of several days to complete. It is therefore practically impossible to carry out an extensive evaluation on the nature of the waves for a range of parameter values. For this reason, one has to be selective in choosing which aspects to investigate. The primary objective is to evaluate the appropriateness of the cavity-resonance type mechanism for describing Pi 2 pulsations. Particular attention is given to those aspects for which observational descriptions exist, in this way allowing for a comparison between theory and observation. Aspects of investigation include the spatio-temporal nature of the cavity and transverse Alfvén modes, the effect of plasmapause position on these waves, the variation of polarization with latitude and longitude, and the variation of phase with latitude.

Since parameters $P(x, z, \tau)$ and $T(x, z, \tau)$ are the most fundamental representations of the isotropic (cavity) and transverse Alfvén modes respectively, investigations in this thesis are carried out in terms of these descriptors. The electric field components are directly related to these field parameters in a simple way i.e. $E_z \propto P(x, z, \tau)$ and $E_x \propto T(x, z, \tau)$, (see equations 4.9 and 4.10).

6.1 The Nature of the Cavity-Resonance Wave

We begin the investigation with an analysis of the interaction between the cavity and transverse Alfvén wave modes. The cavity modes are excited by the application of a suitable impulsive source centred about the near midnight magnetospheric boundary.

The impulse chosen for this study has temporal form defined by

$$H(\tau) = H_1(\tau) = -13.8571 i\tau e^{-5\tau} e^{i\tau}$$

where $H_1(\tau)$ is given in Fig 5.1. The spatial part of the impulse is defined by

$$M(z) = A[e^{-\frac{z^2}{w^2}} + e^{-\frac{(z_0 - z)^2}{w^2}}] + C$$

where $w = 30^0(\times\frac{\pi}{180^0})$ and $C = -0.05$. This function is displayed in Fig. 5.2b.

The temporal evolution of the cavity-resonance waves at various radial distances within the cavity is shown in Fig. 6.1. Fig. 6.1a comprises two panels. The upper panel shows the evolution of the cavity mode component as viewed in the midnight meridian i.e. $P(x, z = 0, \tau)$. The lower panel of Fig. 6.1a is merely the spectral content of the perturbations shown in the upper panel. The upper panel of Fig. 6.2a shows the oscillations of the transverse Alfvén mode $T(x, z = constant, \tau)$ as viewed along a meridian plane slightly displaced from the midnight meridian (specifically at $z = \frac{9}{128}z_0$, or about $\approx 25^0$ from midnight). $T(x, z, \tau)$ is viewed in a meridian displaced from $z = 0$ because, (as will be shown later), $T(x, z, \tau)$ actually has a node in its azimuthal structure at $z = 0$. The lower panel of Fig. 6.2a shows the computed spectra of $T(x, z = \frac{9}{128}z_0, \tau)$.

The temporal coordinate is measured in terms of τ. The unit of time in seconds is easily computed from τ because $t(s) = \tau t_0$, where $t_0 = r_0/A_0 \approx 100$ s, and hence $t(s) \approx 100\tau\ (s)$. The same axis is used to measure frequency in units of $1/\tau$ ($\approx$ 10mHz). Radial distance is measured in terms of normalized coordinate $x = r/r_0$ where $r_0 \approx 10$ earth radii (recall that $r = 0$ and $r = r_0$ correspond to the position of the ionosphere and magnetopause respectively). The radial Alfvén speed profile is chosen such that the plasmapause is located at $L = L_{pp} = 5.5$ (see Fig 5.7, except $L_{pp} = 5.5$). Further assumptions include a fundamental (odd mode) field aligned mode (i.e. $f_n(\theta) = f_1(\theta)$, see equation 4.13) which is generally inferred from observation (see chapter 2), and an ionospheric damping parameter $\kappa \approx 0.01$.

Discussion

The variations in $P(x, z = 0, \tau)$ (upper panel, Fig 6.1a) have a form similar to that of Pi 2. The signal is dominated by oscillations with periods at T $\approx$ 60 s and 120 s. As expected, the temporal nature of the cavity mode, $P(x, z = 0, \tau)$, is consistently similar in amplitude, period and duration over most of the cavity. Of particular note is that the magnitude of the variations are fairly substantial at small radial distances (i.e $x < 0.2$, corresponding to low latitudes). The nature of the wave perturbations

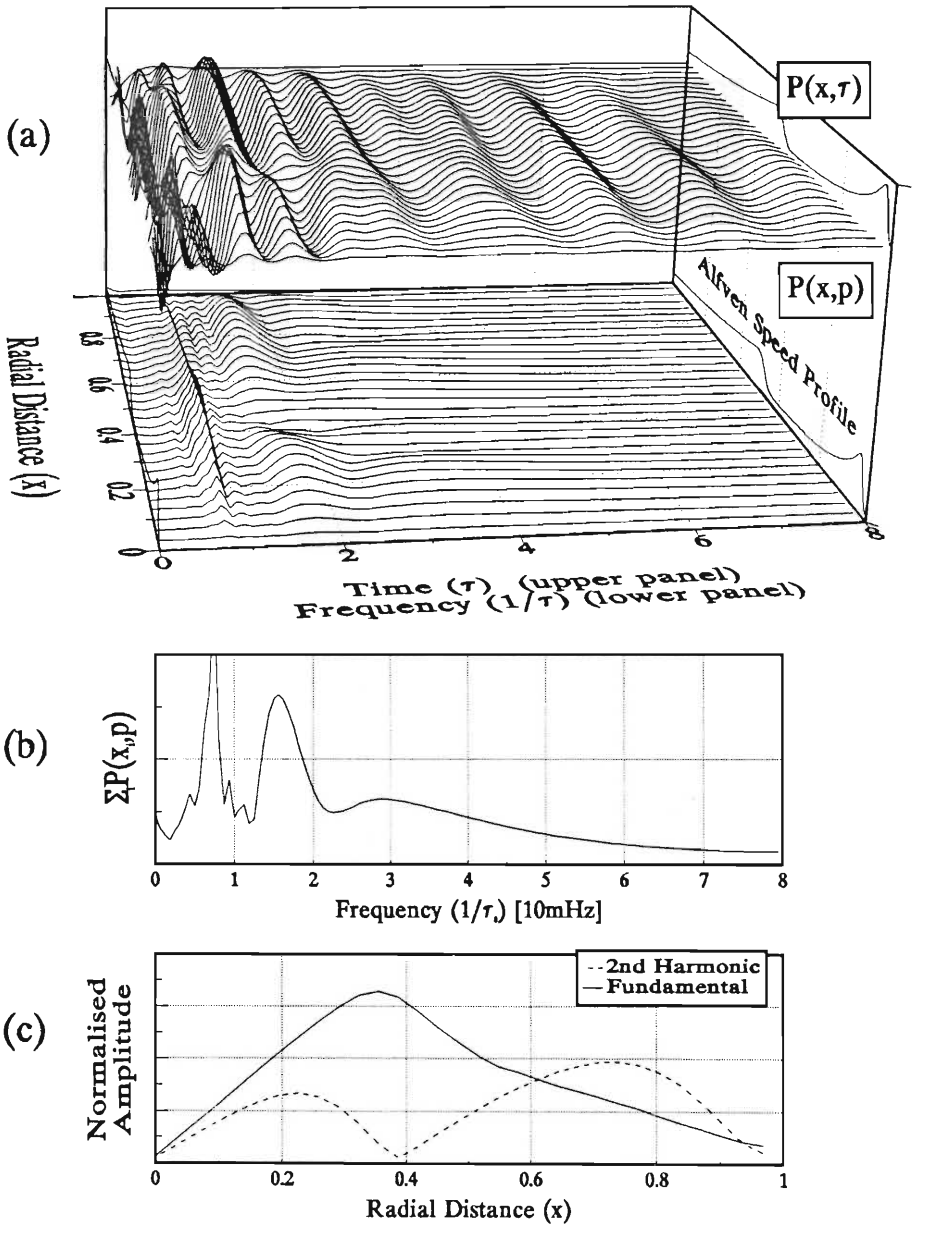

Figure 6.1: (a) Temporal evolution of the cavity $P(x, z, \tau)$ mode at different radial distances in the cavity. (b) Spectral profile, and (c) fundamental and second harmonic mode amplitude variations with radial distance. ($\kappa = 0.01$, $n = 1$ and $L_{pp} = 5.5$). Amplitudes shown are in normalized units.

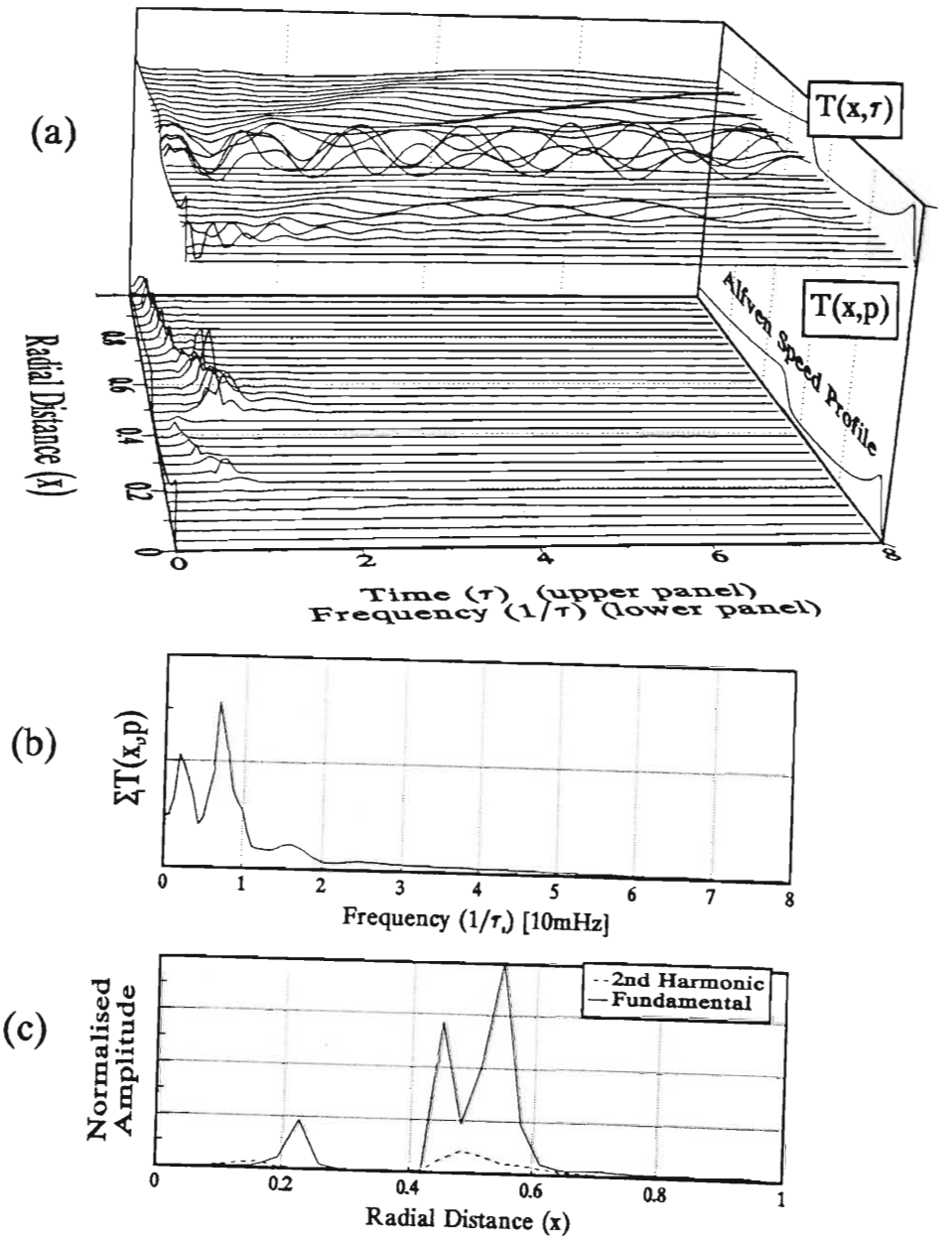

Figure 6.2: (a) Temporal evolution of the transverse Alfvén $T(x, z, \tau)$ mode at different radial distances in the cavity. (b) Spectral profile, and (c) fundamental and second harmonic mode amplitude variations with radial distance. ($\kappa = 0.01, n = 1$ and $L_{pp} = 5.5$). Amplitudes shown are in normalized units.

is in agreement with that found by *Allan et al*, [1986a]. However, the cavity mode oscillations appear to decay faster.

Perturbations in $T(x, z = \frac{9}{128}z_0, \tau)$, (Fig 6.2a, upper panel) display characteristic transverse Alfvén wave form with latitude dependent oscillation frequency. From the figure it is clear that wave frequency increases with decreasing radial distance from the ionosphere, except across the plasmapause where wave frequency temporarily decreases. Damping of these waves appears to be negligible in the outer magnetosphere. As a result, in the plasmatrough the total wave signal comprises significant contributions of both the cavity and the transverse Alfvén mode. Near the plasmapause the amplitude of the waves is enhanced. Earthward of the plasmapause (plasmasphere) the oscillations are evanescent indicating the possible existence of a critical point in the vicinity of the plasmapause.

6.2 Spectra

The excitation of a transverse Alfvén resonance through coupling to the cavity mode, depends on whether the cavity mode spectral peak lies within the Alfvén continuum. The cavity-resonance modelling of *Krauss-Varban and Patel* [1988] indicated the likelihood of two discrete spectrum solutions (i.e. cavity modes) situated inside the frequency range of the Alfvén continuum in a box model magnetosphere.

The cavity mode spectra for the waves in the upper panel Fig 6.1a are displayed in the lower panel of Fig 6.1a ($P(x, p)$). It is clear that the spectral peaks remain at constant frequency at all radial distances, as expected for cavity modes. When the spectral profiles shown in the lower panel of Fig 6.1a are summed (this is the integrated spectra through the cavity), a profile is produced given by Fig. 6.1b. This profile is dominated by two spectral peaks one at frequency $\approx 13/128\tau_0^{-1}$ or period T $\approx$ 120 s (corresponding to the fundamental cavity mode) and the other at frequency $\approx 26/128\tau_0^{-1}$ or period T $\approx$ 60 s (corresponding to the second harmonic cavity mode). The frequency of these cavity modes fall within the Pi 2 range. *Yeoman and Orr* [1989] have observed a Pi 2 event (at BGS) that had fundamental and second harmonic components.

In Fig 6.1c the spectral amplitude of the fundamental (solid line) and second harmonic cavity mode (broken line) is plotted as a function of radial distance. The second harmonic cavity mode has a node at about $x \approx 0.4$ which would correspond to a point just earthward of the plasmapause. (This node may be mistaken for a reflection point if it were observed on the ground at latitudes where the field lines would intersect the equatorial plane at $x \approx 0.4$). These results compare favourably with those of *Allan et al.*, [1986b], (see in particular fig 4, *Allan et al.*, [1986b]). For this spectral

component there is an amplitude maximum in the outer magnetosphere (plasmatrough) and a secondary maximum just earthward of the plasmapause. Secondary amplitude maxima in Pi 2 have been observed equatorward of the plasmapause (e.g. *Lester and Orr*, [1982]; see also section 2.6).

From Fig 6.1a, one can see that most of the transients have decayed by a time $\tau = 3$, and the waves oscillate with a dominant period $\tau \approx \frac{4}{5}t_0$ (or T $\approx$ 120 s), which corresponds to the fundamental cavity mode. For this simulation then, the second harmonic cavity oscillations decay before those of the fundamental cavity mode. The lower panel of Fig 6.2a displays the spectral profiles of the transverse Alfvén waves. It can be seen that the frequency of the waves is dependent on radial distance. From Fig 6.1b, one can see that the largest contribution to the wave spectra from each radial position is made by that component corresponding to the fundamental cavity mode ($\tau^{-1} \approx 0.8\tau_0^{-1}$). The amplitude of the transverse Alfvén waves corresponding to the first and second cavity modes (these are the Alfvén resonance waves) are plotted in Fig 6.2c as a function of radial distance. It is apparent that coupling between the cavity mode and the transverse Alfvén wave is more efficient for the fundamental rather than the second harmonic cavity mode. The amplitude of the Alfvén resonance which corresponds to the second cavity mode, should be maximum at slightly lower latitudes than the resonance due to the first cavity. This is not the case because at $x \approx 0.4$, (where the second harmonic mode should potentially couple to the field line resonance), the cavity mode has a node, (or is very nearly zero), and hence there is very little mode coupling. (The L-shell at which the cavity mode couples to the transverse Alfvén mode depends on the characteristic Alfvén period of that L-shell which in turn depends on the magnetic field strength, length of field line and plasma density).

6.3 Phase as a Function of Radial Distance

We now investigate the phase of the cavity-resonance waves as a function of radial distance. Because the ambient magnetic field lines within the cavity map down to the ionosphere, phase variations in the magnetosphere will be seen at the ionosphere and hence by ground based observatories. The transverse Alfvén waves undergo a phase change as they pass through the ionosphere. The magnitude of this phase change depends largely on the ionospheric conductivity. In general, a highly conducting ionosphere means that the transverse Alfvén resonance waves undergo a 90^0 phase change while the phase of the fast or cavity wave mode is independent of ionospheric conductivity (*Kivelson and Southwood*, [1988]).

Of particular interest is the phase of the two major cavity modes and associated transverse Alfvén resonances. For convenience we have re-plotted the amplitude of the cavity and transverse modes as a function of radial distance in Fig. 6.3a and 6.3d. The phase[1] corresponding to these wave components is plotted in Fig 6.3b and 6.3e. In Fig 6.3b we see that the phase of the fundamental cavity mode (solid line) is fairly constant over most of the cavity (except near the magnetopause boundary). For the second cavity mode (broken line), there is a 180^0 phase change at a point just earthward of the plasmapause (refer to Fig. 6.3c for the normalized Alfvén speed profile). This feature compares well with the 180^0 phase change observed by ground based magnetometers chains (e.g *Yeoman and Orr*, [1989]; see also section 2.5.5).

The phase variations of the associated transverse Alfvén resonance components is plotted in Fig 6.3e. Outside of the enhanced region the amplitudes are negligible and the phase is not really meaningful. However, the phase of the transverse Alfvén resonance mode associated with the fundamental cavity mode (solid line) undergoes an approximate 180^0 change on entering and exiting the resonance region.

From the above discussions, it is clear that the nature of the cavity mode is very different to that of the transverse Alfvén mode components. Since total observed wave signal is the sum of the components $T(x, z, \tau)$ and $P(x, z, \tau)$ observations of the cavity-resonance wave should reveal these differences. In the case of Pi 2, there is observational evidence showing a difference in the nature between magnetic components B_H and B_D. These components often appear to be decoupled and display a different spectral peak (see *Lester et al.*, [1983]), phase and wavenumber characteristics.

[1] We define the phase in this context as the arctangent of the ratio of the imaginary and real parts of the signal.

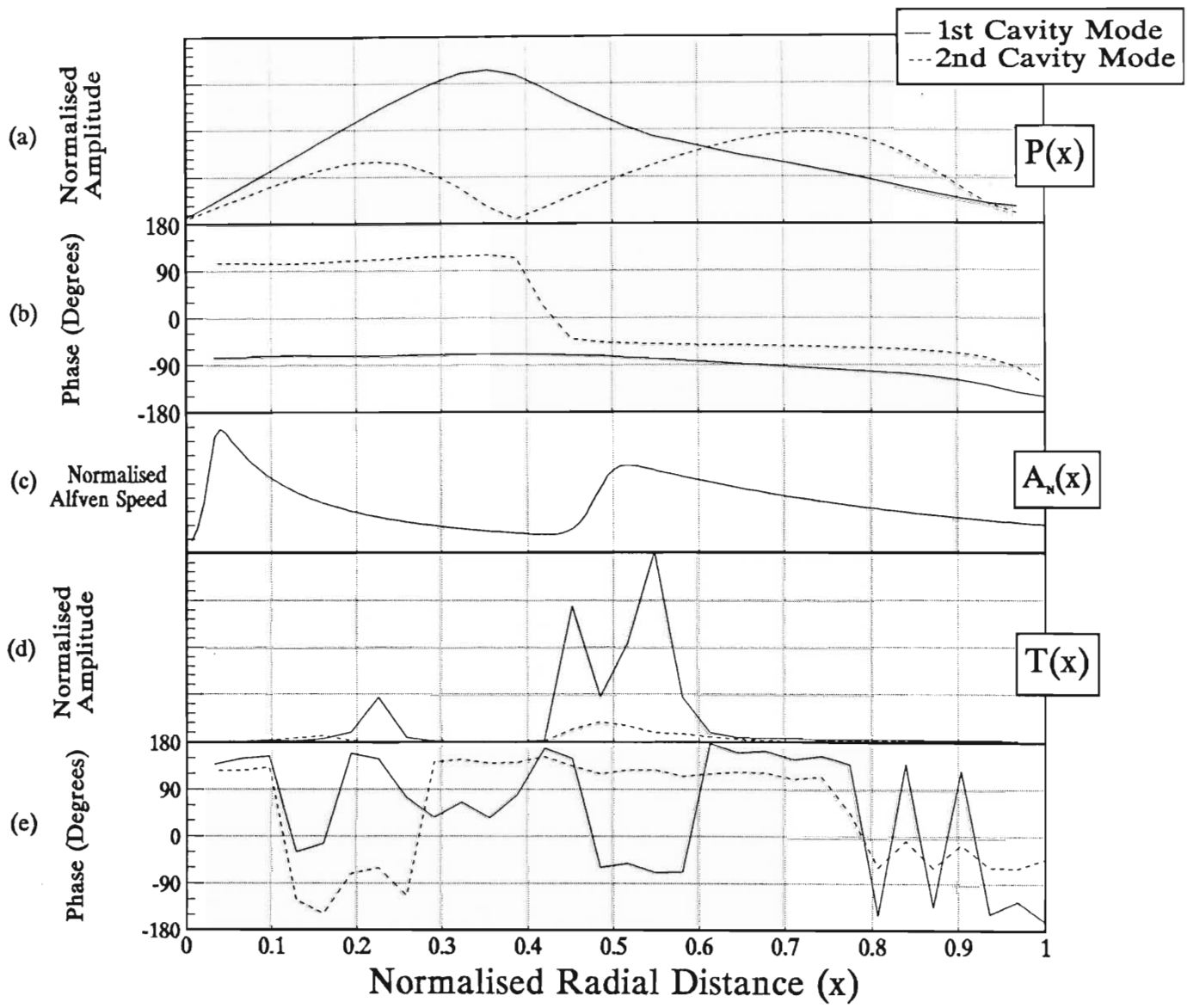

Figure 6.3: (a) Amplitude and (b) Phase versus radial distance for the fundamental (solid curve) and secondary (broken curve) cavity modes. Panels (d) and (e) are plots of the associated amplitude and phase of the field line Alfvén resonance wave. The normalized Alfvén velocity profile is given in panel (c) for reference.

6.4 Polarization Azimuth

From extensive, multi-station observations of Pi 2, a fairly clear picture exists for the Pi 2 horizontal polarization pattern[2], in the ionosphere, as a function of Local Time (see section 2.8.1). At mid to high latitudes, and within the region defined by the current wedge, (a zone extending several hours in Local Time and centred about a point in the near midnight region), the major axis of the Pi 2 horizontal polarization ellipse is observed to point approximately toward the centre of the substorm current wedge (*Lester et al.*, [1989]). This means that if one had to proceed westward from a point to the east of the substorm current wedge centre, the major axis of polarization would rotate in a right handed sense (i.e northern hemisphere and looking down the field lines). At low and equatorial latitudes, the horizontal polarization pattern is observed to be approximately linearly polarized along the magnetic meridian at all Local Times.

Fig. 6.4 shows the calculated major axis of the polarization azimuth, in the equatorial plane, as a function of longitude (or Local Time) for the components of oscillation corresponding to the fundamental cavity-resonance mode, at radial distances x = 0.3, 0.4, 0.5 and 0.6. Within the plasmasphere, the cavity mode component dominates and as a result, the polarization is predominantly north-south at all local times. For $x > 0.5$ (plasmatrough), the transverse Alfvén mode makes a greater contribution to the total field giving rise to a polarization pattern which compares favourably with observations (see section 2.8.1, Fig. 2.8). Within the region 21 - 3 LT, the polarization azimuth points roughly northward and toward the 0 LT meridian. The major axis of polarization rotates in a right handed sense (CW) as one moves westward with a maximum at 0 LT. The figure also illustrates that, for the given initiating pulse that is spatially confined in Local Time to within two to three hours about midnight (see Fig. 5.2b), the waves generated within the cavity travel to the dayside cavity to set up oscillations that spread through the entire cavity. The cavity mode also appears to peak at noon, which may be explained by constructive interference between the various modes of the azimuthal waves.

As pointed out, the transverse Alfvén resonance mode makes a significant contribution to the total wave field at high latitudes. It is worth noting that Pi 2 have been interpreted as transient standing wave resonances of the auroral field lines (*Maltsev et al.*, [1974]; *Saito et al.*, [1976a]; *Olson and Rostoker*, [1971]; *Kuwashima*, [1978]).

[2]The horizontal polarization pattern is determined by the two horizontal magnetic perturbation components (B_H and B_D) in the ionosphere as viewed by ground based magnetometers.

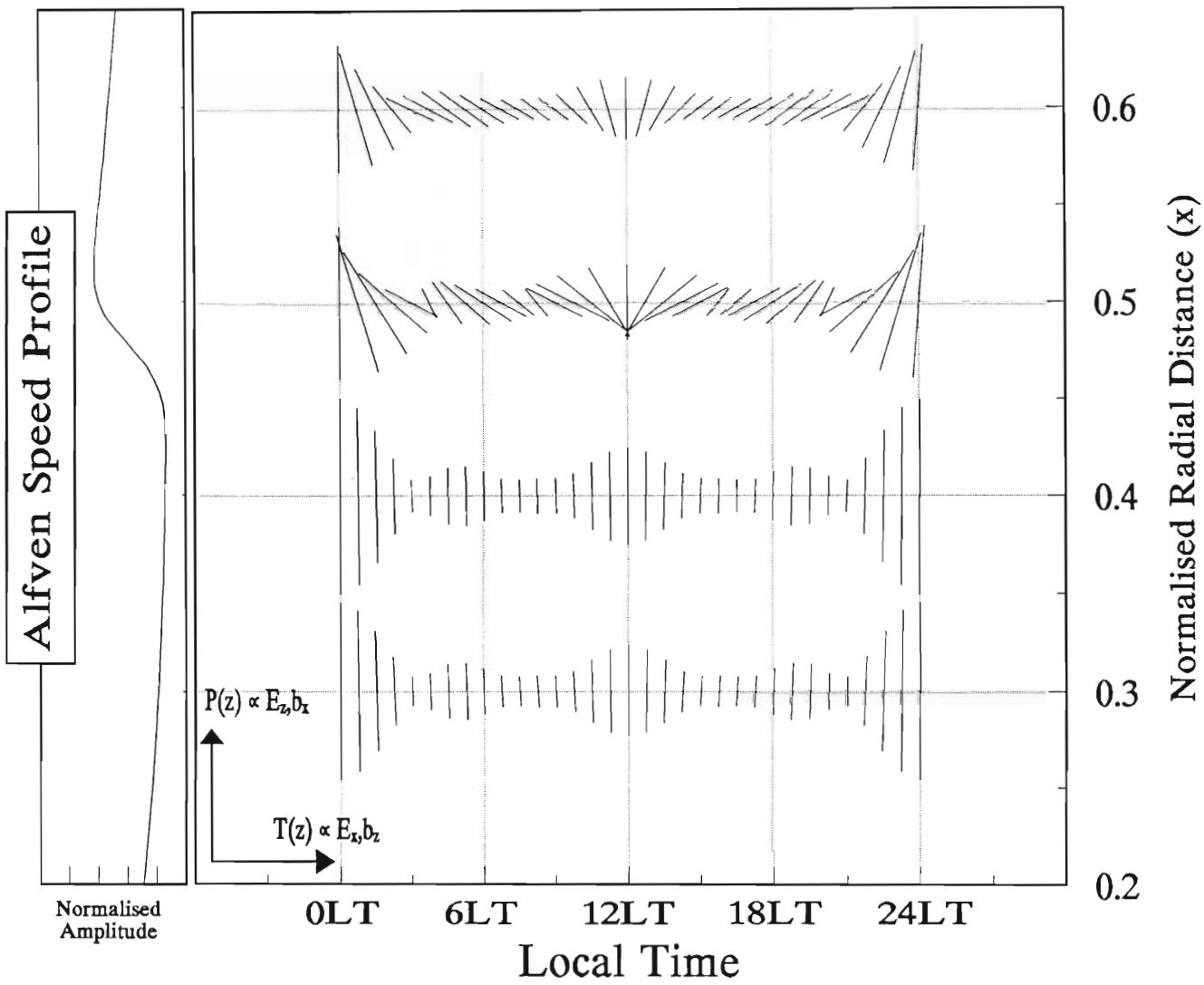

Figure 6.4: Major axis of the fundamental cavity-resonance polarization pattern as a function of Local Time at radial distances $x = 0.3,\ 0.4,\ 0.5$ and 0.6. ($\kappa = 0.01, L_{pp} = 5.5$).

6.5 Effect of Damping Decrement, κ

The effect of the ionospheric dissipation rate is illustrated by comparing the structure of the polarization azimuth in Fig 6.4 where $\kappa = 0.01$, with that of Fig 6.5 where $\kappa = 0.04$. It is evident that the cavity mode component (vertical component) is significantly smaller in the day sector for the case when $\kappa = 0.04$ (Fig 6.5) than in the case when $\kappa = 0.01$ (Fig. 6.4). In effect, a higher ionospheric dissipation value means that the propagation of the waves to the day sector is weaker.

6.6 Role of Plasmasphere

We now investigate the effect of the plasmapause position on the nature of the cavity-resonance waves. In Fig. 6.6, the temporal evolution of the cavity (upper panel) and the transverse Alfvén (lower panel) components is shown when the plasmapause is located at $L_{pp} = 4.5$. A fundamental (odd mode) field aligned structure is assumed (i.e. $f_n(\theta) = f_1(\theta)$, in equation 4.13), with a damping decrement $\kappa \approx 0.04$.

Discussion

The temporal variations of the cavity mode components, $P(x,\tau)$, (upper panel) are damped and have a dominant period T $\approx$ 100 s. As expected, the temporal variations in the cavity mode components are of similar amplitude, period and duration over most of the cavity. The wave frequency of the transverse Alfvén resonance mode $T(x,\tau)$ (lower panel) increases with decreasing latitude. In the outer magnetosphere oscillations appear to be less damped than those within the plasmasphere. Near the plasmapause the waves are enhanced indicating a cavity-resonance coupling. In practice, observation of the resonance near the plasmapause may be mistaken for a plasmapause surface wave (surface waves may occur at steep plasma gradient interfaces, see also section 3.2.3).

In Fig. 6.7 the plasmapause has been excluded from the simulation (with the rest of the integration parameters remaining unchanged). $P(x,\tau)$ displays similar temporal evolution as in the case when the plasmapause was included (Fig 6.6) except that the oscillations are noticeably smaller at small radial distances from the ionosphere (i.e. low latitudes). At very low latitudes, the amplitudes of the oscillations in $P(x,\tau)$ are negligible. This clearly illustrates that the plasmapause plays an important role in the structure of the cavity mode. The presence of the plasmapause appears to cause the cavity mode oscillations within the plasmasphere to be larger, such that even at

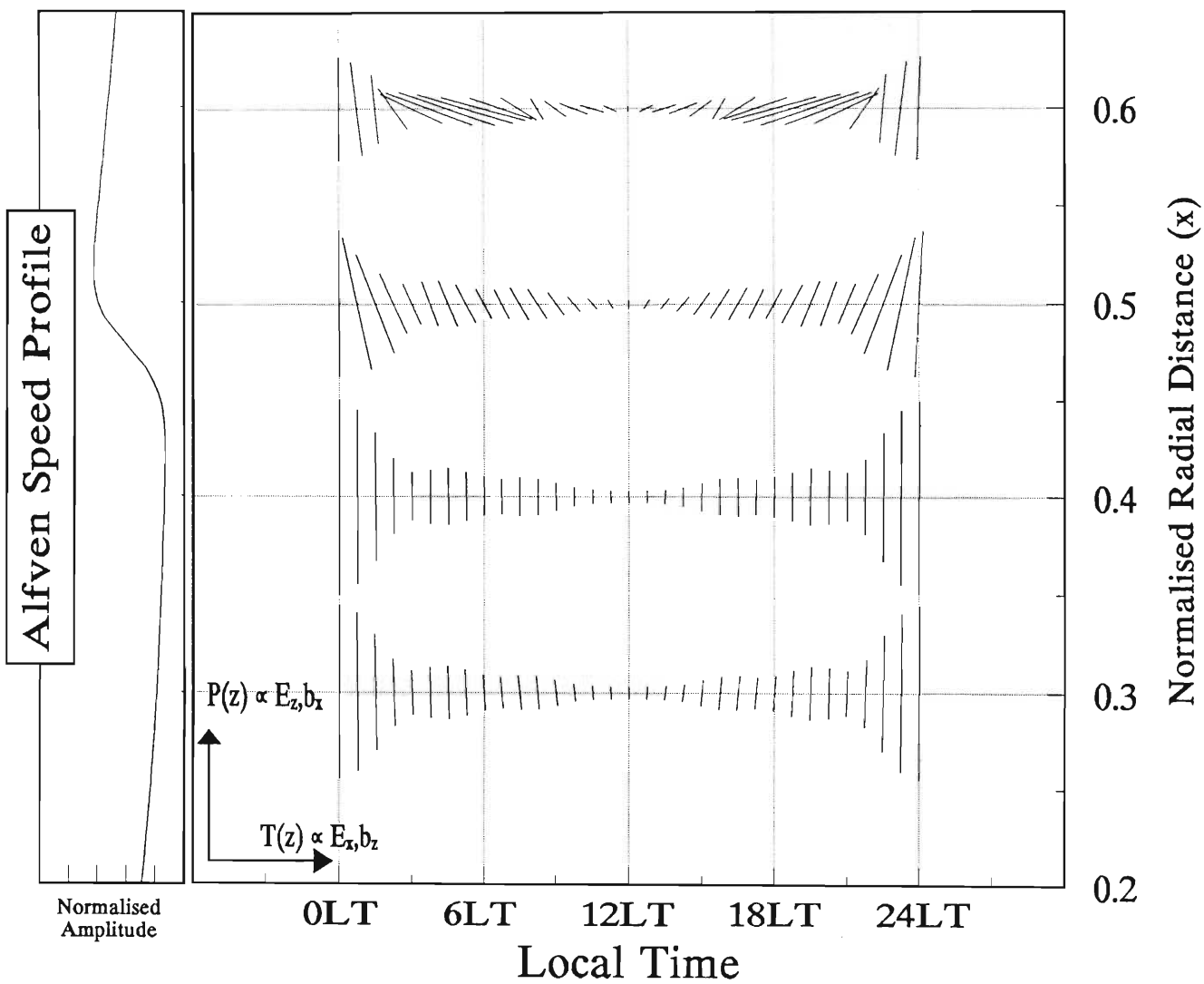

Figure 6.5: Major axis of the fundamental cavity-resonance polarization ellipse as a function of Local Time at radial distances $x = 0.3$, 0.4, 0.5 and 0.6. ($\kappa = 0.04$, $L_{pp} = 5.5$).

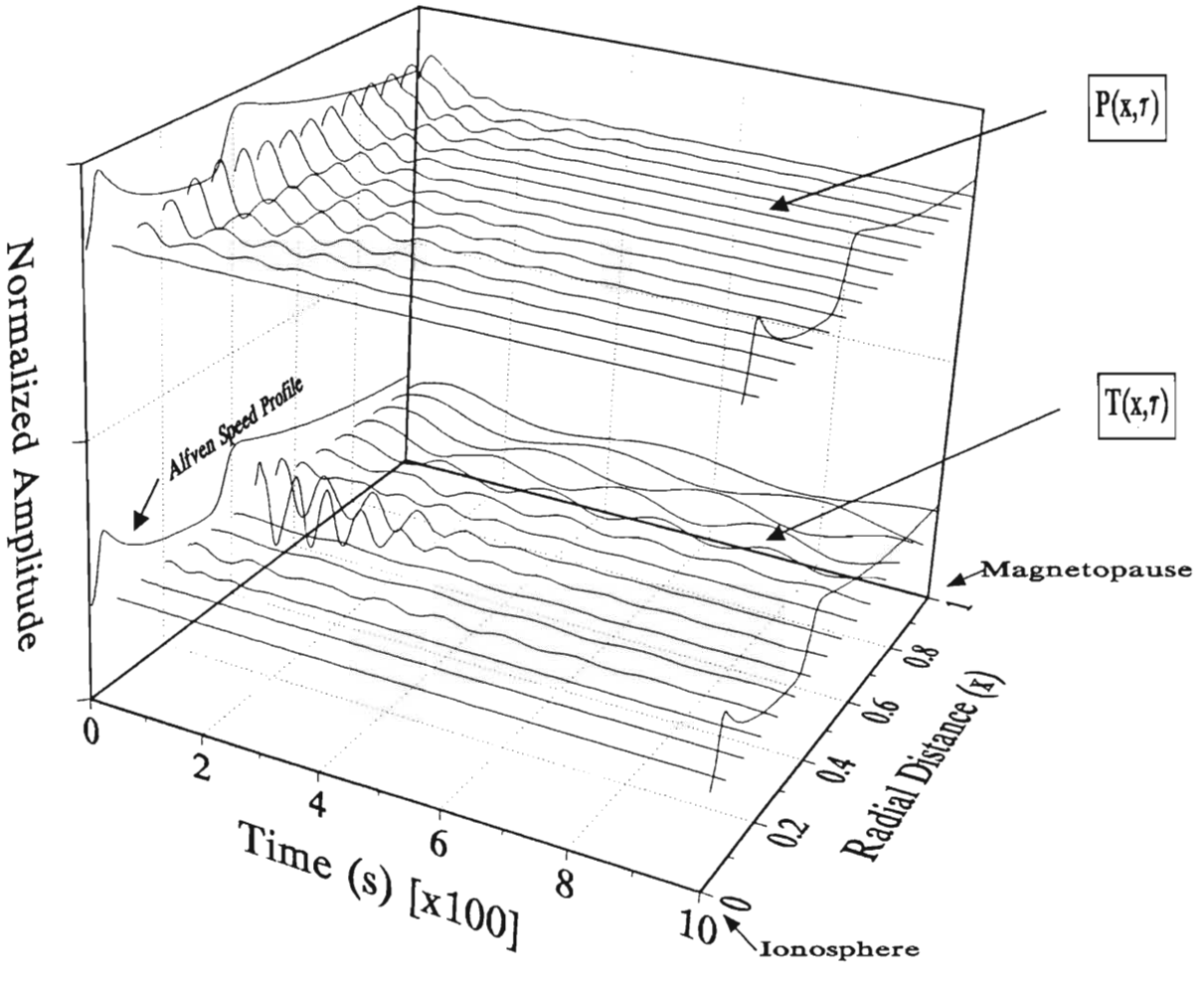

Figure 6.6: Temporal evolution of the cavity $P(x,\tau)$ and transverse resonance Alfvén $T(x,\tau)$ modes within the cavity. ($\kappa = 0.04$ and $L_{pp} = 4.5$).

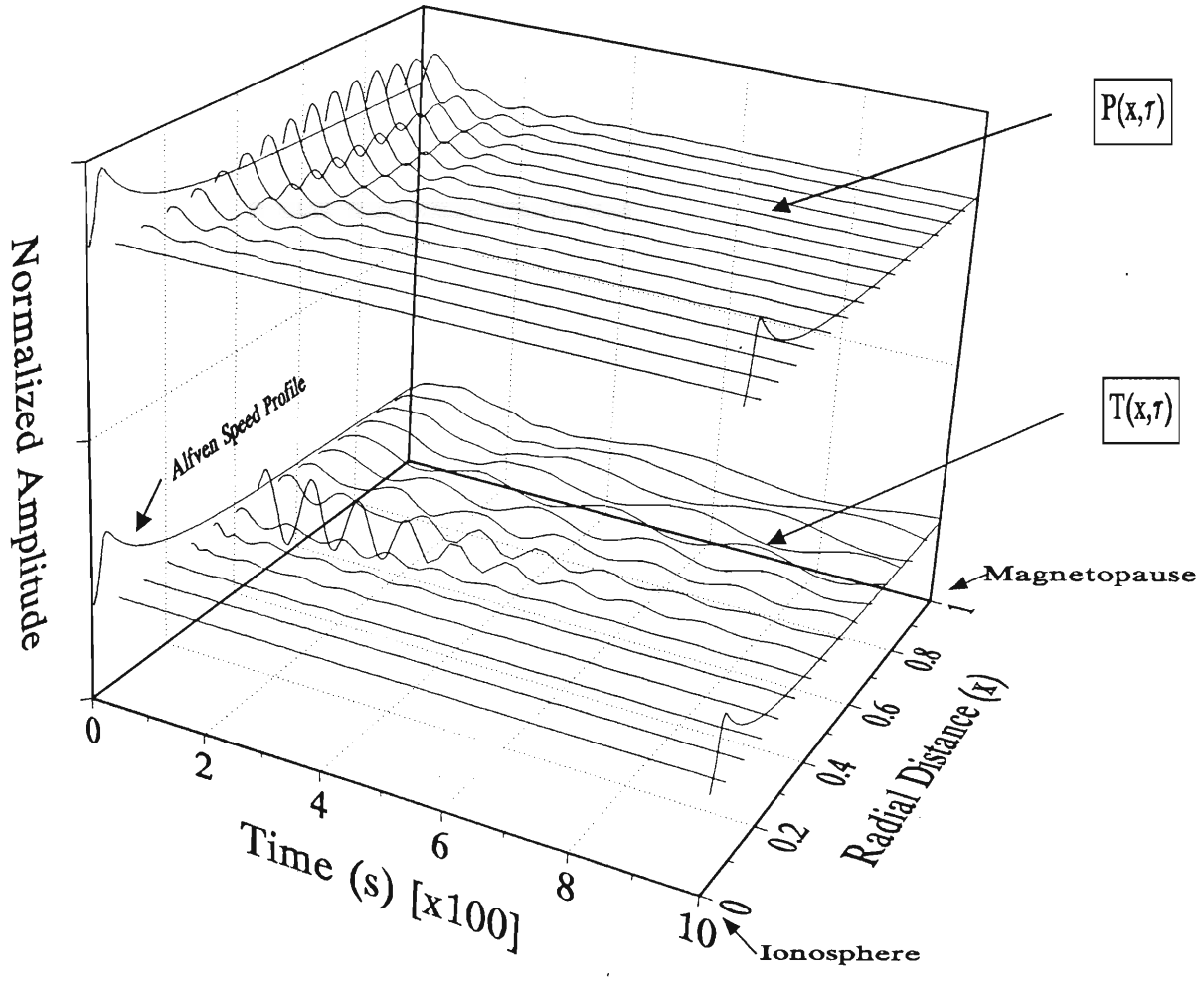

Figure 6.7: Temporal evolution of cavity and transverse Alfvén modes within the model cavity. No plasmapause case. $\kappa = 0.04$.

very low latitudes, the amplitude of the oscillations are significant. *Yeoman and Orr* [1989] pointed out that the plasmasphere cavity resonance is the likely mechanism for the mid-latitude Pi 2. The frequency and amplitude of the transverse Alfvén wave modes $T(x,\tau)$ in Fig 6.7, are similar to the case when the plasmapause was present (Fig. 6.6). A significant difference is that the waves appear to decay more slowly in Fig. 6.7. As in Fig. 6.6, large resonances occur where the frequency of the transverse Alfvénwave matches that of the dominant cavity modes. This resonance appears to occur at roughly the same radial position as in Fig. 6.7, this being coincidental as will be demonstrated in the next paragraph.

In Fig. 6.8 the plasmapause is located at $L_{pp} = 7$. The dominant cavity period is $\approx 2\tau_0$, approximately twice as long as in the case when the plasmapause is located at $L_{pp} = 4.5$ (in that case, the dominant period was $\tau_0 \approx 100$ s). This demonstrates that the location of the plasmapause directly affects the period of the cavity-mode oscillations. Furthermore, the oscillations are less damped in Fig 6.8 and appear to resemble Pc-type oscillations. The resonance in the transverse Alfvén mode (i.e where $T(x,\tau)$ has maximum amplitude, near the plasmapause) has period corresponding to that of the dominant cavity mode. Because of the longer fundamental cavity period, the Alfvén resonance is located deeper within the cavity (at higher latitudes) than in the case when the plasmapause was situated at $L_{pp} = 4.5$. From the above discussion, it is clear that the position of the plasmapause influences the frequency of the cavity modes which in turn affects the L-shell position at which the cavity-resonance coupling occurs.

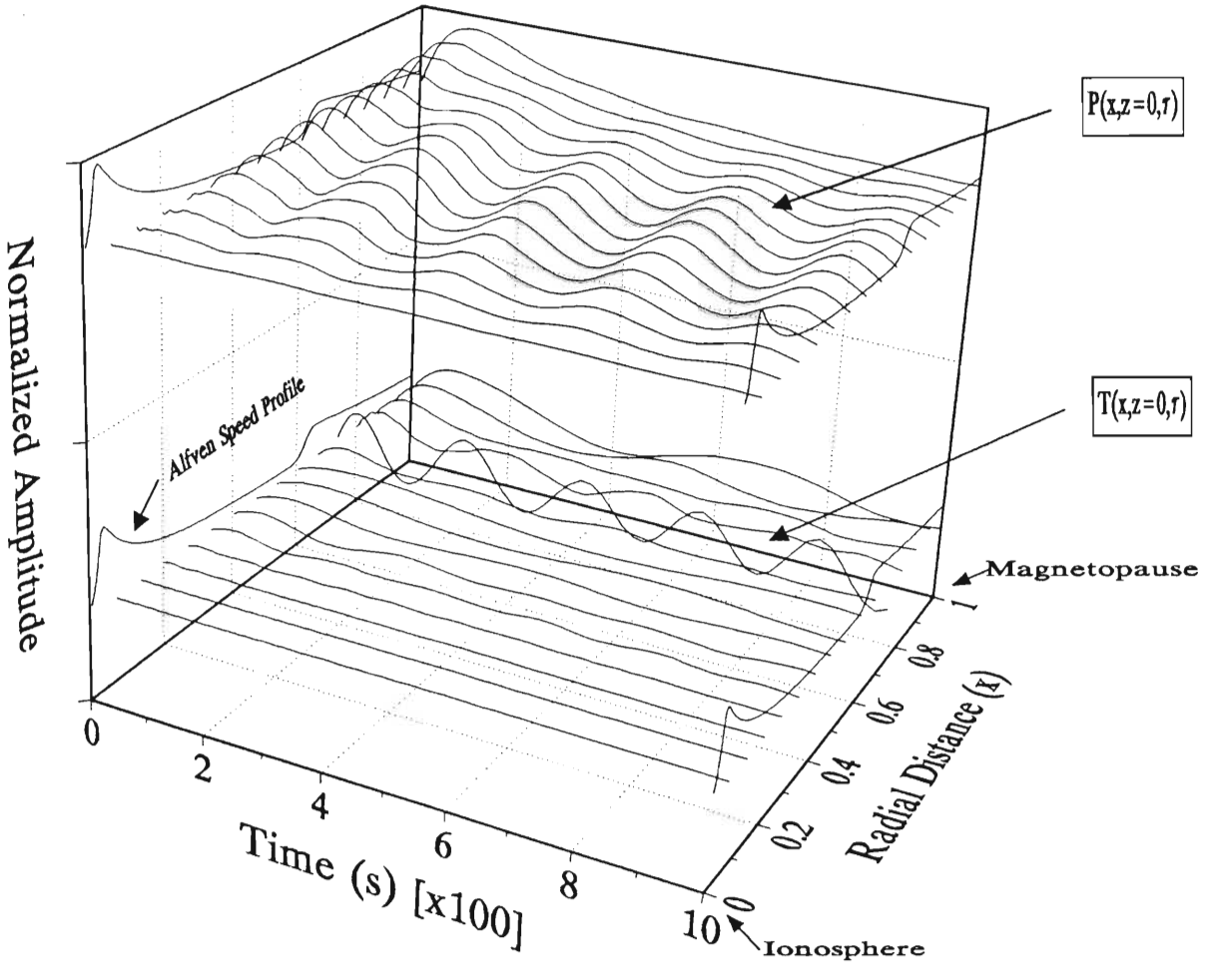

Figure 6.8: Temporal evolution of cavity and transverse Alfvén modes within the model cavity. Plasmapause is located at $L = L_{pp} = 7$. $\kappa = 0.04$.

6.7 The Effect of Field Aligned Harmonic Structure

Thus far we have investigated the nature of the cavity-resonance waves assuming a field aligned wave structure which exhibits a fundamental standing wave (i.e. $n = 1$ in equation 4.13). The cavity and transverse Alfvén components are plotted in Fig. 6.9 and Fig. 6.10 respectively for the case when $n = 2$, (i.e. a second harmonic field aligned wave structure is assumed). The spectral composition of the waves has changed (compare with Fig. 6.1 and Fig. 6.2) with the fundamental and second harmonic cavity modes now having periods T $\approx$ 53 s and T $\approx$ 76 s respectively. Within the plasmapause, the amplitudes of both wave modes are small such that at small radial distances (low latitudes), the oscillations are negligible. This conflicts with Pi 2 observations which show that, even at very low latitudes, they exhibit significant amplitude and are easily observable by ground based magnetometers. A similar trend is found in the case when $n = 3$ (third harmonic field aligned standing wave). The rapid decrease in wave amplitude at low latitudes for $n = 2$ and 3, make these modes unsuitable for describing Pi 2. This is in keeping with suggestions made from observations that Pi 2 have a fundamental (odd mode) field aligned structure.

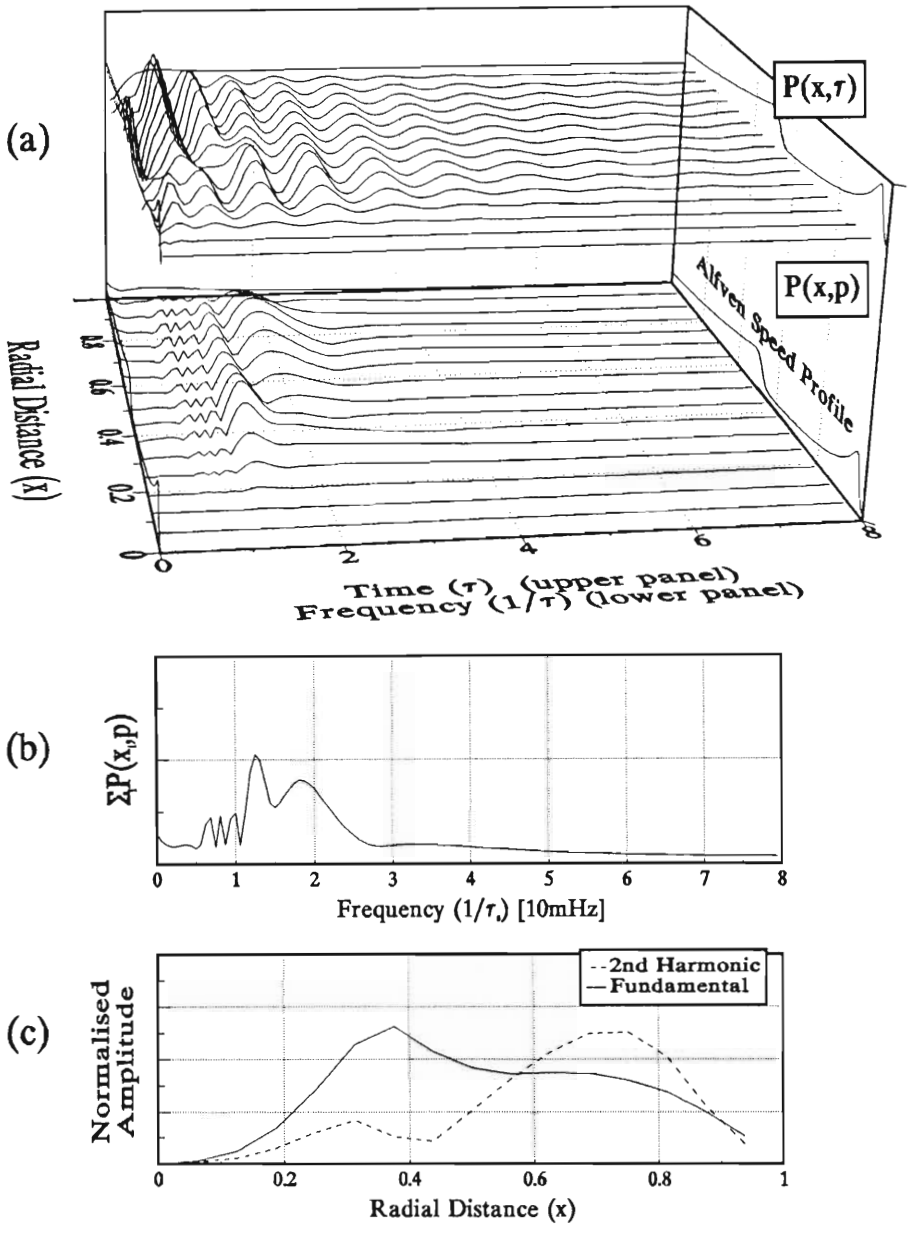

Figure 6.9: Temporal and spectral plots of the cavity waves for the case when the field aligned wave structure is assumed to be second harmonic, i.e. $n = 2$. ($\kappa = 0.04$ and $L_{pp} = 5.5$).

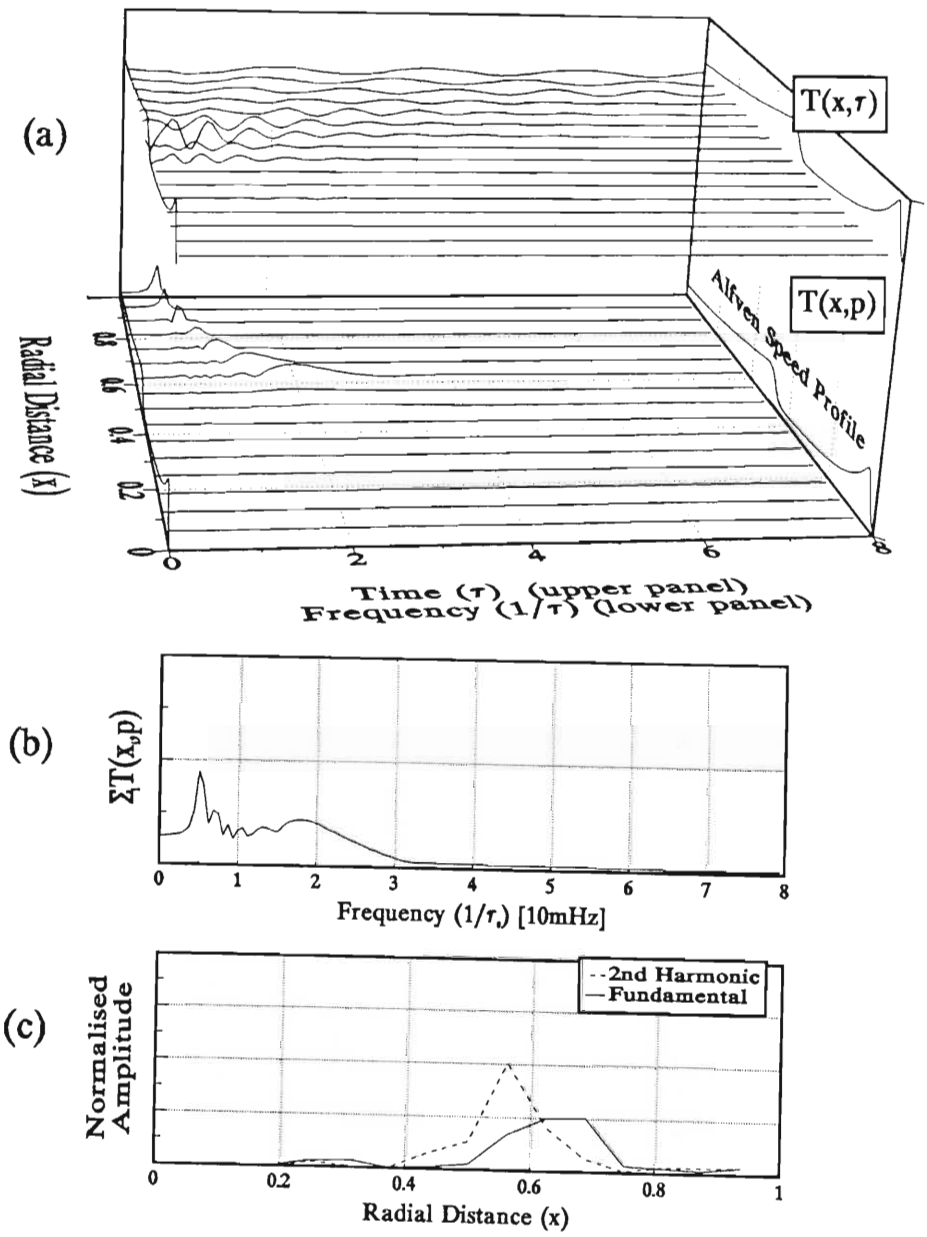

Figure 6.10: Temporal and spectral plots of the transverse Alfvén waves for the case when the field aligned wave structure is assumed to be second harmonic, i.e. $n = 2$. ($\kappa = 0.04$ and $L_{pp} = 5.5$).

6.8 Variation of Azimuthal Wavenumber with Radial Distance

In the simulations carried out by *Allan et al.*, [1987] with single azimuthal wavenumber, m, it was found that when a large m value was chosen, (they chose $m = 10$), the waves were more evanescent from the outer boundary than in the case for small m, ($m = 3$). In Fig 6.11 the azimuthal spectral/Fourier components corresponding to azimuthal wavenumbers $m = 1, 2, ...10$ are plotted as a function of radial distance. These curves were computed for the fundamental cavity mode excited by an impulse with an azimuthal form shown in Fig 5.2b. Within the cavity, low azimuthal wavenumber components have greater amplitude than those with high azimuthal wavenumber. The amplitudes of the low m components increase rapidly away from the outer boundary (i.e. with decreasing radial distance), while that of the high m components increase less rapidly, with some even decreasing in amplitude.

We now consider relative variation between the low and high m components. In Fig 6.12, the ratio of spectral amplitudes corresponding to azimuthal wavenumbers $m = 2$ and $m = 9$ (i.e. $\frac{A(m=2)}{A(m=9)}$) is plotted. In the proximity of the outer cavity boundary, the ratio $\frac{A(m=2)}{A(m=9)}$ decreases rapidly, which may be interpreted as a relative faster growth of the higher m components than the lower m components. The general trend thereafter is that the amplitude of the higher m component decreases faster with decreasing radial distance than that of the lower m component. (The exception is near the plasmapause where $\frac{A(m=2)}{A(m=9)}$ temporarily increases with decreasing radial distance).

The general nature of azimuthal wavenumber variations with radial distance described above is in agreement with that of *Allan et al.*, [1987]. In particular, the finding that high m components decay more rapidly than low m components away from the outer boundary corroborates well with the trend for Pi 2. The important difference is that, at high latitudes, (which would correspond an area near the outer boundary of this model), the amplitude of the high m components of Pi 2 are found to be larger than that of the low m components. From Fig 6.11 it is clear that near the outer boundary, the amplitudes of the low m components are greater than the high m components. We conclude that, on order to obtain an azimuthal wave structure that has larger high m components than low m components, the width of the disturbance must be necessarily narrower than that chosen for this work (Fig 5.2b). (The reader is reminded of the conditions imposed on the width of the spatial disturbance by the limitations of the inverse Laplace algorithm, see section 4.2.3).

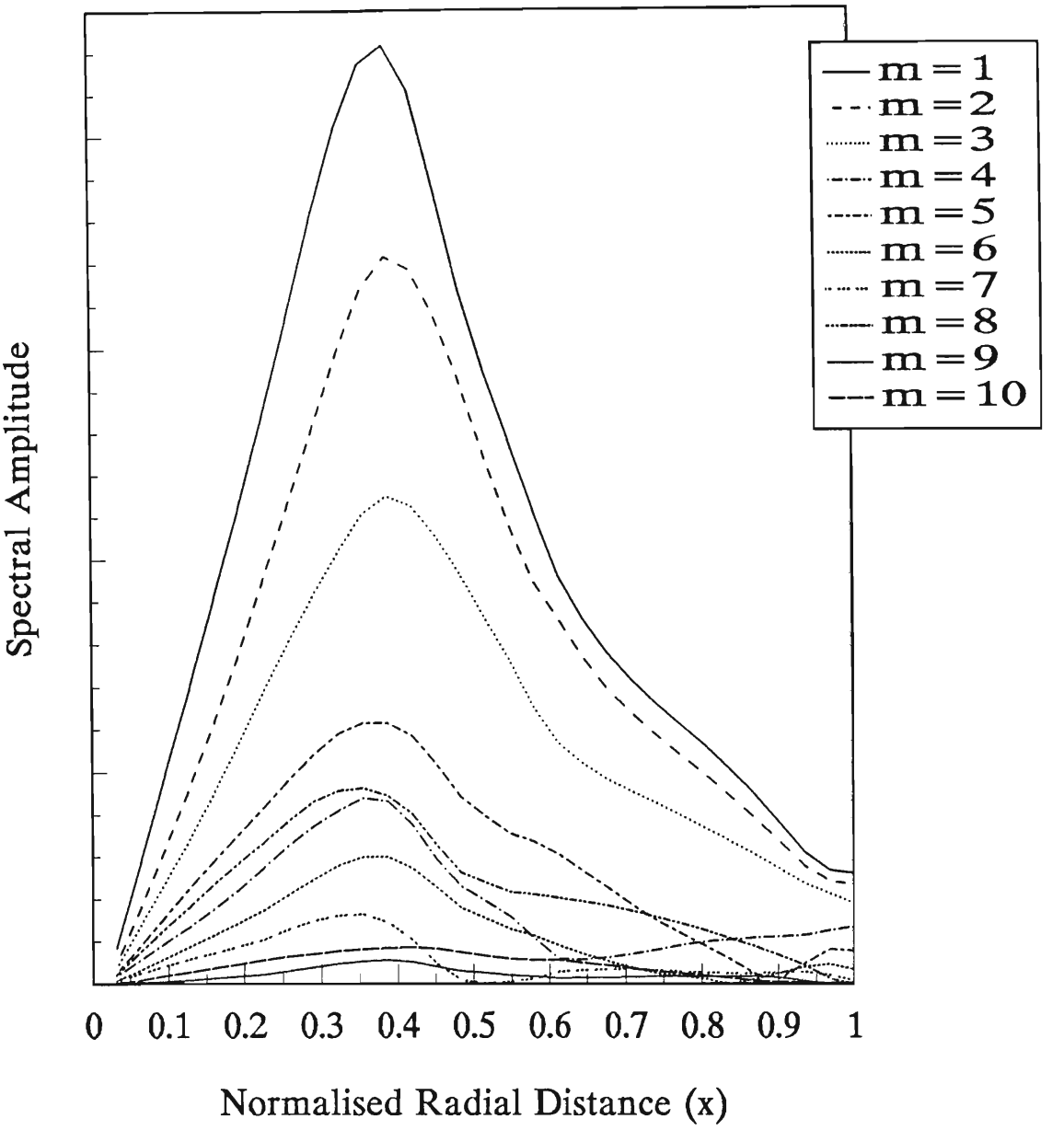

Figure 6.11: Amplitude variation with radial distance for azimuthal wavenumber spectra $m = 1, 2, .., 10$. (Constants for the integration: $\alpha = 0.01, n = 1, \Delta L_{pp} = \frac{1}{20} R_e$).

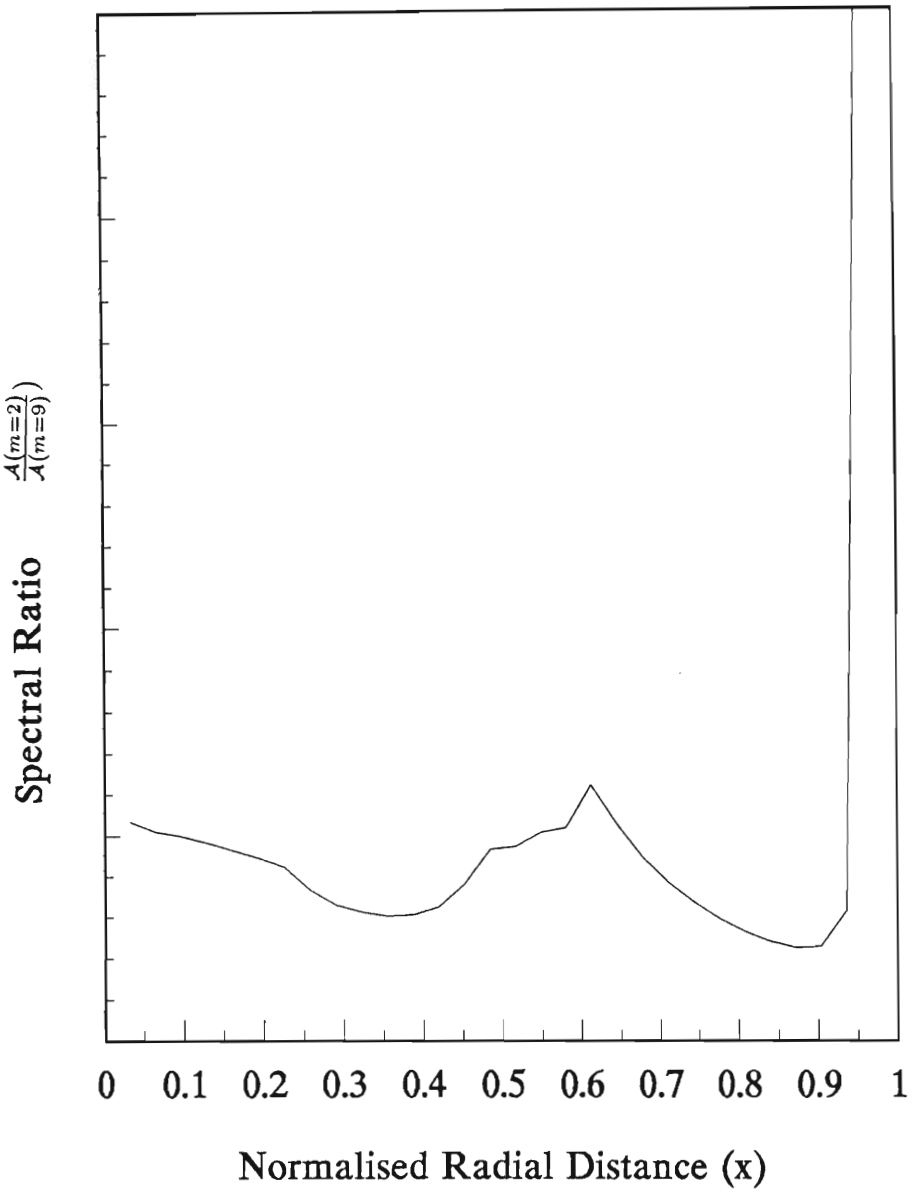

Figure 6.12: Ratio of spectral amplitudes $\frac{A(m=2)}{A(m=9)}$ as a function of radial distance for the components given in Fig (6.12).

Chapter 7

Conclusion

In this thesis, a three-dimensional MHD cavity-resonance model was developed to study the spatio-temporal response of a model magnetosphere to an externally imposed pressure perturbation (chapter 4). As an application, this model was used to investigate the nature of the magnetosphere's response to an impulse representative of the causative mechanism of the Pi 2.

In chapter 2, the major observational features of Pi 2 were reviewed. It was found that the nature of the events at high latitudes conflicts with that observed at mid and low latitudes. In particular, at auroral latitudes Pi 2 are observed to be spatially localized in Local Time to within a few hours about the midnight sector. Low-latitude Pi 2, on the other hand, are observed at all local times and have features which tends to suggest a global mode structure. Further features alluding to the global nature of low-latitude Pi 2 are the low azimuthal (or axial) wavenumber ($m \approx 1$) and, the lack of arrival time difference and a similarity between spectra, of events at globally separate observatories.

In chapter 3, some of the more important Pi 2 propagation mechanisms were reviewed. This was followed by some of the more recent developments in MHD cavity mode modelling. A scenario for the propagation of Pi 2 in terms of the cavity mode excitation was proposed.

In chapter 4, a MHD cavity-resonance model was developed to study the ULF response in the magnetosphere to a generalized, external compressional impulse. The MHD differential equations were derived in a cold, non-uniform plasma imbedded in a cylindrical ambient magnetic field geometry. The important feature of the model is that the response to a spatio-temporal impulse can be investigated at any point within the three-dimensional cavity.

For the study of Pi 2, a signal was chosen reflecting the causal mechanism of the event

thought to be the sudden, short circuiting of the cross tail current to the auroral oval. This model was used to investigate the nature of the cavity and transverse Alfvén modes. The effect of the plasmapause position was investigated. Further aspects of investigation included the polarization azimuth and phase between wave components as a function of Local Time. Where possible, computed results were compared with observation. Important findings of the investigation follow.

- Amplitude variations of the cavity-resonance waves compare favourably with that of Pi 2.
- Two dominant cavity modes lie within the Alfvén continuum. The period of these cavity modes fall within the Pi 2 range.
- At radial distances (or L-shells) where the cavity periods match that of the local transverse Alfvén period of oscillation, Alfvén resonances are established.
- The fundamental cavity mode is found to couple to the transverse Alfvén mode in the vicinity of the plasmapause (mid-latitudes).
- The second harmonic cavity mode has a node just earthward of the plasmapause. Associated with this node is a 180^0 phase change. On the other hand, the phase of the fundamental cavity mode is fairly constant with radial distance.
- The major azimuth of the equivalent mid latitude horizontal polarization ellipse (for the fundamental cavity component) is found to rotate in a right-handed sense (northern hemisphere) as one moves westward, and points north-south at Local Midnight. Within the plasmapause, the cavity-resonance waves are linearly polarized along the north-south meridian for all Local Time.
- The plasmapause appears to cause the cavity mode oscillations to be enhanced within the plasmapause. The position of the plasmapause affects the frequency of the cavity modes, with the period of the cavity modes longer for larger plasmaspheres.
- The waves in the outer cavity (plasmatrough) comprise both the cavity and transverse Alfvén modes.
- Along the field lines, a fundamental standing wave is found to be the best-fit for describing Pi 2.
- The high azimuthal wavenumber components are found to decay faster than the low azimuthal wavenumber components.

The fundamental nature of the cavity-resonance model shows pleasing agreement with that of Pi 2. Furthermore, the model satisfactorily describes some hitherto unexplained Pi 2 features. From this preliminary study, we conclude that the MHD cavity-resonance approach is a plausible one.

The model has its limitations. For example, the observed Pi 2 amplitude enhancements along the equatorial inner boundary (ionosphere) and the high latitude electrojet region (*Samson and Rostoker*, [1983]), are not accounted for by the model. Rather, amplitude enhancements in the Alfvén resonance waves calculated in this thesis have occurred in the plasmapause region, earthward of the auroral electrojet. A more realistic ionospheric conductivity function which would account for latitudinal as well as longitudinal variations would possibly explain this deficiency. A further model improvement would be to assume a dipole geometry representing the geomagnetic field rather than the cylindrical geometry chosen for this thesis. An advantage of the dipolar coordinate system is that azimuthal distances scale with radial distance, significant when studying, for example, the azimuthal wavenumber variations with latitude.

Further improvements may be made to the impulse signal by including a spatial perturbation along the field line. Another important enhancement in the modelling would be the numerical integration of the field aligned wave structure $f(\theta)$, rather than assuming it to be of a pre-determined standing wave form. However, it must be noted that each of these modifications represents an increase in the number of computational iterations required in order to obtain solutions. Each modification must be carefully weighed against the computational penalty of the modification. The choice of a dipolar field geometry, for example, would necessitate the use of a supercomputer (e.g. X-MP CRAY).

The model developed in this thesis does not represent a complete solution of the Pi 2 problem. This was not the aim. Our primary aim was to investigate the plausibility of the ULF cavity-resonance approach as an alternative model description for Pi 2. We have shown that the cavity-resonance waves have characteristics which correlate well with that of Pi 2, hence justifying the model approach adopted in this thesis.

References

Akasofu, S.-I., *Physics of Magnetospheric Substorms*, Reidel, Dordrecht, 1977.

Allan, W., Phase variation of ULF pulsations along the geomagnetic field line, *Planet. Space Sci., 30*, 339, 1982.

Allan, W., and F. B. Knox, A dipole field model for axisymmetric Alfvén waves with finite ionospheric conductivities, *Planet. Space Sci., 27*, 79, 1979.

Allan, W., E. M. Poulter, K. -H. Glassmeier and H. Junginger, Spatial and temporal structure of a high - latitude transient pulsation, *Planet. Space Sci., 33*, 159-173, 1985a.

Allan, W., S. P. White and E. M. Poulter, Magnetospheric coupling of hydromagnetic waves - initial results, *Geophys. Res. Lett., 12*, 287, 1985b.

Allan, W., S. P. White and E. M. Poulter, Impulse excited hydromagnetic cavity and fieldline resonances in the magnetosphere, *Planet. Space Sci., 34*, 371, 1986a.

Allan, W., S. P. White and E. M. Poulter, Hydromagnetic wave coupling in the magnetosphere — plasmapause effects on impulse-excited resonances, *Planet. Space Sci., 34*, 1189, 1986b.

Allan, W. E. M. Poulter and S. P. White, Hydromagnetic wave coupling in the magnetosphere - magnetic fields and poynting fluxes, *Planet. Space Sci., 35*, 1181, 1987.

Atkinson, G., The expansive phase of the magnetospheric substorm, in *Dynamics of the Magnetosphere*, (Edited by Akasofu, S.-I.), p.461. Reidel, Dordrecht., 1979.

Baumjohann, W., and K.-H. Glassmeier, The transient response mechanism and Pi 2 pulsations at substorm onset — review and outlook, *Planet. Space Sci., 32*, 1361, 1984.

Baumjohann, W., H. Junginger, G. Haerendel, and O. H. Bauer, Resonant Alfvén waves excited by a sudden impulse, *J. Geophys. Res., 89*, 2765, 1984.

Bjőrnsson, A., O. Hillebrand, and H. Voelker, First observational results of geomagnetic Pi 2 and Pc 5 pulsations on a north-south profile through Europe, *Zeitshr,*

Geophys., 37, 1031, 1971.

Chen, L., and A. Hasegawa, A theory of long period magnetic pulsations, 1, Steady state excitation of field line resonances, *J. Geophys. Res., 79,* 1024, 1974.

Clauer, C. R., and R. L. McPherron, Mapping the local time-universal time development of magnetospheric substorms using mid-latitude magnetic observatories, *J. Geophys. Res., 79,* 2811, 1974.

Cummings, W. D., O'Sullivan, R. J., and Coleman, P. J., Jr., Standing Alfvénwaves in the magnetosphere, *J. Geophys. Res., 74,* 778, 1969.

Doobov, A. L., *J. Atmos. Terr. Phys.,* 35, 971, 1973.

Doobov, A. L., and J. S. Mainstone, Investigations of Pi 2 micropulsations, I, Frequency spectra and polarization, *Planet. Space Sci., 21,* 721, 1973.

Dungey, J. W., Electrodynamics of the outer atmosphere, *Tech. Rep., 69* Pa. State Univ., University Park, Pa., 1954.

Dungey, J. W., Hydromagnetic waves, In *Physics of Geomagnetic Phenomena, edited* by W. H. Campbell and S. Matsushita, p.913, San Diego, Calif., 1968.

Friis-Christensen, E., M. A. McHenry, C. R. Clauer, and S. Vennerstrom, Ionospheric travelling convection vortices observed near the polar cleft: A triggered response to sudden changes in the solar wind, *Geophys. Res. Lett., 15,* 253, 1988.

Fukunishi, H., and Hirasawa, *Rep. Ionosph. Space. Res. Japan, 24,* 45, 1970.

Fukunishi, H., Polarization changes of geomagnetic Pi 2 pulsations associated with the plasmapause, *J. Geophys. Res., 80,* 98, 1975.

Gelpi, C., W. J. Hughes, and H. J. Singer, Longitudinal phase and polarization characteristics in mid latitude Pi 2 pulsations, *J. Geophys. Res., 90,* 9905, 1985a.

Gelpi, C., W. J. Hughes, H. J. Singer, and M. Lester, Mid-latitude Pi 2 polarization pattern and synchronous orbit magnetic activity, *J. Geophys. Res., 90,* 6451, 1985b.

Gelpi, C.,H. J. Singer, and W. J. Hughes, A comparison of magnetic signatures and DMSP auroral images at substorm onset: Three case studies, *J. Geophys. Res., 92,* 2447, 1987.

Glassmeier, K.-H., H. Volpers, and W. Baumjohann, Ionospheric Joule dissipation as a damping mechanism for high latitude ULF pulsations: Observational evidence, *Planet. Space Sci., 32,* 1463, 1984.

Glassmeier, K.-H., W. Baumjohann, A. Korth, and P. Gough, High latitude Pi 2 pulsations, ELF intensity, and particle flux variations, A case study, *Ann. Geophys., 6,* 287-296, 1988.

Green, C. A., and W. F. Stuart, Apparent phase velocities of Pi 2s, *Paper presented in IAGA General Assembly*, Canberra, Australia, 1979

Hasegawa, A. K., H. Tsui, and A. S. Assis, A theory of long-period magnetic pulsations, 3, Local field line oscillations, *Geophys. Res. Lett.*, *10*, 765, 1983.

Hattingh, S. K. F., A realistic model for determining the eigenperiods of ULF geomagnetic pulsations at low latitudes, *M. Sc. thesis, University of Natal*, 1987.

Holmberg, E. R., Rapid periodic fluctuations of the geomagnetic field, I, *Mon. Not. R. Astron. Soc., Geophys. Suppl.*, *6*, 476, 1953.

Hopcraft, K. I., and P. R. Smith, Polarization characteristics of Pi 2 oscillations, *Planet. Space Sci.*, *34*, 1259, 1986.

Hughes, W. J., Hydromagnetic waves in the magnetosphere, *Rev. Geophys.*, *21*, 508, 1983.

Inhester, B., Numerical modeling of hydromagnetic wave coupling in the magnetosphere, *J. Geophys. Res.*, *92*, 4751, 1987.

Jacobs J. A., *Geomagnetic Micropulsations,* Heidelberg Springer-Verlag, New York, 1970.

Jacobs, J. A., and K. Sinno, Worldwide characteristics of geomagnetic micropulsations, *Geophys. J.*, *3*, 333, 1960.

Jacobs J. A., Y. Kato, S. Matsushita, and V. A. Troitskaya, Classification of geomagnetic pulsations, *J. Geophys. Res.*, *69*, 180, 1964.

Jamet, F., R. Remoit, J. Roquet, and E. Selzer, *C.r. hebd. Séanc. Acad. Sci., Paris*, 269 442, 1969.

Kan, J. R., D. U. Longenecker, and J. V. Olson, A transient response model of Pi 2 pulsations, *J. Geophys. Res.*, *87*, 7483, 1982.

Kan, J. R., and W. Sun, Simulation of the westward traveling surge and Pi 2 pulsation during substorms, *J. Geophys. Res.*, *90*, 10911, 1985.

Kato, Y., J. Osaka, and M. Okuda, Investigation of the magnetic disturbance by the induction magnetograph, III, On the magnetic storms, *Sci. Rep. Tohuku Univ., Ser. 5, 3*, 85, 1953.

Kitamura, T.-I., O. Saka, M. Shimoizumi, H. Tachihara, T. Oguti, T. Araki, N. Sato, M. Ishitsuka, O. Veliz, J. B. Nyobe, Global mode of Pi2 waves in the equatorial region — Difference of Pi2 mode between high and equatorial latitudes, *J. Geomagn. Geoelectr.*, *40*, 621, 1988.

Kivelson G. K., Etcheto, J., and J. G. Trotignon, Global compressional oscillations of the terrestrial magnetosphere: The evidence and a model, *J. Geophys. Res.*, *89*, 9851, 1984.

Kivelson, M. G., and D. J. Southwood, Resonant ULF waves: A new interpretation, *Geophys. Res. Lett., 12*, 49, 1985.

Kivelson, M. G., and D. J. Southwood, Coupling of global magnetospheric MHD eigen modes to field line resonances, *J. Geophys. Res., 91*, 4345, 1986.

Kivelson, M. G., D. J. Southwood, Hydromagnetic waves and the ionosphere, *Geophys. Res. Lett., 15*, 1271, 1988.

Krauss-Varban, D., and V. L. Patel, Numerical analysis of the coupled hydromagnetic wave equations in the magnetosphere, *J. Geophys. Res., 93*, 9721, 1988.

Kuwashima, M., *Mem. Nat. Inst. Polar Res. Series A, No. 15*, 1978.

Kuwashima, M., and T. Saito, Spectral characteristics of magnetic Pi 2 pulsations in the auroral region and lower latitudes, *J. Geophys. Res., 86,* 4686, 1981.

Lanzerotti, L. J., and H. Fukunishi, Modes of magnetohydrodynamic waves in the magnetosphere, *Rev. Geophys., 12,* 724, 1974.

Lanzerotti, L. J., and L. V. Medford, Local night, impulsive (Pi 2 type) hydromagnetic wave polarization at low latitudes, *Planet. Space Sci., 32,* 135, 1984.

Lee, D. H., and R. L. Lysak, Magnetospheric ULF wave coupling in the dipole model: the impulsive excitation, *J. Geophys. Res., 94*, 17097, 1989.

Lee, D. H., and R. L. Lysak, Effects of azimuthal asymmetry on ULF waves in the dipole magnetosphere, *Geophys. Res. Lett., 17*, 53, 1990.

Lester, M., and D. Orr, The spatio-temporal characteristics of Pi 2's *J. Atmos. Terr. Phys., 43,* 947, 1981.

Lester, M., and D. Orr, Correlation between ground observations of Pi 2 geomagnetic pulsations and satellite plasma density observations, *Planet. Space Sci., 31,* 143, 1983.

Lester, M., W. J. Hughes, and H. J. Singer, Polarization patterns of Pi 2 magnetic pulsations and the substorm current wedge, *J. Geophys. Res.*, 88, 7958, 1983.

Lester, M., W. J. Hughes, and H. J. Singer, Longitudinal structure in Pi 2 pulsations and the substorm current wedge, *J. Geophys. Res., 89*, 5489, 1984.

Lester, M., K.-H. Glassmeier, and J. Behrens, Pi 2 pulsations and the eastward electrojet: a case study, *Planet. Space Sci., 33,* 351, 1985.

Lester, M., H. J. Singer, D. P. Smits, and W. J. Hughes, Pi 2 pulsations and the substorm current wedge: low-latitude polarization, *J. Geophys. Res., 94*, 17133, 1989.

Lin, C. C., L. J. Cahill, Jr., Pi 2 pulsations in the magnetosphere, *Planet. Space Sci., 23,* 693, 1975.

Lysak, R. L., C. T. Dum, Dynamics of magnetosphere-ionosphere coupling including turbulent transport, *J. Geophys. Res.*, *88*, 365, 1983.

Mainstone, J. S., *Ann. Géophys.*, 26, 735, 1970.

Maltsev, Y. P., S. V. Leontyev, and W. B. Lyatsky, Pi 2 pulsations as a result of evolution of an Alfvén impulse originating in the ionosphere during a brightening of aurora, *Planet. Space Sci.*, *22*, 1519, 1974.

McPherron, R. L., Substorm associated micropulsations at synchronous orbit, *J. Geomagn. Geoelectr.*, *32*, suppl. II, SII57, 1980.

McPherron, R. L., C. T. Russell, and M. P. Aubry, Satellite studies of hydromagnetic substorms on August 15, 1968, 9, Phenomenological model for substorms, *J. Geophys. Res.*, *78*, 3131, 1973.

McPherron, R. L., Magnetospheric substorms, *Rev. Geophys. Space Phys.*, *22*, 1519, 1979.

Mier-Jedrzejowicz, W. A. C., and D. J. Southwood, The east-west structure of mid-latitude geomagnetic pulsations in the 8-25 mHz band, *Planet. Space Sci.*, *27*, 617, 1979.

Moortgat, K. T., Cattell, C. A., Mozer, F. S., Elphic, R., On the search for evidence of fast mode compressions in the near-earth tail: ISEE observations, *J. Geophys. Res.*, *95*, 18887, 1990.

Nagai, T., Observed magnetic substorm signatures at synchronous altitude, *J. Geophys. Res.*, *87*, 4405, 1982.

Newton, R. S., D. J. Southwood, and W. J. Hughes, Damping of geomagnetic pulsations by the ionosphere, *Planet. Space Sci.*, *26*, 201, 1978.

Nishida, A., Geomagnetic Diagnosis of the Magnetosphere, *Springer-Verlag, New York*, 1978.

Olson, J. V., and G. Rostoker, Latitude variations of the spectral components of auroral zone Pi 2, *Planet. Space Sci.*, *25*, 663, 1977.

Orr, D., Magnetic pulsations within the magnetosphere: A review, *J. Atmos. Terr. Phys.*, *35*, 1, 1973.

Orr, D., Probing the plasmapause by geomagnetic pulsations, *Ann. Geophys.*, *31*, 77, 1975.

Orr, D., and H. G. Barsczus, Geomagnetic micropulsations, Pi 2, at low latitudes, *Planet. Space Sci.*, *17*, 497, 1969.

Pashin, A. B., K.-H. Glassmeier, W. Baumjohann, O. M. Raspopov, A. G. Yaknin, H. H. Opgenoorth, and R. J. Pellinen, Pi 2 magnetic pulsations, auroral break-ups, and the substorm current wedge: a case study, *J. Geophys.*, *51*, 223, 1982.

Pekrides, H., Numerical modelling of Pc 4-5 compressional pulsations in the magnetosphere, *MSc Thesis*, University of Natal, Durban, South Africa, 1989.

Piessens, R., and M. Branders, Numerical inversion of the Laplace transform using generalized Laguerre polynomials, *Proc. IEEE,. 118*, 1517, 1971.

Potemra, T. A., H. Lűhr, L. J. Zanetti, K. Takahashi, R. E. Erlandson, G. T. Marklund, L. P. Block, L. G. Blomberg, and R. P. Lepping, Multisatellite and ground-based observations of transient ULF waves, *J. Geophys. Res., 94*, 2543, 1989.

Poulter, E. M., and E. Nielsen, The hydromagnetic oscillation of individual shells of the geomagnetic field, *J. Geophys. Res., 87*, 10432, 1982.

Press, H., B. P. Flannery, S. A. Teukolsky, and W. T. Vetterling, *Numerical Recipes: The art of scientific computing,* Cambridge University Press, Cambridge, 1986.

Radoski, H., A theory of latitude dependent geomagnetic micropulsations: the asymptotic fields, *J. Geophys. Res., 79*, 595, 1974.

Raspopov, O. M., *Geomag. and Aeronomy, 8*, 257, 1968.

Raspopov, O. M., V. A. Troitskaya, L. N. Baranskiy, B. N. Belenkaya, V. K. Koshelevskiy, L. T. Afans'yeva, J. Rox, and O. Fambitokoya, Properties of geomagnetic Pi 2 pulsation spectra along a meridional profile, *Geomagn., Aeronomy, 12,* 772, 1972.

Rostoker, G., Propagation of Pi 2 micropulsations through the ionosphere, *J. Geophys. Res., 70,* 4388, 1965.

Rostoker, G., The polarization characteristics of Pi 2 micropulsations and their relation to the determination of possible source mechanisms for the production of nighttime impulsive micropulsation activity, *Can. J. Phys., 45,* 1319, 1967.

Rostoker, G., and J. V. Olson, Pi 2 micropulsations as indicators of substorm onsets and intensifications, *J. Geomag. Geoelectr., 30*, 135, 1978.

Rostoker, G., and J. C., Samson, Polarization characteristics of Pi 2 pulsations and implications for their source mechanisms: location of source regions with respect to the auroral electrojets., *Planet. Space Sci., 29*, 255, 1981.

Rothwell, P. L., M. B. Silevitch, and L. P. Block, Pi 2 pulsation and the westward travelling surge, *J. Geophys. Res., 91*, 6921, 1986.

Rothwell, P. L., M. B. Silevitch, and L. P. Block, and P. Tanskanen, A model of the westward traveling surge and the generation of Pi 2 pulsations, *J. Geophys. Res., 93*, 8613, 1988.

Saito, T., Geomagnetic pulsations, *Space Sci. Rev., 10,* 319, 1969.

Saito, T., and S. Matsushita, *J, geophys. Res., 73*, 267, 1968.

Saito, T., Magnetospheric study, *Proc. Int. Workshop on Selected Topics of Magnetospheric Physics,* Tokyo (Japan), March 1979, p. 104, 1979.

Saito, T., and S. Matsushita, Solar cycle effects on geomagnetic Pi 2 pulsations, *J. geophys Res., 73*, 267, 1968.

Saito, T., T. Sakurai, and Y. Koyama, Mechanism of association between Pi 2 pulsation and magnetospheric substorm, *J. Atmos. Terr. Phys., 38*, 1265, 1976a.

Saito, T., K. Yumoto, and Y. Koyama, Magnetic pulsation Pi 2 as a sensitive indicator of magnetospheric substorm, *Planet. Space Sci., 24*, 1025, 1976b.

Saka, O., T. Kitamura, M. Shimoizumi, T. Araki, T. Oguti, O. Veliz, and M. Ishitsuka, The effects of non-uniform ionosphere on the equatorial Pc pulsations, *J. Geomag. Geoelectr., 40*, 635, 1988.

Sakurai, T., and R. L. McPherron, Satellite observations of Pi 2 activity at synchronous orbit, *J. Geophys. Res., 88,* 7015, 1983.

Sakurai, T., and T. Saito, Magnetic pulsation Pi 2 and substorm onset, *Planet. Space Sci., 24*, 573, 1976.

Samson, J. C., Pi 2 pulsations: High latitude results, *Planet. Space Sci., 30*, 1239, 1982.

Samson, J. C., Large-scale studies of Pi-2's associated with auroral breakups, *J. Geophys., 56*, 133, 1985.

Samson, J. C., and B. G. Harrold, Maps of the polarizations of high latitude Pi 2's, *J. Geophys. Res., 88,* 5736, 1983.

Samson, J. C., and B. G. Harrold, Characteristic time constants and velocities of high-latitude Pi 2s, *J. Geophys. Res., 90*, 12173, 1985.

Samson, J. C., and G. Rostoker, Polarization characteristics of Pi 2 pulsations and implications for their source mechanisms, 2, Influence of the westward travelling surge, *Planet. Space Sci., 31,* 435, 1983.

Samson, J. C., and B. G. Harrold, and K. L. Yeung, Characteristic time constants and velocities of mid-latitude Pi 2's, *J. Geophys. Res., 90*, 3448, 1985.

Samson, J. C., R. A. Greenwald, J. M. Ruohoniemi, T. J. Hughes, and D. D. Wallis, Magnetometer and radar observations of magnetohydrodynamic cavity modes in the earth's magnetosphere, *Can. J. Phys., 69*, 929, 1991.

Sastry, T. S., Y. S. Sarma, S. V. S. Sarma, and P. V. Sanker Narayan, Day-time Pi pulsations at equatorial latitudes, *J. Atmos. Terr. Phys., 45*, 733, 1983.

Sato, T., Auroral physics, in *Magnetospheric Plasma Physics*, edited by A. Nishida, pp. 197-243, D. Reidel, Hingham, Mass., 1982.

Sibeck, D. G., W. Baumjohann, and R. E. Lopez, Solar wind dynamic variations and transient magnetospheric signatures, *Geophys. Res. Lett., 16*, 13, 1989.

Singer, H. J., W. J. Hughes, P. F. Fougere, and D. J. Knecht, The localization of Pi 2 pulsations: Ground-satellite observations, *J. Geophys. Res.*, *88*, 7029, 1983.

Singer, H. J., W. J. Hughes, M. Lester, D. J. Knecht, and C. Gelpi, Ground-satellite observations of substorm related Pi 2 pulsations and current systems, Proceedings of Conference on Achievements of the International Magnetospheric Study, Eur. Space Agency Spec. Publ., *ESA SP-217*, 697, 1984.

Smith B. P., On the occurrence of Pi 2 micropulsations, *Planet. Space Sci.*, *21,* 831, 1973.

Southwood, D. J., Some features of field line resonance in the magnetosphere, *Planet. Space Sci.*, *22*, 483, 1974.

Southwood, D. J., and W. J. Hughes, Concerning the structure of Pi 2 pulsations, *J. Geophys. Res.*, *90*, 386, 1985.

Southwood, D. J., and M. G. Kivelson, The magnetohydrodynamic response of the magnetospheric cavity to changes in solar wind pressure, *J. Geophys. Res.*, *95*, 2301, 1990.

Southwood, D. J., and W. F. Stuart, Pulsations at the substorm onset, In *Dynamics of the Magnetosphere,* edited by S.-I. Akasofu, pp. 341, D. Reidel, Hingham, Mass., 1980.

Stuart, W. F., *J. Atmos. Terr. Phys.*, *34*, 817, 1972.

Stuart, W. F., A mechanism of selective enhancement of Pi 2's by the plasmasphere, *J. Atmos. Terr. Phys.*, *36*, 851, 1974.

Stuart, W. F., and H. G. Barsczus, Pi's observed in the daylight hemisphere at low latitudes, *J. Atmos. Terr. Phys.*, *42*, 487, 1980.

Stuart, W. F., L. N. Baranskiy, Simultaneous observations of Pi 2 pulsations on N-S meridians in the U.K. and Scandinavia, *J. Atmos. Terr. Phys.*, 1982.

Stuart, W. F., and D. C. Booth, A study of the power spectra of Pc's and Pi 2's, *J. Atmos. Terr. Phys.*, *36*, 835, 1974.

Stuart, W. F., and A. N. Hunter, *J. Atmos. Terr. Phys.*, *37,* 369, 1975.

Stuart, W. F., P. M. Brett, and T. J. Harris, Mid-latitude secondary resonances in Pi 2's., *J. Atmos. Terr. Phys.*, *41*, 65, 1979.

Sutcliffe, P. R., Some aspects of Pi 2 morphology, *Proceedings of the International Workshop on Selected Topics of Magnetospheric Physics,* Japanese IMS Committee, Tokyo, 94, 1979.

Sutcliffe, P. R., The longitudinal range of Pi2 propagation at low latitudes, *Planet. Space Sci., 28*, 9, 1980.

Sutcliffe, P. R., Ellipticity variations in Pi 2 pulsations at low latitudes, *Geophys. Res. Lett.*, *8*, 91, 1981.

Sutcliffe, P. R., E. Nielsen, STARE observations of Pi 2 pulsations, *Geophys. Res. Lett.*, *17*, 603, 1990.

Sutcliffe, P. R., E. Nielsen, The ionospheric signature of Pi 2 pulsations observed by STARE, *J. Geophys. Res.*, *in press*, 1992.

Sutcliffe, P. R., and K. Yumoto, Dayside Pi 2 pulsations at low latitudes, *Geophys. Res. Lett.*, *16*, 887, 1989.

Sutcliffe, P. R., and K. Yumoto, On the cavity nature of low-latitude Pi 2 pulsations, *J. Geophys. Res.*, *96*, 1543, 1991.

Takahashi, K., S.-I. Ohtani, and K. Yumoto, AMPTE CCE observations of Pi 2 pulsations in the inner magnetosphere, *Submitted to Geophys. Res. Lett.*, 1992.

Tamao, T., and A. Miura, Coupling instability of the shear Alfvénwave in the magnetosphere with the ionospheric ion drift wave. 1. Energetic consideration, *J. Geophys. Res.*, *87*, 905, 1982.

Taylor, J. P. H., and A. D. M. Walker, Accurate approximate formulae for toroidal standing hydromagnetic oscillations in a dipolar geomagnetic field, *Planet. Space Sci.*, *32*, 1119, 1984.

Taylor, J. P. H., and A. D. M. Walker, Theory of magnetospheric hydromagnetic standing waves with large azimuthal wavenumber - 2. Eigenmodes of the magnetosonic and Alfvén oscillations, *J. Geophys. Res.*, *92*, 10046, 1987.

Verő, J., Experimental aspects of low-latitude pulsations - A review, *J. Geophys.*, *60*, 106, 1986.

Walker, A. D. M., Theory of magnetospheric hydromagnetic standing waves with large azimuthal wavenumber - 1. Coupled magnetosonic and Alfvén waves, *J. Geophys. Res.*, *92*, 10039, 1987.

Walker, A. D. M., and J. C. Samson, A magnetohydrodynamic model of substorm intensifications, *Submitted to J. Geophys. Res.*, 1992.

Yanagihara, K., and N. Shimizu, Equatorial enhancement of micropulsations Pi - 2, *Mem. Kakioka Magn. Obs.*, *12*, 57, 1966.

Yeoman, T. K., and D. Orr, Phase and spectral power of mid-latitude Pi 2 pulsations: Evidence for a plasmaspheric cavity resonance, *Planet. Space Sci.*, *37*, 1367, 1989.

Yeoman, T. K., D. K. Milling, and D. Orr, Pi 2 polarization patterns on the U.K. subauroral magnetometer network (SAMNET), *Planet. Space Sci.*, *38*, 589, 1990.

Yeoman, T. K., M. Lester, D. K. Milling, and D. Orr, Polarization, propagation and MHD wave modes of Pi 2 pulsations: SABRE/SAMNET results, *Planet. Space Sci., 39,* 983, 1991.

Yumoto, K., Generation and propagation mechanisms of low-latitude magnetic pulsations - A review, *J. Geophys., 60,* 79, 1986.

Yumoto, K., Characteristics of daytime bay and Pi 2 magnetic variations: A case study, *Planet. Space Sci., 35,* 799, 1987.

Yumoto, K., External and internal sources of low-frequency MHD waves in the magnetosphere - A review, *J. Geomagn. Geoelectr., 40,* 292, 1988.

Yumoto, K., T. Saito, T. Tamura, Y. Tanaka, M. Nishino, M. Kunitake, K. Nishimuta, and H. Mitsudome, Polarization characteristics of Pi 2 magnetic pulsations in conjugate area around $L = 1.2 - 2.1$, paper presented at 83rd Meeting Soc. of Geomagn., of Earth, Planet. and Space Sci., Koganei, Japan, April 26-28, 1988.

Yumoto, K., K. Takahashi, T. Saito, F. W. Menk, B. J. Fraser, T. A. Potemra, and L. J. Zanetti, Some aspects of the relation between Pi 1-2 magnetic pulsations observed at L = 1.3 - 2.1 on the ground and substorm-associated magnetic field variations in the near-earth magnetotail observed by AMPTE/CCE, *J. Geophys. Res., 94,* 3611, 1989.

Yumoto, K., K. Takahashi, T. Sakurai, P. R. Sutcliffe, S. Kokubun, T. Saito, M. Kuwashima, and N. Sato, Multiple ground-based and satellite observations of global Pi 2 magnetic pulsations, *J. Geophys. Res., 95,* 15,175, 1990.

Zhu, X., and M. G. Kivelson, Analytic formulation and quantitative solutions of the coupled ULF wave problem, *J. Geophys. Res., 93,* 8602, 1988.

Zhu, X., and M. G. Kivelson, Global mode ULF pulsations in a magnetosphere with a nonmonotonic Alfvén velocity profile, *J. Geophys. Res., 94,* 1497, 1989.

Appendix A

Derivation of the Cavity-Resonance Equations in a Cylindrical Coordinate Geometry

Since $\nabla.\mathbf{E} = 0$, wave equation 4.5 may be written as

$$\nabla\times(\nabla\times\mathbf{E}(r,\theta,s,t)) = \nabla^2\mathbf{E}(r,\theta,s,t) = \frac{1}{A^2}\frac{\partial^2}{\partial t^2}\mathbf{E}(r,\theta,s,t)$$

or in the (x,θ,z) coordinate system as

$$\nabla^2\mathbf{E}(x,\theta,z,\tau) = \frac{1}{A_N^2}\frac{\partial^2}{\partial\tau^2}\mathbf{E}(x,\theta,z,\tau) \tag{A.1}$$

The components of the electric field are defined by

$$\mathbf{E} = \begin{bmatrix} E_x \\ E_\theta \\ E_z \end{bmatrix} = \begin{bmatrix} T(x,z,\tau)f(\theta) \\ 0 \\ iP(x,z,\tau)f(\theta) \end{bmatrix}$$

In cylindrical coordinates,

$$\begin{aligned} \nabla.\mathbf{E} = 0 \quad &\Rightarrow \quad \frac{1}{x}\frac{\partial}{\partial x}(xE_x) + \frac{1}{x}\frac{\partial E_\theta}{\partial\theta} + \frac{\partial E_z}{\partial z} = 0 \\ &\Rightarrow \quad \frac{1}{x}\frac{\partial}{\partial x}(xE_x) = -\frac{\partial E_z}{\partial z} \\ &\Rightarrow \quad \frac{1}{x}\frac{\partial}{\partial x}(xT) = -i\frac{\partial P}{\partial z} \end{aligned} \tag{A.2}$$

with the Laplacian given by

$$\nabla^2 \equiv \frac{1}{x}\frac{\partial}{\partial x}(x\frac{\partial}{\partial x}) + \frac{1}{x^2}\frac{\partial^2}{\partial \theta^2} + \frac{\partial^2}{\partial z^2}$$

Now consider equation A.1,

$$\begin{aligned}
\nabla^2\mathbf{E} &= \begin{bmatrix} \nabla^2 E_x - \frac{1}{x^2}E_x - \frac{2}{x^2}\frac{\partial E_\theta}{\partial \theta} \\ \nabla^2 E_\theta - \frac{1}{x^2}E_\theta + \frac{2}{x^2}\frac{\partial E_x}{\partial \theta} \\ \nabla^2 E_z \end{bmatrix} \\
&= \begin{bmatrix} \nabla^2 E_x - \frac{1}{x^2}E_x \\ 0 \\ \nabla^2 E_z \end{bmatrix} = \frac{1}{A_N^2}\frac{\partial^2}{\partial \tau^2}\begin{bmatrix} E_x \\ 0 \\ E_z \end{bmatrix} \qquad \text{(A.3)}
\end{aligned}$$

From the first row,

$$\left(\nabla^2 E_x - \frac{1}{x^2}\right)E_x = \left(\frac{1}{x}\frac{\partial}{\partial x}(x\frac{\partial}{\partial x}) + \frac{1}{x^2}\frac{\partial^2}{\partial \theta^2} + \frac{\partial^2}{\partial z^2} - \frac{1}{x^2}\right)E_x = \frac{1}{A_N^2}\frac{\partial^2}{\partial \tau^2}E_x$$

Substituting the expression $Tf(\theta)$ for E_x and dividing through by $f(\theta)$ we have

$$\begin{aligned}
\frac{1}{x}\frac{\partial}{\partial x}(x\frac{\partial T}{\partial x}) + \frac{1}{x^2}\frac{T}{f(\theta)}\frac{\partial^2 f(\theta)}{\partial \theta^2} + \frac{\partial^2 T}{\partial z^2} - \frac{T}{x^2} - \frac{1}{A_N^2}\frac{\partial^2 T}{\partial \tau^2} &= 0 \\
\Rightarrow \left[\frac{1}{A_N^2}\frac{\partial^2}{\partial \tau^2} - \frac{1}{x^2}\frac{1}{f(\theta)}\frac{\partial^2 f(\theta)}{\partial \theta^2} - \frac{\partial^2}{\partial z^2}\right]T &= \left[\frac{1}{x}\frac{\partial}{\partial x}(x\frac{\partial}{\partial x}) - \frac{1}{x^2}\right]T \\
&= \frac{\partial}{\partial x}\left[\frac{1}{x}\frac{\partial}{\partial x}(xT)\right] \\
&= -i\frac{\partial}{\partial x}\left[\frac{\partial}{\partial z}P(x,z,\tau)\right]
\end{aligned} \qquad \text{(A.4)}$$

where we have used equation (A.2) in the last step. For the third row,

$$\nabla^2 E_z = \left(\frac{1}{x}\frac{\partial}{\partial x}(x\frac{\partial}{\partial x}) + \frac{1}{x^2}\frac{\partial^2}{\partial \theta^2} + \frac{\partial^2}{\partial z^2}\right)iP(x,z,\tau)f(\theta) = \frac{1}{A_N^2}\frac{\partial^2}{\partial \tau^2}iP(x,z,\tau)f(\theta)$$

where we have substituted $E_z = iP(x,z,\tau)f(\theta)$.

Following the same procedure as before, we have

$$\begin{aligned}
\frac{1}{x}\frac{\partial}{\partial x}(x\frac{\partial iP}{\partial x})+\frac{1}{x^2}\frac{iP}{f(\theta)}\frac{\partial^2 f(\theta)}{\partial\theta^2}+\frac{\partial^2 iP}{\partial z^2} &= \frac{1}{A_N^2}\frac{\partial^2 iP}{\partial\tau^2} \\
\Rightarrow\left[\frac{1}{A_N^2}\frac{\partial^2}{\partial\tau^2}-\frac{1}{x^2}\frac{1}{f(\theta)}\frac{\partial^2 f(\theta)}{\partial\theta^2}-\frac{1}{x}\frac{\partial}{\partial x}(x\frac{\partial}{\partial x})\right]iP &= \frac{\partial^2}{\partial z^2}iP \\
&= -\frac{\partial}{\partial z}\left[-i\frac{\partial P}{\partial z}\right] \\
&= -\frac{\partial}{\partial z}\left[\frac{1}{x}\frac{\partial}{\partial x}(xT(x,z,\tau))\right]
\end{aligned} \tag{A.5}$$

where A.2 has been used in the last step. The coupled cavity-resonance equations are hence

$$\left[\frac{1}{A_N^2}\frac{\partial^2}{\partial\tau^2}-\frac{1}{x^2}\frac{1}{f(\theta)}\frac{\partial^2}{\partial\theta^2}f(\theta)-\frac{\partial^2}{\partial z^2}\right]T(x,z,\tau) = -i\frac{\partial}{\partial z}\left[\frac{\partial}{\partial x}P(x,z,\tau)\right] \tag{A.6}$$

$$\left[\frac{1}{A_N^2}\frac{\partial^2}{\partial\tau^2}-\frac{1}{x^2}\frac{1}{f(\theta)}\frac{\partial^2}{\partial\theta^2}f(\theta)-\frac{1}{x}\frac{\partial}{\partial x}(x\frac{\partial}{\partial x})\right]iP(x,z,\tau) = -\frac{\partial}{\partial z}\left[\frac{1}{x}\frac{\partial}{\partial x}(xT(x,z,\tau))\right] \tag{A.7}$$

Appendix B

Finite Difference Integration

There are various numerical methods used for solving the two point boundary value problem. A well known integration technique is the 'shooting' method. In this method, the differential equations are integrated from the one boundary to the other where the value of the solution is compared to a given value at the boundary. The eigenfrequency is varied after each iteration until the computed solution matches the boundary condition.

In the relaxation integration method, both boundary values are used for each integration process. This method is often used in preference to the 'shooting' method in cases when the equations to be integrated are inherently unstable near one of the boundaries (see *Press et al.*, [1986]). It is clear that the cavity-resonance equation 4.30 is unstable for small x and hence the relaxation method is preferred for this work.

Finite Difference method

We are faced with the problem of integrating equation 4.30 i.e.

$$\left(\frac{m^2}{\alpha} - 1\right)\frac{\partial^2}{\partial x^2}\bar{\mathcal{P}} + \left(\frac{m^2}{x}\left(\frac{\partial}{\partial x}\frac{x}{\alpha}\right) - \frac{1}{x}\right)\frac{\partial}{\partial x}\bar{\mathcal{P}} + \beta\bar{\mathcal{P}} = 0 \tag{B.1}$$

where

$$\begin{aligned} \alpha &= \frac{p^2}{A_N^2} + \frac{(n+i\kappa)^2}{x^2} + m^2 \\ \beta &= \alpha - m^2 \end{aligned}$$

This equation is in a finite difference form

$$A\bar{\mathcal{P}}'' + B\bar{\mathcal{P}}' + C\bar{\mathcal{P}} = 0 \tag{B.2}$$

(where we have used the superscript $'$ ($\equiv \frac{\partial}{\partial x}$) for convenience), with boundary conditions

$$\bar{\mathcal{P}}(x=0,m,p) = \mathcal{I}(m)\bar{G}(p) = 0 \tag{B.3}$$

$$\text{and } \bar{\mathcal{P}}(x=1,m,p) = \mathcal{M}(m)\bar{H}(p) \tag{B.4}$$

Notice that equation B.2 involves the derivative of the Alfvén speed $A_n(x)$ with respect to x. This derivative is determined in Appendix E. The domain of integration, $0 \leq x \leq 1$, is divided into a grid of N segments each with size $h = \Delta x = \frac{1}{N}$. The value at each grid point depends on the adjacent grid points as follows:

$$\bar{\mathcal{P}}''_n = \frac{\bar{\mathcal{P}}_{n+1} - 2\bar{\mathcal{P}}_n + \bar{\mathcal{P}}_{n-1}}{h^2} \tag{B.5}$$

$$\bar{\mathcal{P}}'_n = \frac{\bar{\mathcal{P}}_{n+1} - \bar{\mathcal{P}}_{n-1}}{2h} \tag{B.6}$$

Replacing $\bar{\mathcal{P}}''_n$ and $\bar{\mathcal{P}}'_n$ in equation B.2 by B.5 and B.6 leads to an equation which is in the general finite difference form, i.e.

$$a_n\bar{\mathcal{P}}_{n-1} + b_n\bar{\mathcal{P}}_n + c_n\bar{\mathcal{P}}_{n+1} = d_n \tag{B.7}$$

where

$$\begin{aligned} a_n &= 2A - hB \\ b_n &= 2Ch^2 - 4A \\ c_n &= 2A + hB \\ \text{with } d_{n=0} &= \mathcal{I}(m)\bar{G}(p) \\ \text{and } d_{n=N+1} &= \mathcal{M}(m)\bar{H}(p) \end{aligned}$$

where $n = 1, 2, \ldots$ N,N+1 and N is the number of grid intervals in the domain $0 \leq x \leq 1$. This N dimensional system is solved using the Thomas algorithm, a variation of the Gaussian elimination process, the details of which are beyond the scope of this thesis.

Appendix C

Magnetic Components

The integral form of equations 4.31, 4.32 and 4.32 are given by

$$b_x(\tau) = -\frac{i}{x}\frac{df(\theta)}{d\theta}\int_0^\tau P(x,z,\tau')d\tau' \tag{C.1}$$

$$b_z(\tau) = \frac{1}{x}\frac{df(\theta)}{d\theta}\int_0^\tau T(x,z,\tau')d\tau' \tag{C.2}$$

$$b_\theta(\tau) = f(\theta)\int_0^\tau \left(i\frac{\partial}{\partial x}P(x,z,\tau') - \frac{\partial}{\partial z}T(x,z,\tau')\right)d\tau' \tag{C.3}$$

Applying the Laplace transform identity

$$\mathcal{L}\{\int_0^\tau F(\tau')d\tau'\} = \frac{1}{p}\bar{F}(p) \tag{C.4}$$

(where $\bar{F}(p) \equiv \mathcal{L}\{F(\tau)\}$), to equations C.1, C.2 and C.3 we have that

$$b_x(x,z,\tau) = -\frac{i}{x}\frac{df(\theta)}{d\theta}\int_0^\tau P(x,z,\tau')d\tau' = -\frac{i}{x}\frac{df(\theta)}{d\theta}\mathcal{L}^{-1}\left\{\frac{\bar{P}(x,z,p)}{p}\right\} \tag{C.5}$$

$$b_z(x,z,\tau) = \frac{1}{x}\frac{df(\theta)}{d\theta}\int_0^\tau T(x,z,\tau')d\tau' = \frac{1}{x}\frac{f(\theta)}{d\theta}\mathcal{L}^{-1}\left\{\frac{\bar{T}(x,z,p)}{p}\right\} \tag{C.6}$$

$$\begin{aligned} b_\theta(x,z,\tau) &= f(\theta)\int_0^\tau \left(i\frac{\partial}{\partial x}P(x,z,\tau') - \frac{\partial}{\partial z}T(x,z,\tau')\right)d\tau' \\ &= f(\theta)\mathcal{L}^{-1}\left\{i\frac{\partial}{\partial x}\frac{\bar{P}(x,z,p)}{p} - \frac{\partial}{\partial z}\frac{\bar{T}(x,z,p)}{p}\right\} \\ &= f(\theta)\left[i\frac{\partial}{\partial x}\mathcal{L}^{-1}\left\{\frac{\bar{P}}{p}\right\} - \frac{\partial}{\partial z}\mathcal{L}^{-1}\left\{\frac{\bar{T}}{p}\right\}\right] \end{aligned} \tag{C.7}$$

Thus b_x, b_z and b_θ are obtained during the numerical integration procedure by computing

$$\mathcal{L}^{-1}\left\{\frac{\bar{P}}{p}\right\} \text{ and } \mathcal{L}^{-1}\left\{\frac{\bar{T}}{p}\right\}$$

Appendix D

Poynting Vectors

We are required to expand (4.34) i.e.

$$\mathbf{F}(\tau) = \int_0^\tau \Re(\mathbf{E}) \times \Re(A_0 \mathbf{b}) d\tau'$$

where $\mathbf{E} = \mathbf{E}_R + i\mathbf{E}_I$ and $\mathbf{b} = \mathbf{b}_R + i\mathbf{b}_I$, i.e.

$$\mathbf{E} = \begin{bmatrix} E_x^R \\ E_\theta^R \\ E_z^R \end{bmatrix} + i \begin{bmatrix} E_x^I \\ E_\theta^I \\ E_z^I \end{bmatrix} \quad \text{and} \quad \mathbf{b} = \begin{bmatrix} b_x^R \\ b_\theta^R \\ b_z^R \end{bmatrix} + i \begin{bmatrix} b_x^I \\ b_\theta^I \\ b_z^I \end{bmatrix}$$

Evaluating the cross product of the real parts

$$\Re(\mathbf{E}) \times \Re(\mathbf{b}) = \begin{bmatrix} E_x^R \\ E_\theta^R \\ E_z^R \end{bmatrix} \times \begin{bmatrix} b_x^R \\ b_\theta^R \\ b_z^R \end{bmatrix} = \begin{bmatrix} -b_\theta^R E_z^R \\ b_\theta^R E_x^R \\ b_x^R E_z^R - b_z^R E_x^R \end{bmatrix}$$

and hence

$$\mathbf{F}(\tau) = \int_0^\tau \begin{bmatrix} -b_\theta^R E_z^R \\ b_\theta^R E_x^R \\ b_x^R E_z^R - b_z^R E_x^R \end{bmatrix} d\tau'$$

Appendix E

The Alfvén Speed Derivative

Firstly, note that

$$\frac{d}{dx}A_N(R) = \frac{dA_N(R)}{dR}\frac{dR}{dx} \tag{E.1}$$

Each derivative is obtained as follows

$$R = \frac{r_0 x}{a} + 1 \Rightarrow \frac{dR}{dx} = \frac{r_0}{a} \tag{E.2}$$

From equation 5.9

$$A_N(R) = \frac{A_i}{A_0}R^{-3}f(R)^{-\frac{1}{2}} \Rightarrow \frac{dA_N(R)}{dR} = -\frac{A_i}{A_0}\left(3R^{-4}f(R)^{-\frac{1}{2}} + \frac{1}{2}f(R)^{-\frac{3}{2}}\frac{df(R)}{dR}R^{-3}\right) \tag{E.3}$$

and therefore

$$\frac{dA_N(x)}{dx} = \frac{A_i r_0}{A_0 a}R^{-3}f(R)^{-\frac{1}{2}}\left(-\frac{3}{R} - \frac{1}{2f(R)}\frac{df(R)}{dR}\right)$$

All that remains is to compute the derivative $\frac{df(R)}{dR}$. The function $f(R)$ is given by equations 5.16 i.e.

$$\begin{aligned} n = \rho_{eq} = \rho_i f(R) \;=\; & \alpha e^{\beta R} \\ & + \frac{n_i}{2}\left[\frac{1-\exp^{\frac{R-R_{pa}}{\Delta R}}}{1+\exp^{\frac{R-R_{pa}}{\Delta R}}} + 1\right]\left(\frac{1}{R}\right)^{N_1} \\ & + \frac{n_p}{2}\left[\frac{1-\exp^{\frac{R_{pb}-R}{\Delta R}}}{1+\exp^{\frac{R_{pb}-R}{\Delta R}}} + 1\right]\left(\frac{R_{pb}}{R}\right)^{N_2} \\ & + n_{IMF} \end{aligned} \tag{E.4}$$

Consider the term

$$\frac{n_i}{2}\left[\frac{1-\exp^{\frac{R-R_{pa}}{\Delta R}}}{1+\exp^{\frac{R-R_{pa}}{\Delta R}}}+1\right]\left(\frac{1}{R}\right)^{N_1}$$

First note that for the exponent

$$\frac{d}{dR}e^{\frac{R-R_{pa}}{\Delta R}} = e^{\frac{R-R_{pa}}{\Delta R}}\frac{1}{\Delta R}$$

and therefore

$$\begin{aligned}\frac{d}{dR}\left[\frac{1-\exp^{\frac{R-R_{pa}}{\Delta R}}}{1+\exp^{\frac{R-R_{pa}}{\Delta R}}}+1\right] &= -\frac{(1+\exp^{\frac{R-R_{pa}}{\Delta R}})e^{\frac{R-R_{pa}}{\Delta R}}\frac{1}{\Delta R}-(1-\exp^{\frac{R-R_{pa}}{\Delta R}})e^{\frac{R-R_{pa}}{\Delta R}}\frac{1}{\Delta R}}{(1+\exp^{\frac{R-R_{pa}}{\Delta R}})^2}\\ &= -\frac{2e^{\frac{R-R_{pa}}{\Delta R}}\frac{1}{\Delta R}}{(1+\exp^{\frac{R-R_{pa}}{\Delta R}})^2}\end{aligned}$$

and finally

$$\begin{aligned}&\frac{d}{dR}\left[\frac{n_i}{2}\left[\frac{1-\exp^{\frac{R-R_{pa}}{\Delta R}}}{1+\exp^{\frac{R-R_{pa}}{\Delta R}}}+1\right]\left(\frac{1}{R}\right)^{N_1}\right] =\\ &\quad\frac{n_{io}}{2}R^{-N_1}\left[-\frac{N_1}{R}\left(\frac{1-\exp^{\frac{R-R_{pa}}{\Delta R}}}{1+\exp^{\frac{R-R_{pa}}{\Delta R}}}+1\right)-\frac{-2e^{\frac{R-R_{pa}}{\Delta R}}\frac{1}{\Delta R}}{(1+\exp^{\frac{R-R_{pa}}{\Delta R}})^2}\right]\end{aligned}$$

Similarly it can be shown that

$$\begin{aligned}&\frac{d}{dR}\left[\frac{n_p}{2}\left[\frac{1-\exp^{\frac{R_{pb}-R}{\Delta R}}}{1+\exp^{\frac{R_{pb}-R}{\Delta R}}}+1\right]\left(\frac{R_{pb}}{R}\right)^{N_2}\right] =\\ &\quad\frac{n_p}{2}\left(\frac{R_{pb}}{R}\right)^{N_2}\left[-\frac{N_2}{R}\left(\frac{1-\exp^{\frac{R_{pb}-R}{\Delta R}}}{1+\exp^{\frac{R_{pb}-R}{\Delta R}}}+1\right)+\frac{-2e^{\frac{R_{pb}-R}{\Delta R}}\frac{1}{\Delta R}}{(1+\exp^{\frac{R_{pb}-R}{\Delta R}})^2}\right]\end{aligned}$$

The total derivative of equation E.4 also includes the derivative of the ionospheric term ($\alpha = e^{\beta R}$), which is trivial.

Appendix F

Toroidal Resonance Eigenperiod Formulae

Taylor and Walker [1984] presented empirical formulae from which the eigenfrequency of toroidal-resonance modes (in a dipolar magnetic field) may by determined. We make use of their calculations to determine the characteristic periodicity of the Alfvén guided wave mode at any give L-shell.

Assuming a plasma density variation along the field line of r^{-N}, they determined the following set of formulae for the eigen-wavenumber k,

$$N = 2, \quad k = \frac{(\pi/s_0)}{[1-(a_1 s_0^2 - a_2 s_0^4 + a_3 s_0^6)]^{\frac{1}{2}}}$$

$$N = 3, \quad k = \frac{(\pi/s_0)}{[1-(a_5 s_0^2 - a_6 s_0^4 + a_7 s_0^6)]^{\frac{1}{2}}}$$

$$N = 4, \quad k = \frac{(\pi/s_0)}{[1-(a_8 s_0^2 - a_9 s_0^4)]^{\frac{1}{2}}}$$

$$N = 6, \quad k = \frac{\pi}{s_0}$$

where the values for the constants $a_i, i = 1,9$ are given in table F.1

Constant	Value
a_1	0.1307
a_2	0.0154
a_3	0.0011
a_4	0.00004
a_5	0.0980
a_6	0.0077
a_7	0.0003
a_8	0.0653
a_9	0.0026

Table F.1: Values for the coefficients a_i.

Given the wavenumber, the eigenperiod is easily determined using

$$T(t) = \frac{1}{f} = \frac{1}{A(s)k(s)} = \frac{1}{A(x)k(x)} = \frac{1}{A_0 A_N(x)k(x)} \tag{F.1}$$

$$\Rightarrow T(\tau) = \frac{T(t)}{t_0} = \frac{1}{A_0 A_N(x)k(x)t_0} = \frac{1}{A_N(x)k(x)r_0} \tag{F.2}$$

where the relationship between x and s is described in appendix G.

Appendix G

Relationship between coordinates x and s.

In a dipole field, *Taylor and Walker* [1984] defined the coordinates z and s as

$$z = \sin\theta, \text{ and}$$

$$s = z + z_0$$

where $s = z_0$ defines the position of the southern ionosphere. A point along the dipole field is defined by

$$r = aL\cos^2\theta,$$

$$\Rightarrow \quad r = aL(1 - z^2), (\text{ using } z = \sin\theta)$$

$$\Rightarrow \quad r = aL(1 - (\frac{s_0}{2})^2), (\text{ using } s_0 = 2z_0)$$

The points along the ionosphere are given by

$$r = a = aL(1 - (\frac{s_0}{2})^2)$$

$$\Rightarrow \quad L = \frac{1}{(1 - (s/2)^2)}$$

Hence

$$x = \frac{r_0}{a}(L - 1) = \frac{r_0}{a}(\frac{1}{(1 - (s/2)^2)} - 1) \tag{G.1}$$

or

$$s = 2(1 - \frac{1}{(\frac{a}{r_0}x + 1)})^{\frac{1}{2}} \tag{G.2}$$